ISSN 1000-9620

Marine Science Bulletin

Volume 5 • Number 1 2003

ISSN 1000-9620

NATIONAL MARINE DATA AND
INFORMATION SERVICE OF CHINA

MARINE SCIENCE BULLETIN

Vol.5 No.1 May, 2003

CONTENTS

Research on the Propagation Acting of the Equatorial Planetary Waves on the Western Equatorial Pacific Warm Pool Heat ····· *Shi Qiang* (石 强) *et al.* (1)

Multi-beam Sonar and Side-scan Sonar Image Co-registering and Fusing ····· *Yang Fanlin* (阳凡林) *et al.* (16)

A Study on Snowstorm Weather in Coastal Area of Western Antarctic ····· *Huang Yaorong* (黄耀荣) *et al.* (24)

Biochemical Mechanism of the Eutrophication and Its Prevention — the Deep Treatment of Waste Water and Its Denitrification and Dephosphorization ····· *Li Hongshan* (李红山) *et al.* (32)

Effect of Temperature on the Fatty Acid Composition of Four Species of Marine Microalgae ····· *Li Wenquan* (李文权) *et al.* (40)

Reanalysis of the Atmospheric Flux of Nutrient Elements to the Southern Yellow Sea and the East China Sea ····· *Wan Xiaofang* (万小芳) *et al.* (45)

Chemical Associations of Heavy Metals in the Sediments near Bailonggang Sewage Discharge Outlet of Shanghai ····· *Bi Chunjuan* (毕春娟) *et al.* (52)

Accumulation and Cycle of Heavy Metals in *Sonneratia apetala* and *S. caseolaris* Mangrove Community at Futian of Shenzhen, China ····· *Wang Bosun* (王伯荪) *et al.* (59)

Effect of $NaNO_3$ Concentrations on the Growth and Fatty Acid Compositions of *Nitzschia closterium* and *Chaetoceros gracilis* ····· *Liang Ying* (梁 英) *et al.* (69)

Characteristics of Heavy Minerals Composition and Distribution in Jiulong River Estuary Sediment ····· *Xu Maoquan* (徐茂泉) *et al.* (75)

Study on the Release of Grouper *Epinephelus* for Stock Enhancement ····· *Bo Zhili* (薄治礼) *et al.* (88)

LIBRARY
SEP 30 2003
National Oceanic & Atmospheric Administration
U.S. Dept. of Commerce

Research on the Propagation Acting of the Equatorial Planetary Waves on the Western Equatorial Pacific Warm Pool Heat

Shi Qiang (石 强)[1,3], Xu Jianping (许建平)[2,3], Zhu Bokang (朱伯康)[1]

1 *North China Sea Branch, State Oceanic Administration (SOA), Qingdao* 266033

2 *Second Institute of Oceanography, SOA, Hangzhou* 310012

3 *Key Lab of Ocean Dynamic Processes and Satellite Oceanography, SOA, Hangzhou* 310012

Abstract Based on the long-term buoy data from the Tropical Atmosphere Ocean (TAO) array during the TOGA (Tropical Ocean and Global Atmosphere) Program (1980—1996), the propagation acting of the Equatorial planetary waves on the Western Equatorial Pacific warm pool heat is analyzed. Results show that the zonal heat transmission in the Western Equatorial Pacific takes palace mainly in the subsurface water and spreads eastwards along the thermocline; while the seasonal westward-spreading heat change structure occurs in the mixed layers in the middle and western Pacific. The standing-form transmission in the western Pacific appears in the thermocline layer, while in the eastern pacific, it exists in the mixed layer as well as in the thermocline layer. The standing-form and eastward-spreading sign of zonal heat transmitting in the upper water is predominant and strong, and the westward sign is weak.

The component force of Kelvin Equatorial wave pressure runs through the western and eastern Equatorial pacific, and transmits heat energy eastwards. And the heat transmitted by zonal current component occurs mostly in the western Pacific; The heat transmitted by the component force of Rossby wave pressure mainly appears in the eastern and middle areas of the Pacific, while the zonal current component transmitting occurs mainly in the western Pacific; Mixed-Rossby gravity wave's action on the zonal current is stronger than that of the thermocline layer. In the mean state, the standing wave model of Equatorial Pacific up layer ocean temperature confines the transport of western Pacific warm pool heat to the eastern Pacific. Under abnormal conditions, the standing wave model of Equatorial Pacific up layer ocean temperature weakens, the eastwardly transmitting model enhances, and subsequently the El Niño event occurs.

Keywords Equatorial Planetary Wave, Equatorial Kelvin Wave, Rossby Wave, Mixed Rossby Gravity Wave, Heat, Western Equatorial Pacific Warm Pool

1 Introduction

In the Equatorial Pacific, due to the difference between the atmospheric circulation and air-sea interaction, the near-surface seawater heat structure in the eastern and western Pacific presents two obviously different characteristics: warm pool (> 28℃) in the western equatorial Pacific and cold tongue (< 24℃) in the eastern equatorial Pacific. The water bodies of these two heat structures would give rise to change in spatial distribution under the action of the equatorial Pacific circulation. During

Received on March 10, 2003; accepted on April 15, 2003

LIBRARY
Pacific Islands Fisheries Science Center
NOAA Fisheries
Honolulu, Hawai'i

the El Niño-Southern Oscillation (ENSO), the magnitude of spatial variations of these two water bodies reaches the extreme. During the El Niño event, the easterly margin of the western Pacific warm pool may spread 8 000 km eastwards from the mean position; while in the anti-El Niño event, the westerly margin of the eastern Pacific cold tongue may extend 1 500 km westwards from the mean position[1]. Under the mean conditions, the eastern margin of the western equatorial Pacific warm pool depicts a seasonal swing about 170° W; The western cold tongue of the equatorial eastern Pacific cold tongue moves to the east of 115° W. Many scholars have studied the seasonal change of the equatorial Pacific sea area by using many methods and they conclude that the seasonal variations in the upper ocean are subjected to the local response of sea surface wind stress and controlled by the excitation and propagation of Kelvin Wave and Rossby Wave. Of late, based on the analysis of the calculated results of the TOGA-TAO buoy data by using the linear dynamic model, Yu *et al.* suggested that the seasonal variations of the ocean between 5° N and 5° S are mainly controlled by the wind-driven equatorial Kelvin Wave, and the first and second baroclinic modal Rossby Wave. In addition, there also exists the influence of the mixed-Rossby gravity wave[2]. However, in the previous studies, little has been known about how these three low-frequency forced oscillations have affected the process of heat energy transmission in the upper equatorial ocean. Recently, MacPhden *et al.* have made a summary of the research on the roles of the TOGA data in revealing the ENSO circulation phenomenon, checking the ENSO theory, developing new theoretical concepts on air-sea interaction, the ocean and atmospheric models, and the air-sea coupling model, and the marine data assimilation. Owing to the fact that the delayed oscillation theory cannot always explain the ENSO event, they propose the necessity of establishing a new physical hypothesis and the need of making new theoretical explorations into the air-sea interaction on the interannual-seasonal time scale. In the research program of climate change and prediction for the next fifteen years (1995—2012), data from TOGA and other observing systems would make contributions to the research on new theories[3].

Based on the long-term hydrological and meteorological data observed by the TOGA-TAO buoy array in the sea area of the equatorial Pacific, this paper first analyses the space-time structure of the ocean temperature and zonal current propagation in the upper equatorial Pacific as well as the space-time structure of the equatorial Kelvin Wave, Rossby Wave and mixed-Rossby gravity wave and their zonal heat transmission action. And, on this basis, it further discusses the relationship between the time -space structure of heat transmission in the western Equatorial Pacific warm pool and the equatorial Pacific warm pool and equatorial Pacific planetary wave so as to improve the understanding of the interaction between ENSO and the mean seasonal circulation of the equatorial Pacific, thus contributing to the knowledge of dynamic process of ENSO and improving the precision of ENSO prediction.

2 Data and analytical methods

The paper calculates the multi-year daily mean values of such elements as sea surface quasi-wind stress, ocean temperature (1 ~ 200 m) and equatorial zonal current (10 ~ 200 m) as well as the depth of thermocline (20℃ isothermal line depth) by using the daily mean values given by the historical observations of the TOGA-TAO buoy array between March, 1980 and May, 1996. The locations of statistical stations and the data time for various elements are shown in Table 1 and 2.

Tab. 1 Station locations of ocean temperature, and wind speed of observation, and years of data statistics

	165° E	140° W	110° W
0° N	1986. 1—1996. 3	1983. 4 —1995. 12	1980. 3—1995. 5
2° N	1985. 7—1996. 5	1986. 10—1996.2	1985. 11—1996. 5
2° S	1985. 7—1996. 5	1986. 6—1996. 4	1985. 6—1996. 5
5° N	1988. 2—1996. 5	1988. 5—1996. 5	1985. 11—1996. 5
5° S	1987. 1—1996. 4	1990. 10—1996. 5	1985. 11—1996. 5

Tab. 2 Station locations of zonal current observation and years of data statistics

165° E, 0° N	140° W, 0° N	110° W, 0° N
(10 m) 1986. 1—1993.1 2	(10 m) 1983. 4—1995. 9	(10 m) 1983. 11—1995. 8
(50 m) 1986. 11—1993. 12	(45 m) 1983. 10—1995. 9	(45 m) 1983. 11—1995. 8
(100 m) 1986. 11—1993. 12	(80 m) 1983. 4—1995. 9	(80 m) 1983. 11—1995. 2
(150 m) 1986. 12—1993. 12	(120 m) 1983. 4—1995. 9	(120 m) 1980. 3—1995. 8
(200 m) 1986. 1—1993. 12	(200 m) 1987. 10—1995. 9	(200 m) 1980. 3—1995. 8

According to the marine waveguide theory, within the equatorial ocean Rossby deformation radius (approximately the zonal sea area of 2.5°N ~ 2.5°S), the marine low-frequency disturbance would be reflected within the waveguide range and propagates zonally[4]. Therefore, assuming that each analytical element is composed of the many harmonics, as shown in the formula (1), its low-frequency disturbance propagates zonally within the equatorial waveguide while the directions of the various harmonic disturbances may be determined by comparison and judgment of the initial phases of the harmonics of the same period between different station locations.

$$F(T,h,u) = A_0^{T,h,u} + \sum_{i=1}^{N} A_i^{T,h,u} \cos(\omega_i^{T,h,u} t - g_i^{T,h,u}) + e \tag{1}$$

Where F (···) represents the sequence of elements analysed; T, the ocean temperature; h, the depth of thermocline (20 ℃ isothermal line depth); u, zonal current speed; t, the times; ω_i, the harmonic angular frequency of each element analysed; A_i, the harmonic amplitude of each element analysed; g_i, the harmonic initial phase of each element analysed; N, the number of harmonics; A_0, the

mean value of each element analysed and *e*, the noise.

As there does not exist a fixed frequency range in the seasonal and intraseasonal ocean oscillation periods, many researchers choose different wave period ranges to study in the light of the problems they fee interested in. For example, some take 60 ~ 120 d[4], 60 ~ 90 d[5], others take 40 ~ 60 d[6] or 36 ~ 73 d[7] *etc.*. In this study, the harmonics period is taken as 20 ~ 365 d while the disturbances with periods less than 20 d are neglected.

The Fourier power spectrum analysis is made of the time series of each element analysed to identify the angular frequency ω_i in the time series of each element analysed corresponding to the significant power spectrum peak value. Then, the least square method is employed to calculate the harmonic constants A_i and g_i of the angular frequency ω_i corresponding to the significant power spectrum peak value.

The judgment criterion for the initial phase g of the distubance zonal propagation forms of the same (or near) standard layer, and the same angular frequency is:

g (165° E) < g (140° W) < g (110° W) harmonic disturbance propagating eastwards;

g (165° E) > g (140° W) > g (110° W) harmonic disturbance propagating westwards;

g (165° E) > g (140° W) < g (110° W) or

g (165° E) < g (140° W) > g (110° W) harmonic disturbance propagating in standing wave.

Resuperimposing and combining the harmonic disturbances with the same form of propagation of the elements analysed constitute the elemental time series with the same form of propagation, *i. e.*:

$$f_{E、W、S}(T,h,u) = \sum_{i=1}^{M} A_i^{T,h,u} \cos(\omega_i^{T,h,u} t - g_i^{T,h,u}) \tag{2}$$

Where $f(\cdots)$ denotes the elemental series with propagating characteristics. The subscripts E, W and S represent the analytical element series of eastward propagation, westward propagation and standing-wave propagation respectively. Other symbols have the same meanings as those in formula (1).

In making space-time analysis of the above-mentioned elemental series $f_{E,W,S}(T, h, u)$ with the same form of propagation, we adopted the empirical orthogonal decomposition method based on the optimal variance matrix and its analytical results are similar to those obtained by using the singular eigenvalue orthogonal decomposition (SVD) method.

In order to calculate the velocity of the propagation phase of the analytical series decomposed main modal, we use the delayed cross-correlation coefficient analysis method between the east boundary and internal data for the expansion coefficients corresponding to the station locations of 165° E, 140° W and 110° W[8, 9], to estimate the propagating time and then calculate the velocity of the propagation phase.

3 Calculated results and analysis

3.1 Propagating characteristics of the low-frequency planetary wave of the equatorial Pacific

3.1.1 Equatorial Kelvin Wave

The relaxation of the monsoonal zonal component in the western Pacific excites Kelvin Wave in

the west boundary and propagates eastwards along the equator. This eastward transmitting equatorial Kelvin Wave is considered the triggering mechanism for the El Niño event. Then, under the mean conditions, how does the equatorial Kelvin Wave propagate? We have made space-time analysis of the eastward-propagating thermocline sequence and the results show that the eastward-propagating thermocline variations are mainly controlled by the equatorial Kelvin Wave. The spatial distribution of the equatorial Kelvin Wave shows the largest amplitude at the equator, which attenuates toward the two sides of the equator (Fig. 1a). Such spatial distribution is consistent with the theoretical results of the equatorial Kelvin Wave. It is found from the distribution of the thermocline expansion coefficients at the 165° E and 110° W stations (Fig. 1b) that the period of the equatorial Kelvin Wave is about 120 d, it takes about 75 d for the equatorial Kelvin Wave to transmit from 165° E to 110° W with the eastward-propagating phase velocity of about 1.46 m/s, which is very close to the theoretical calculated result of the modal phase velocity (1.40 m/s)[2] of the second baraclinic equatorial Kelvin Wave model.

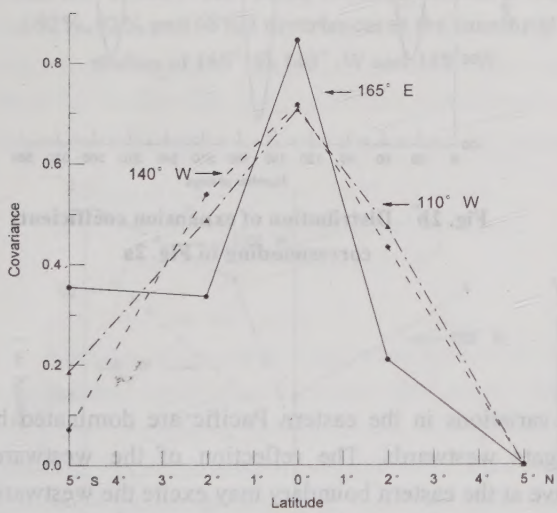

Fig. 1a Kelvin Wave of thermocline main modals (86%, 62% and 87%) covariances at the equatorial station of 165° E, 140° W and 110° W

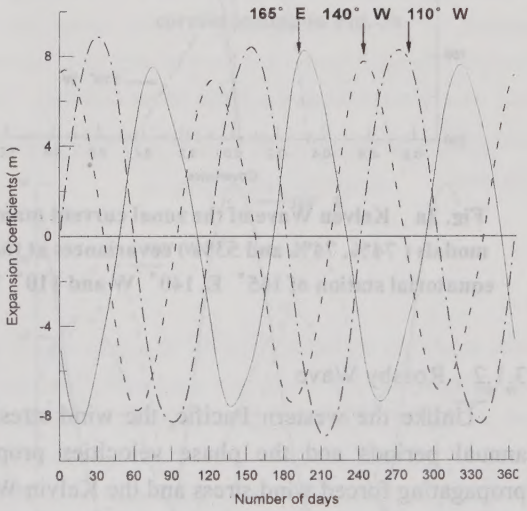

Fig. 1b Distribution of expansion coefficients corresponding to Fig. 1a

Space-time analysis of the eastward-propagating zonal current sequence in the four standard layers is made. Fig. 2a shows the vertical structure of the eastward-propagating zonal currents at the three equatorial observation stations. The variations in the eastward-propagating zonal current mainly originate from the joint action of the dynamic processes of westerly stress and equatorial Kelvin Wave. Analysis of the surface mean quasi-wind stress at the three equatorial observation stations of 165° E, 140° W and 110° W indicates that the zonal quasi-wind stress has the eastward-propagating intraseasonal Kelvin Wave disturbances with a period of about 60.83 d and that the propagating characteristics are more obvious between 165° E and 140° W, its mean phase velocity being 2.36 m/s

or so. Under the joint action of the eastward-propagating zonal wind stress and the equatorial Kelvin Wave pressure gradient force, the eastward-propagating mean phase velocity of the equatorial zonal current is approximately 3.64 m/s and it only takes 30 d for the zonal current disturbance to propagate from 165° E to 110° W, which is similar to the vertical structure obtained from the theoretical analysis of the equatorial Kelvin Wave[2].

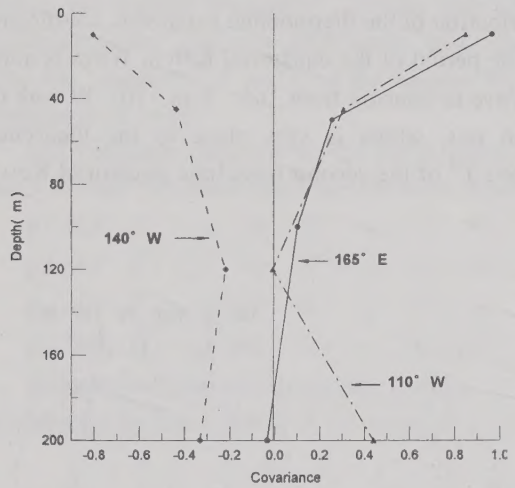

Fig. 2a Kelven Wave of the zonal current main modals (74%, 74% and 53%) covariances at the equatorial station of 165° E, 140° W and 110° W

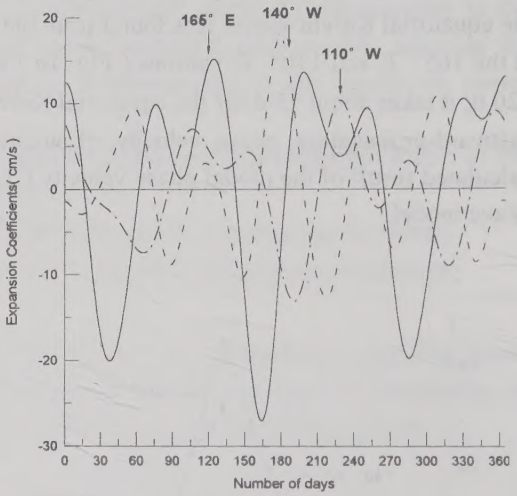

Fig. 2b Distribution of expansion coefficients corresponding to Fig. 2a

3.1.2 Rossby Wave

Unlike the western Pacific, the wind stress variations in the eastern Pacific are dominated by annual periods and the phase velocities propagate westwards. The reflection of the westward-propagating forced wind stress and the Kelvin Wave at the eastern boundary may excite the westward-going Rossby Wave in the equatorial ocean. Space-time analysis of the westward-propagating thermocline sequences indicates that the radial distribution of Rossby Wave shows the maximum disturbance at 5° N, the secondary at 5° S and the minimum on the equator and at 2° S, the disturbance presenting an asymmetric distribution relative to the equator (Fig. 3a), which is consistent with the analytical results given by Gent *et al.*[10] and Kessler *et al.*[11] based on the CTD data in the tropic Pacific. It may be concluded from the distribution of thermocline expansion coefficients at 165° E and 110° W station locations (Fig. 3b) that the period of the equatorial Rossby Wave is about 360 d and that it takes about 100 d for the equatorial Rossby Wave to propagate from 110° W to 165° E, the westward-propagating phase velocity being 1.09 m/s or so, which is close to the modal phase velocity (0.91 m/s) of the first baroclinic equatorial Rossby Wave model as theoretically calculated by Yu *et al.*[2]. The above-mentioned proportional characteristics of period and phase velocity between the equatorial Kelvin Wave and Rossy Wave are basically consistent with the theoretical analytical results (3/1).

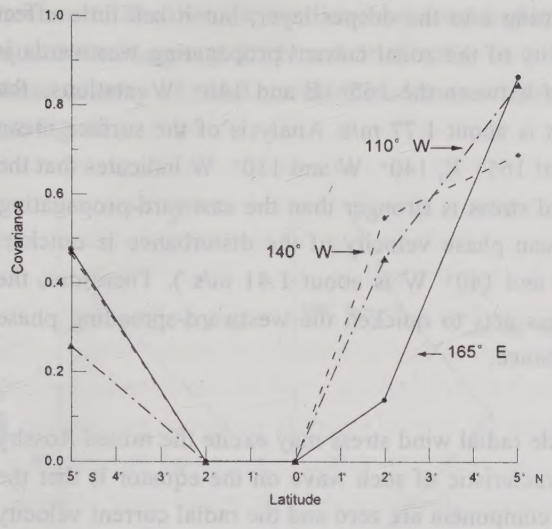

Fig. 3a Rossby Wave of the thermocline main modals (92%, 92% and 68%) covariances at the equatorial station of 165° E, 140° W and 110° W

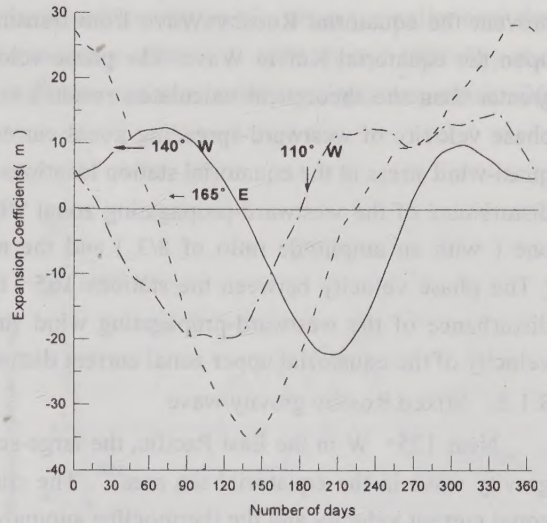

Fig. 3b Distribution of expansion coefficients corresponding to Fig. 3a

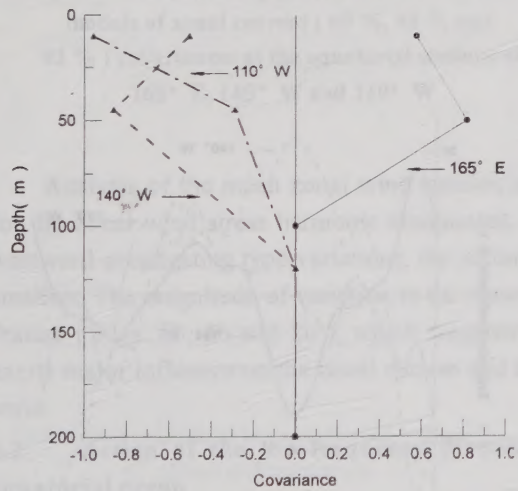

Fig. 4a Rossby Wave of the zonal current main modals (85%, 89% and 71%) covariances at the equatorial station of 165° E, 140° W and 110° W

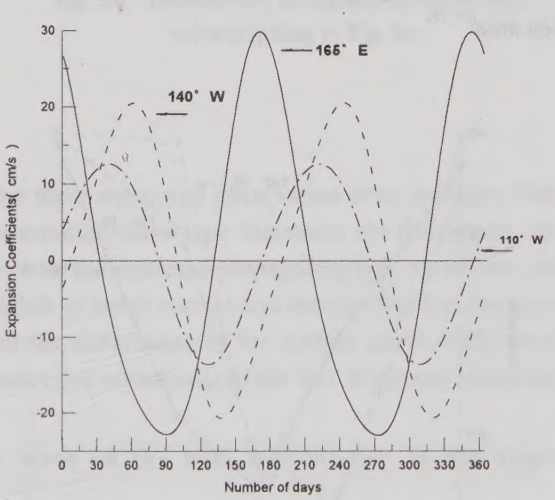

Fig. 4b Distribution of expansion coefficients corresponding to Fig. 4a

The difference between the vertical structure of the westward-going zonal current at the three equatorial station locations (Fig. 4a) and the analytical results of the theoretical linear dynamic model [2] lies in the disappearance of the vertical reserve variations of the zonal current velocity. Philanders [12] analysis indicates that the phase velocity of the equatorial Rossby Wave corresponds to the maximum velocity of the Equatorial Undercurrent. Therefore, the Equatorial Undercurrent may

prevent the equatorial Roosby Wave from transmitting into the deeper layer, but it has little effect upon the equatorial Kelvin Wave. The phase velocity of the zonal current propagating westwards is greater than the theoretical calculated result[2], and between the 165° E and 140° W stations, the phase velocity of westward-spreading zonal current is about 1.77 m/s. Analysis of the surface mean quasi-wind stress at the equatorial station locations of 165° E, 140° W and 110° W indicates that the disturbance of the westward-propagating zonal wind stress is stronger than the eastward-propagating one (with an amplitude ratio of 8/3) and the mean phase velocity of the disturbance is quicker. (The phase velocity between the stations 165° E and 140° W is about 1.41 m/s). Therefore, the disturbance of the westward-propagating wind stress acts to quicken the westward-spreading phase velocity of the equatorial upper zonal current disturbance.

3.1.3 Mixed Rossby gravity wave

Near 125° W in the East Pacific, the large-scale radial wind stress may excite the mixed Rossby gravity wave in the equatorial sea area[13]. The characteristic of such wave on the equator is that the zonal current velocity and the thermocline anomaly component are zero and the radial current velocity is the largest. Under the condition of the near-equatorial conservation of potential vorticity, the radial current of the mixed-Rossby gravity wave may induce the disturbance of the thermocline, which reaches the maximum near the equator and decreases toward the two sides, and propagates in the east and west directions at the same phase velocity. The thermocline disturbance may also induce the zonal current[9]. During the non-El Niño, such mixed Rossby gravity wave is found to exist in the equatorial sea area[14, 15].

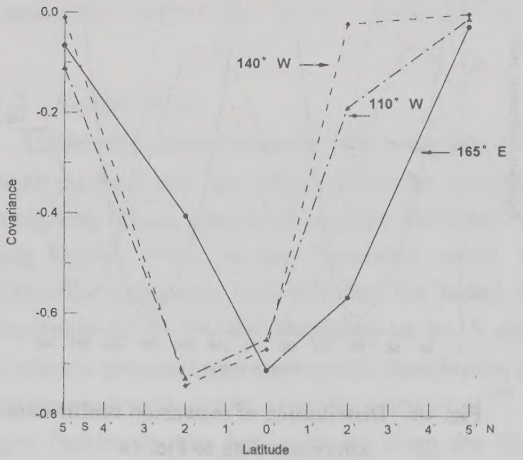

Fig. 5a Mixed Rossby gravity wave of the thermocline main modals (75 %, 92 % and 60 %) covariances at the equatorial stations of 165° E, 140° W and 110° W

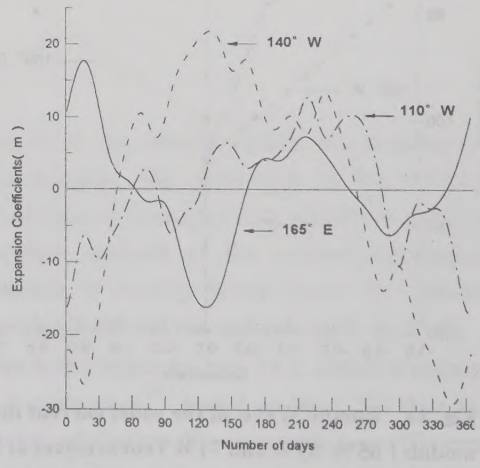

Fig. 5b Distribution of expansion coefficients corresponding to Fig. 5a

As the three observation stations are located on the two sides of 125° W in the equatorial eastern Pacific respectively, the mixed-Rossby Wave should present the characteristic of standing-wave

movement. The thermocline disturbance induced by the mixed Rossby gravity wave is smaller near the equator and larger at 5° N and 5° S (Fig. 5a). Between the stations of 165° E and 140° W, the phase velocity of zonal current disturbance is about 0.88 m/s and the disturbing depth may reach 120 m (Fig. 6a).

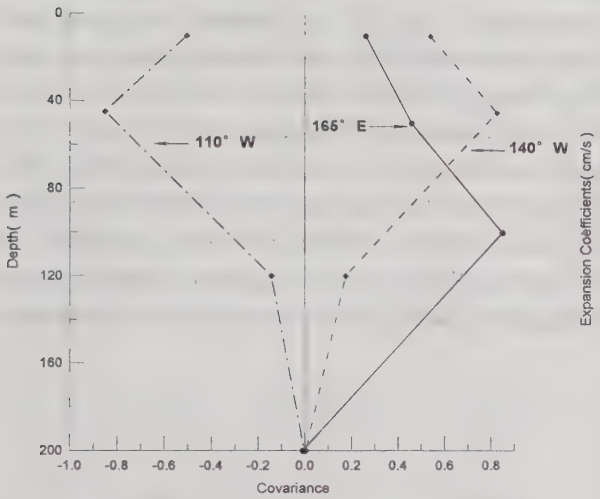

Fig. 6a Mixed Rossby gravity wave of the main modals of zonal current (69 %, 93 % and 93 %) covariances at the equatorial stations of 165° E, 140° W and 110° W

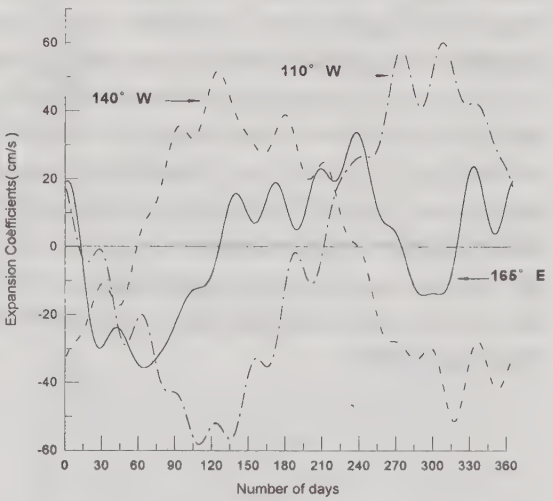

Fig. 6b Distribution of expansion coefficients corresponding to Fig. 6a

Analysis of the mean zonal wind stresses at the three equatorial observation sites indicates that, for the zonal wind stress harmonic component, the standing-wave type variations are the largest; the westward-propagating type variations, the secondary and the eastward-propagating type variations, the smallest. The magnitude of variation in the main modals of zonal current and thermocline has the same feature (Figs. 6b, 4b and 2b), which suggests that the disturbance of the surface zonal wind stress exerts major influence on the zonal current and thermocline component of the low-frequency planetary wave.

3.2 Action of the low-frequency planetary wave on the heat transmission in the upper equatorial ocean

Model research shows that, for seasonal cycle, the equatorial SST annual period harmonic variations are mainly driven by the wind stress while the air-sea interactions strongly affect the semi-annual period harmonic variations[16]. Observations indicate that during the non-ENSO, the marginal lines of the west Pacific warm pool and the east Pacific cold tongue move only within the fixed longitudinal range. Now we use the observed daily mean ocean temperature sequence and adopt the methods mentioned in section 2 to analyse the action of the equatorial Kelvin Wave, Rossby Wave and mixed-Rossby gravity wave on the zonal heat transmission in the upper equatorial ocean.

3.2.1 Zonal transmission structure of ocean temperature in the upper equatorial ocean

The equatorial station of 165° E is near the eastern edge of the western Equatorial Pacific warm

pool. The existence of the warm pool makes this sea area the one with the most active air-sea interaction in the equatorial Pacific. For the eastward-spreading ocean temperature structure, the subsurface temperature variations around the depth of 140 m are the greatest while those in the mixed layer shallower than 80 m are smaller; The equatorial station of 140° W shows the similar characteristics; The area in the equatorial station of 110° W with greater variations in ocean temperature appears near the depth of the thermocline (Fig. 7a). Therefore, the zonal heat transmission in the west Pacific warm pool is mainly manifested in the fact that the subsurface water (24℃ ～ 26℃) propagates eastwards along the thermocline and its phase velocity (1.46 m/s) is identical with the eastward-propagating velocity of the thmerocline disturbance. In the middle and western Pacific, the westward-propagating seasonal thermal structure variations mainly occur in the mixed layer (Fig. 8a) and the phase velocity is about 1.82 m/s (taking about 60 d to transmit from the station of 140° W to the station of 165° E). The seasonal thermal structure variations propagating in the form of standing waves mainly appear in the thermocline in western Equatorial Pacific, in the mixed layer and the thermocline in the middle Equatorial Pacific and in the mixed layer in eastern Equatorial Pacific.

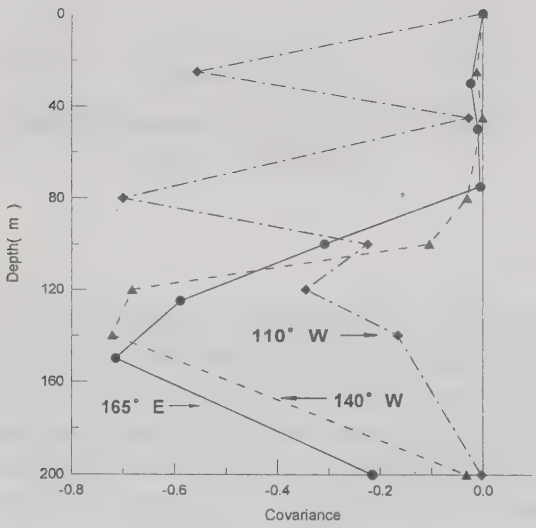

Fig. 7a Covariances of the main modals (82 %, 86 % and 66 %) of the ocean temperature eastward-propagating sequence at the equatorial station of 165° E, 140° W and 110° W

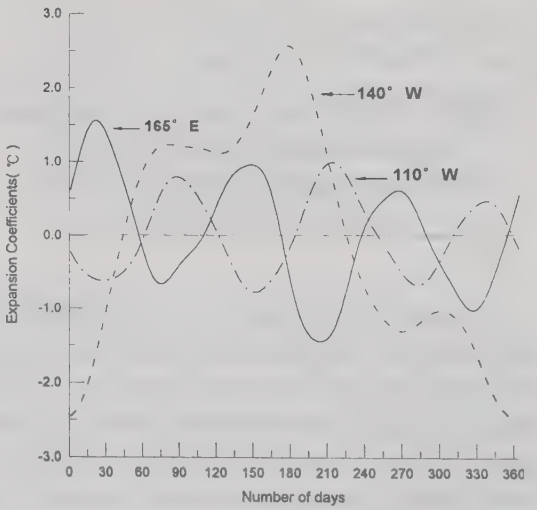

Fig. 7b Distribution of expansion coefficients corresponding to Fig. 7a

It can be seen from analysis of the expansion coefficients in the three forms of propagation that the zonal thermal transmission signals in the upper equatorial Pacific are stronger for the standing-wave and eastward-propagating types and weaker for the westward propagating type (Fig. 7b, 9b and 8b). Under the mean conditions, the standing-wave type variation intensity of ocean temperature in the upper equatorial Pacific is close to the eastward-propagating type, thus restricting the continuous eastward transmission of the western Pacific warm pool heat, and hence results in the normal seasonal

change form of the ocean temperature in the eastern Pacific. But, when the standing-wave type variations of ocean temperature weaken and the eastward-propagating ones intensify, the El Niño phenomenon would ensue.

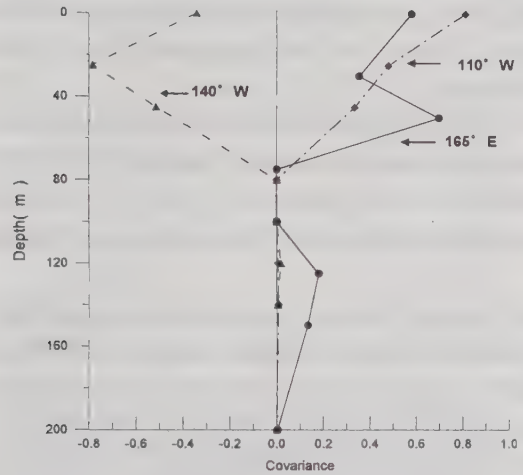

Fig. 8a Covariances of the main modals (49 %, 81 % and 58 %) of the ocean temperature westward -propagating sequence at the equatorial station of 165° E, 140° W and 110° W

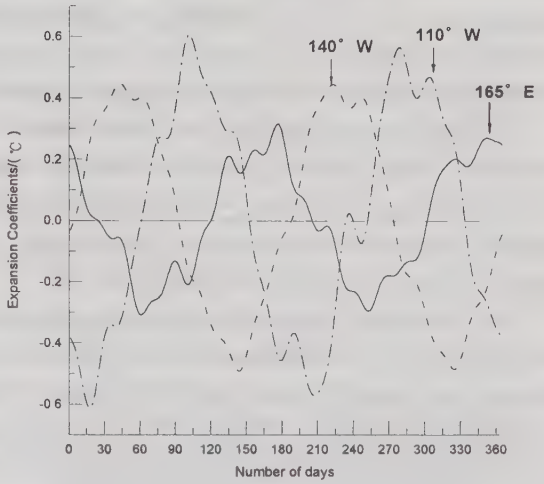

Fig. 8b Distribution of expansion coefficients corresponding to Fig. 8a

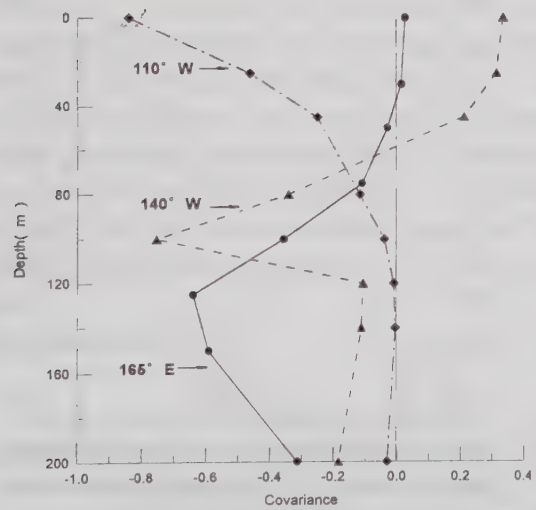

Fig. 9a Covariances of the main modals (56 %, 20 % and 72 %) of the ocean temperature standing-wave propagating sequence at the equatorial station of 165° E, 140° W and 110° W

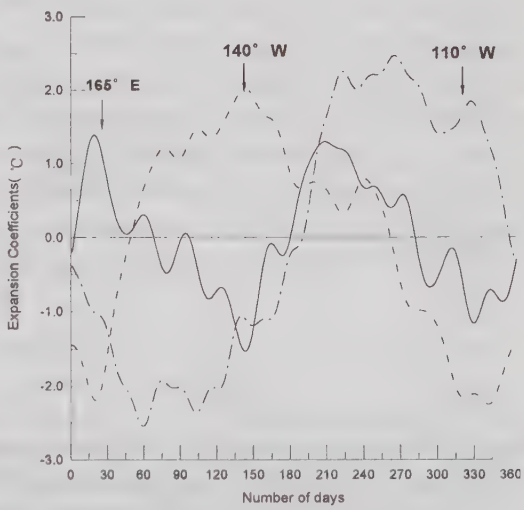

Fig. 9b Distribution of expansion coefficients corresponding to Fig. 9a

3.2.2 Action of the equatorial planetary wave on the zonal heat transmission in the upper ocean

As a result of the complexity of the actual natural condition, the motion effects of the three above-mentioned low-frequency planetary wave motion components (current velocity, pressure) are not obtained according to the prediction of theoretical model, and the transmission action of wave motion components on the ocean temperature are also different. Here, the analytical method of delayed cross-correlation coefficient is adopted to discuss the role of wave motion components in the ocean temperature zonal transmission in the upper equatorial ocean.

Delayed cross-correlation coefficient analysis is made respectively between the eastward and westward propagating zonal currents in the upper equatorial ocean at the eastern boundary (110° W) and the main modal expansion coefficients at the thermocline depth between 5° N and 5° S and the eastward and westward propagating main modal expansion coefficients of ocean temperature in the upper equatorial ocean at 165° E and 140° W.

The role of the eastward-propagating component (Kelvin Wave) of the thermocline disturbance in transmitting the ocean temperature in the upper equatorial ocean is obvious, especially in the heat transmission from the warm pool to the eastern Pacific (Fig. 10); while the role of its westward-propagating component (Rossby Wave) is mainly manifested in the middle and eastern Pacific (Fig. 11). The roles of the eastward-propagating and westward-propagating components of the upper zonal current in the equatorial ocean in transmitting the upper ocean temperature are both manifested in the western Pacific (Figs. 12 and 13), which is consistent with the research findings of Bonjean[17] by adopting the observation and model for the surface (15 m) zonal current and SST advection action within the range of 20° N ~ 20° S in the Pacific.

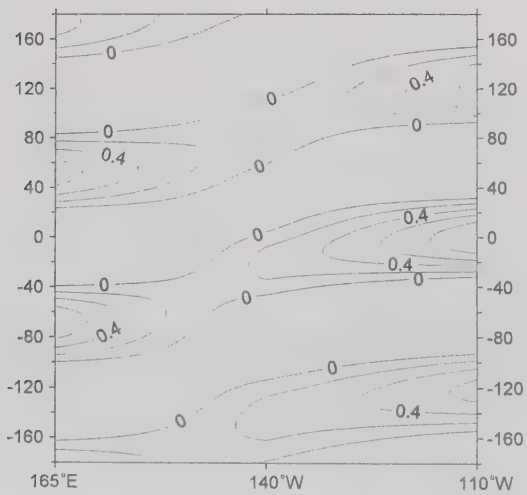

Fig. 10 Delayed cross-correlation coefficients between the thermocline eastward-propagating main model at 110° W and the internal ocean-temperature eastward-propagating main model at the 140° W, 165° E

(The negative values on the vertical coordinate donate the number of days for which the west side leads the east side and the positive values the same number of days for which the west side lags the east side. The same applies to the following three figures)

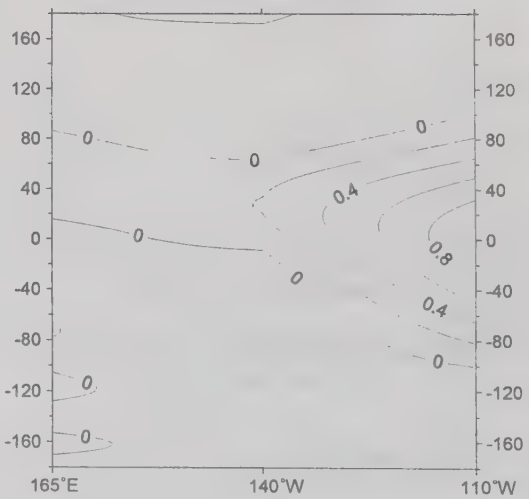

Fig. 11 Delayed cross-correlation coefficients between the westward-propagating main model of the thermocline at 110° W and the westward-propagating main modal of internal ocean temperature at the station of 140° W, 165° E

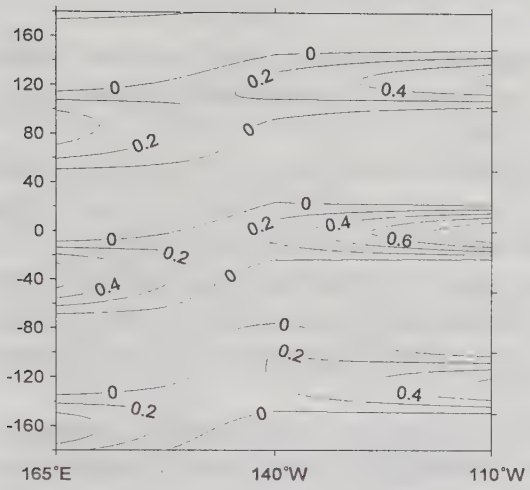

Fig. 12 Delayed cross-correlation coefficients between the eastward-propagating main modal of zonal current at 110° W and the eastward-propagating main modal of internal ocean temperature at 140° W, 165° E

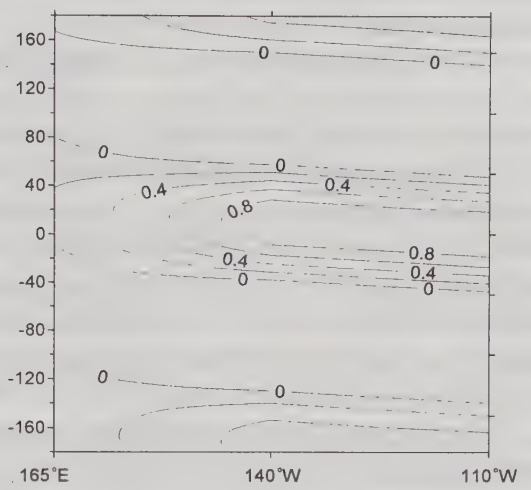

Fig. 13 Delayed cross-correlation coefficients between the westward-propagating main modal of zonal current at 110° W and the westward-propagating main modal of internal ocean temperature at 140° W, 165° E

Gill's research indicates that, under the adiabatic conditions, for the long-wave geostrophic disturbance, most energy exists in the potential energy, while for the short-wave geostrophic disturbance, the kinetic energy is dominant[8]. As far as the upper ocean of the equatorial Pacific is concerned, the eastward and westward transmission of ocean temperature is mainly through the transmission of the thermocline disturbance of Kelvin Wave and Rossby Wave. The role of the zonal current in transmitting the ocean temperature is mainly found in the western Pacific where the thermocline is deeper and thicker, while, in the middle and eastern Pacific, with the gradual shallowing of the thermocline, the vertical gradient of ocean temperature increases and the vertical convection would weaken the heat transmitting role of the zonal current. The role of the mixed-Rossby wave in standing-wave type motion in zonally tranmitting the ocean temperature in the upper equatorial ocean is mainly manifested in the variations of the equatorial zonal current (figure omitted).

4 Conclusion

Analysis of the mean seasonal variations of the long-term (5 ~ 15 years) observations (wind stress, ocean temperature and zonal current, *etc.*) from the TOGA-TAO buoy array indicates that:

(1) The equatorial Kelvin Wave pressure (thermocline disturbance) component propagates eastwards approximately at the phase velocity of the second baraclinic equatorial Kelvin Wave modal (1.46 m/s), and the eastward-propagating phase velocity of the upper equatorial zonal current more than doubles that of the pressure component. The westward-propagating phase velocity of the Rossby Wave pressure component (1.09 m/s) and the phase velocity of the mixed Rossby gravity zonal

current component between 165° E and 140° W (0.88 m/s) are close to that of the first baroclinic equatorial Rossby Wave modal (0.91 m/s).

(2) The eastward- and westward-propagating harmonic components of the equatorial Pacific zonal wind stress have the effect of accelerating the eastward- and westward-propagating phase velocities of the zonal current in the upper equatorial ocean.

(3) The zonal heat transmission of the western Equatorial Pacific warm pool is mainly manifested in the eastward-propagating of the subsurface water (24 ～ 26℃) along the thermocline, and its phase velocity is the same as the eastward-propagating phase velocity of the thermocline disturbance. In the middle and western Pacific, the westward-propagating seasonal thermal structure variations are mainly reflected in the mixed layer. The standing-wave type propagating seasonal thermal structure variations mainly occur in the thermocline in Western Pacific, in the mixed layer and the thermocline in the middle Pacific and in the mixed layer in Eastern Pacific.

(4) The standing-wave and eastward-propagating types of zonal heat transmission signals of ocean temperature in the upper equatorial Pacific are stronger while the westward-propagating type ones are weaker.

(5) The pressure component of the equatorial Kelvin Wave (thermocline disturbance) goes through the western and eastern equatorial Pacific and transmits eastwards the warm pool thermal energy; The heat transmission of the zonal component is mainly manifested in western Pacific while that of the Rossby Wave pressure (thermocline disturbance) mainly in the eastern and middle Pacific. The heat transmission action of zonal current excited by the mixed Rossby gravity wave is stronger than the corresponding thermocline disturbance. Under the mean conditions, the standing-wave type variations of ocean temperature in the upper equatorial Pacific restrict the persistent eastward transmission of the western Pacific warm pool heat, thus resulting in the normal seasonal variation form of ocean temperature in the equatorial Pacific. And when the standing-wave type variations of ocean temperature weaken, the El Niño phenomenon would ensue therefrom.

Acknowledgments

The authors were supported by "National Key Programme for Developing Basic Science" G1998040900 part 1. The first author was supported by the Key Laboratory of Lopso, SOA, China.

References

[1] Picaut J M, Ioualalen M, Menkes C *et al.* Mechanism of the zonal displacements of the Pacific warm pool, implication for ENSO. Science, 1996, 274: 1 486-1 489.

[2] Xu Riyu , McPhaden M J. Seasonal variability in the Equatorial Pacific. J. Phys. Oceanogy, 1999, 29(5): 925-947.

[3] MacPhden M J. Busalacchi A C, Cheney R *et al.* The Tropical Ocean-Global Atmosphere observing system: A decade of progress. J. Geophys. Res., 1998, 103(C7): 14 169-14 240.

[4] Johnson E S, McPhaden M J. Structure of intraseasonal Kelvin waves in the equatorial Pacific Ocean. J. Phys. Oceanogy, 1993, 23: 608-625.

[5] McPhaden M J, Taft B A. Dynamics of seasonal and intraseasonal variability in the eastern equatorial Pacific. J. Phys. Oceanogy, 1988, 18: 1 713-1 732.

[6] Enfield D B. The intraseasonal oscillation in eastern Pacific sea levels; How is it forced? J. Phys. Oceanogy, 1987, 17: 1 860-1 876.

[7] Spillane M C, Enfield D B. Allen Intraseasonal oscillations in sea level along the west coast of the Americas. J. Phys. Oceanogy, 1987, 17: 313-325.

[8] Gill A E. Atmosphere-Ocean Dynamics. Academic Press, Inc. LTD, London. 1982, 662pp.

[9] Busalacchi A J, O'Brine J J. Interannual Variability of the Equatorial Pacific in the 1960's. J. Geophys. Res., 1981, 86(C11): 10 901-10 907.

[10] Gent P R, Luyten J R. How much energy propagates vertically in the equatorial oceans? J. Phys. Oceanogy, 1985, 15: 997-1 007.

[11] Kessler W S, McCreary J P. The annual wind-driven Rossby wave in the subthermocline equatorial Pacific. J. Phys. Oceanogy, 1993, 23: 1 192-1 207.

[12] Philander S G H. Equatorial waves in the presence of the Equatorial Undercurrent. J. Phys. Oceanogy, 1979, 9: 254-262.

[13] Shi Qiang, Pu Shuzhen, Su Jie *et al.* Research on the main current system and equatorial planetary wave of the tropic Pacific under the climatic mean wind field action. Acta Oceanologica Sinica, 1999, 21(3): 40-50.

[14] Chiswell S M, Lukas R. Rossby-gravity waves in the central equatorial Pacific Ocean during the NORPAX Hawaii-to -Tahiti Shuttle experiment. J.Geophys.Res., 1989, 94(C2): 2 091-2 098.

[15] Ripa P, Hayes S P. Evidence for equatorial trapped waves at the Galapagos Islands. J. Geophys. Res., 1981, 86(C7): 6 509-6 516.

[16] Robertson A W, C.-C. Ma, Meohoso C R *et al.* Simulation of the Tropical Pacific Climate with a Coupled Ocean-Atmosphere General Circulation Model. Part I: The Seasonal Cycle. J. of Climate, 1995, 8(5): 1 199 -1216.

[17] Bonjean F. Influence of surface currents on the sea surface temperature in the tropical Pacific Ocean. J. Phys. Oceanogy, 2001, 31: 943-961.

Multi-beam Sonar and Side-scan Sonar Image Co-registering and Fusing

Yang Fanlin[1] (阳凡林), Liu Jingnan[2] (刘经南), Zhao Jianhu[1] (赵建虎)
1 *GPS Engineering Research Center, Wuhan University, Wuhan* 430079
2 *Presidential Secretariat, Wuhan University, Wuhan* 430079

Abstract Multi-beam Sonar and Side-scan Sonar compensate each other. In order to fully utilize all information, it is necessary to fuse two kinds of image and data. And the image co -registration is an important and complicated job before fusion. This paper suggests combining bathymetric data with intensity image, obtaining the characteristic points through the minimal angles of lines, and then deciding the corresponding image points by the maximal correlate coefficient in searching space. Finally, the second order polynomial is applied to the deformation model. After the images have been co-registered, Wavelet is used to fuse the images. It is shown that this algorithm can be used in the flat seafloor or the isotropic seabed. Verification is made in the paper with the observed data.

Keywords Multi-beam Sonar, Side-scan Sonar, Co-registering, Fusion

1 Introduction

Multi-beam Sonar (MES) can obtain high precision position and underwater depth in seafloor points. At the same time, it can also obtain low-resolution seabed images. According to MES, Side-scan Sonar (SSS) can only obtain low precision position and depth but high-resolution image. A new generation of SSS also can measure underwater height all over the area, but the precision is lower than MES[1, 2]. However, MES and SSS can compensate each other. If the digital information of MES and SSS can be fused, it has vital significance in explaining and exploring seabed[3]. In the 1990s, Rongxing Li *et al.* used the slope that was calculated by SSS to interpolate MES underwater depth data[4]. SIO combined 12 Hz Sea Beam with 12 Hz SeaMARC in a vessel to work at the same time in 1989[5].

Because images of MES and SSS are not measured from the same source, their deformations are also not the same. The latter is bigger than the former. So co-registration must be made before fusion. The early image co-registration method is to find the corresponding image points in two images by hand, but this is difficult and easily causes errors. Afterwards, some scholars invented automated methods. They usually utilize the image correlation coefficient. Firstly, the characteristic points are found through the interested arithmetic operators or other methods, and then the corresponding image points are confirmed by the maximal correlation coefficient in the local window. Finally, the deformed model coefficient is calculated with the corresponding image points before the image is resampled through co-registering[6]. Because of the different deformations in the two kinds of images, the correlation coefficient cannot be considered as a measure in co-registration. T. P. LE BAS *et al.* introduced "chamfer" algorithm to co-register MES and SSS images[7, 8]. They didn't consider the big

Received on March 2, 2003; accepted on March 15, 2003

area, so the global model was not inaccurate. Behrooz Kamgar-Parsi *et al.* suggested using the seabed contour to co-register images[9, 10]. The result was satisfactory, but these images were obtained from the same source, *i.e.* the cause of their deformation was the same. Sylvie Daniel *et al.* co-registered SSS image through the pairs of object shadows[11]. The method is only applicable to the slant range uncorrected SSS image. Zhuxun Zhang *et al.* proposed a full-automatic method for the co-registration of remote sensing imagery, and their method used probability relaxation theory and considered the total area[12, 13]. However, sonar imagery is different from the space remote-sensing imagery. The former does not have enough clear terrain points, so some co-registration methods in the remote-sensing imagery cannot be emloyed in the sonar imagery. This paper suggests combining bathymetric data with intensity image. It considers MES data as source image, and obtains the characteristic points through the minimal angles of lines, then decides the corresponding image points by the maximal correlation coefficient in searching space. Then the second order polynomial is applied to the deformation model. Finally the SSS images are resampled through the model.

At present, Wavelet analysis is usually used in the image fusion. It mainly uses Mallat algorithm and à trous algorithm. It replaces low frequency signal of high-resolution image with low frequency signal of low-resolution, and then reverses the combined frequency signal to time domain. So, the fused image is obtained. After the original images are fused, cross entropy is used to evaluate the result. It can show the difference between the resultant image and the original image. The smaller the difference is between the two images, the more the information is in the resultant image obtained from the original image[14].

2 Image preprocessing before co-registrating

SSS image is a slant range image. Because the projector of SSS is too close to the seabed, the objects in the image have some big geometrical deformations, including foreshortening and overlapping and vertex moving forward. In order to co-register images, the slant range image must be corrected to the flat range image through sound curve tracking. And these geometrical deformations must be eliminated. Though the MES image is also the slant range image, MES projector lies in the ocean surface. So its geometrical deformations are very small. When its slant range image is corrected, the used underwater depths of points are highly precise, so MES is considered as reference image and has no deformation.

There are some kinds of causations of deformations in the SSS image. Besides the slant range, there are the velocity change of tow fish, attitude change of the tow fish, unbalanced intensity, and the different scale in the acrosstrack and the alongtrack, *etc.* These deformations will distort the real seabed and cause errors in the interpretation of images. The position of tow fish can be calculated through the length of towline. If high precision is requested, it can be measured by the short baseline system. Some deformations can be corrected by the position and navigational information. If these informations are not recorded, they can also be evaluated. It is assumed that the seafloor is isotropic. Daniel *et al.* evaluated navigational information by using the intensity statistical method[15], but the precision cannot be higher than the measured value. Because the topic is not in correcting deformations, this paper doesn't go into details. Readers can find it from the paper[16~19].

Generally, the MES image has a lower resolution than the SSS image. In order to co-register, two images must have equal resolutions. This can be realized by interpolating the MES data. If the

difference of resolution is too big, it can reduce SSS data when interpolating the MES data.

3 Extracting the characteristic points

3.1 Extracting the characteristic points in seafloor contour

In order to automatically process data, the wrong contour lines produced by computer are not edited. The short lines that are shorter than the threshold value are removed so as to reduce errors. For every pixel in each contour line, the angle is determined by the pixel and the former pixel and latter pixel. In the grid image, there are only eight directions between two pixels. In order to have high accuracy, more pairs of pixels are needed to calculate the value. In Fig.1, five pairs of pixels are used to calculate the angle. The angle is

$$\alpha = \sum_{i=1}^{n} P_i \beta_i \tag{1}$$

$$P_i = \frac{1 / s_i}{\sum_{i=0}^{n} 1 / s_i} \tag{2}$$

n is the number of pairs of pixels. β_i is every angle of the i pair. s_i is the distance between the i pair of pixels and the central pixel o. i is 1…, n.

Fig. 1 The angles of all pairs of pixels

So, every contour can be represented by a set of angles. These angles can be considered as time sequence value, and the corresponding pixels of their minimal value in every segment are the characteristic points. In the same way, those big angles that are bigger than the threshold angle are removed so that errors can be reduced.

3.2 Extracting the characteristic points in seafloor image

Some traditional image processing methods are the first steps. These are edge segmenting, threshold segmenting and profile extracting. After these steps have been finished, image is made of some profile lines. Next step is the same as in the contour line.

4 Image co-registering

Firstly, those characteristic points in contour lines and profile lines are respectively superposed in MES data and SSS data; Secondly, within the scope of position error, the corresponding image points are determined through the correlated coefficient; Thirdly, the polynomial coefficients are calculated through the corresponding image points. Fourthly, the big errors in the corresponding image points are removed through big corrections, and then the model is recalculated; Finally, the SSS data are resampled by the model.

5 Image fusion and evaluation

Wavelet analysis is a good image fusion method. When the scale of resolution of two images is 1: 2, Binary Wavelet fusing can obtain a good result. If the scale is not 1:2, the result cannot be very good. Zhijun Wang presented a method that can divide any frequency space. This method can process under this situation and obtain a good result[20]. In my paper, the scale is 1:2 after the image is resampled, so Binary Wavelet fusing could be used. After images have fused, the cross entropy is used to evaluate the result. Its definition is

$$D(P,Q) = \sum_{i=1}^{n} p_i \ln(p_i / q_i) \tag{3}$$

where p_i and q_i are underwater height or intensity probability. It is assumed that D_1 denotes the cross entropy between the fusing image and the MES image, D_2 denotes the cross entropy between the fusing image and the SSS image. The average and RMS are

$$D_\alpha = (D_1 + D_2)/2 \tag{4}$$

$$D_\beta = \sqrt{(D_1^2 + D_2^2)/2} \tag{5}$$

D_α and D_β describe the total difference of the result and the two original images.

6 Data analysis

The following data are obtained from the offshore of the East China Sea. Sea Beam (MES) and SeaMARC (SSS) are used . Fig. 2 is the seafloor terrain obtained by MES, and Fig. 3 is the same area obtained by SSS. Fig. 4 is the intensity image obtained by MES, and Fig. 5 is the same image obtained by SSS. The maximal depth is 100.8 m, and the minimal depth is 27.3 m. The data have been interpolated and their resolution is equal. Every pixel represents 4 m in real seabed.

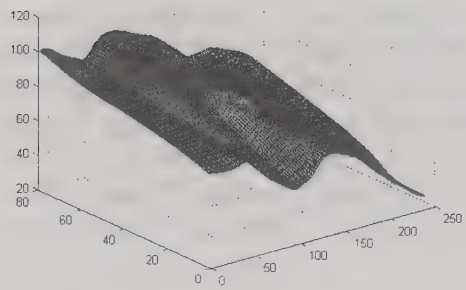

Fig. 2 The terrain measured by MES

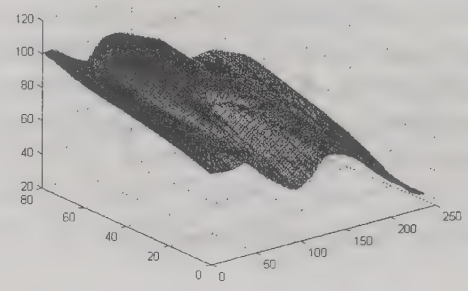

Fig. 3 The terrain measured by SSS

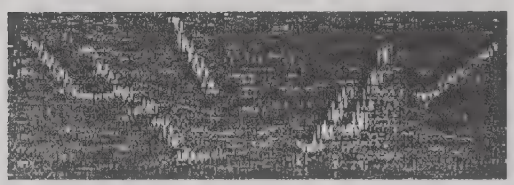

Fig. 4 The intensity measured by MES

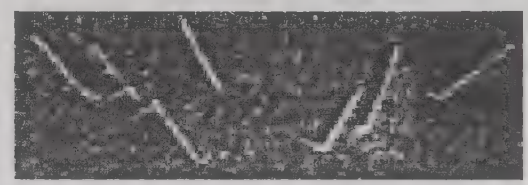

Fig. 5 The intensity measured by SSS

The contours are produced from Fig. 2 and Fig. 3, and then the characteristic points are extracted. When the points are extracted, the threshold value of angle is 150°. As shown in Fig. 6 and Fig. 7, "×"denotes the characteristic points.

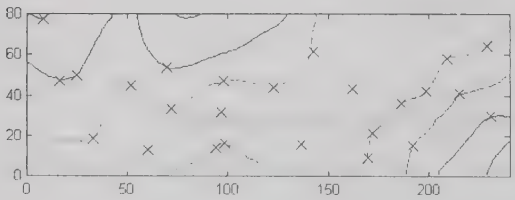

Fig. 6 The characteristic points in Figure 2

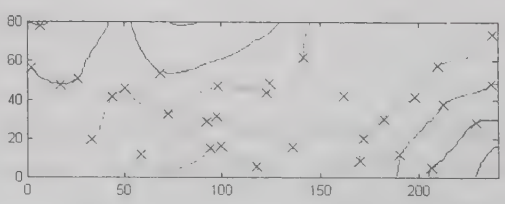

Fig. 7 The characteristic points in Figure 3

Sobel operator is used to segment edge in Fig. 4 and Fig. 5, and then profile lines are extracted. After the too short line segments are removed, the characteristic points are extracted with the same method. The length threshold is 10 pixels. Fig. 8 and Fig. 9 are the result of edge segmenting, and

Fig. 10 and Fig. 11 are the result of profile lines after removing shorter lines. Fig. 12 and Fig. 13 include the characteristic points.

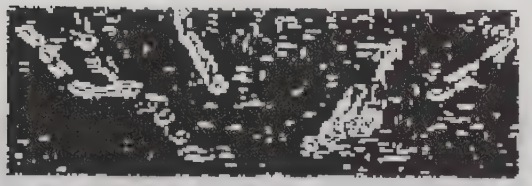

Fig. 8 The edge in Figure 4

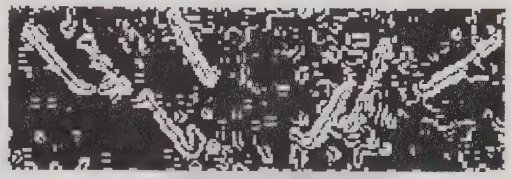

Fig. 9 The edge in Figure 5

Fig. 10 The profile in Figure 8

Fig. 11 The profile in Figure 9

Fig. 12 The characteristic points in Figure 10

Fig. 13 The characteristic points in Figure 11

In SSS data, the measured position error is considered as 20 m through the real operating situation. So the possible corresponding image points are determined by the 10 pixels by 10 pixels window. The measure in co-registering is the correlated coefficient. The searching window is 40 pixels by 40 pixels, and the maximal rotating angle is 10° . If the correlated coefficient is larger than 0.8, the two possible points are considered as the corresponding image points. Then some big errors are removed by using the least square method in the corresponding image points. After these have been finished, the polynomial coefficients are recalculated and RMS are calculated, too. Finally, the SSS data are resampled. In this work, RMS is 0.532, so it is highly accurate co-registration by this algorithm and the precision attains sub-pixel.

After co-registration has been finished, symlets Wavelet is used to fuse the images, as shown in Fig. 14 and Fig. 15. D_α is 0.184 and D_β is 0.296 in seabed terrain. D_α is 0.173 and D_β is

0.277 in intensity image. The cross entropy is small, so the result of fusion is satisfactory. Fig. 16 is the superposition diagram of seabed terrain and intensity image.

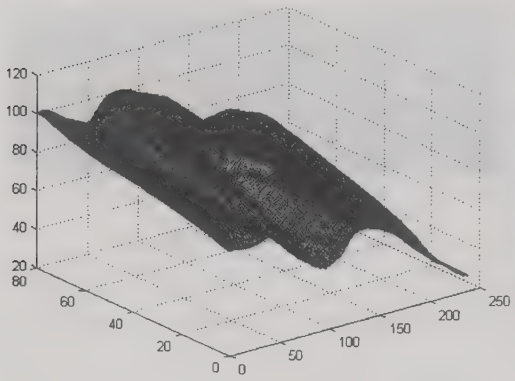

Fig. 14 The fusion terrain

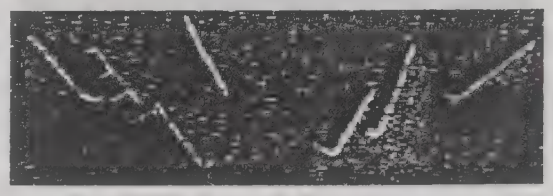

Fig. 15 The fusion intensity

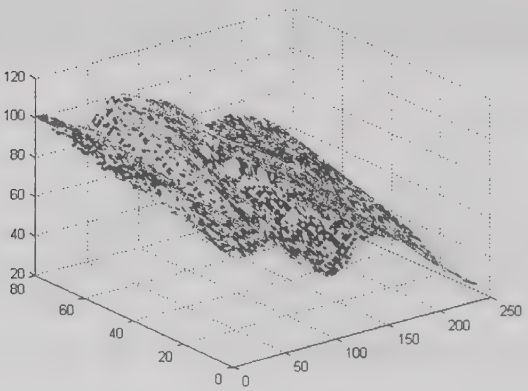

Fig. 16 Figure 14 plus Figure 15

7 Conclusions

Combining contour with intensity image in co-registration can fully utilize useful information and improve the precision. It can be used not only in the flat seafloor that has different intensities, but also in the isotropy seabed that has an uneven terrain. In some traditional SSS, it cannot measure underwater depth, but co-registration can be processed only through intensity image. Its precision may be debased in this situation.

References

[1] L-3 Communications SeaBeam Instruments. Multibeam Sonar Theory of Operation. http://doc.igm.bo.cnr.it/MBEAMS/ELAC_BOOK/thop_toc.pdf

[2] Pierre Cervenka *et al.* Postprocessing and Corrections of Bathymetry Derived from Sidescan Sonar Systems. IEEE JOURNAL OF OCEANIC ENGINEERING, 1994,19(4):619-629.

[3] Jianhu Zhao. Research on Multibeam Depth and Image. Wuhan University, 2002, 125-138.

[4] Rongxing Li *et al.* Improvement of Bathymetric Data Bases by Shape From Shading Technique Using Side-scan Sonar Images. Oceans '91, IEEE Conference Proceedings, 1991, 320-324.

[5] Christian de Moustier *et al.* Simultaneous Operation of the Sea Beam Multibeam Echo-sounder and the SeaMARC II Bathymetric Sidescan Sonar System. IEEE JOURNAL OF OCEANIC ENGINEERING, 1990, 15(2):84-94.

[6] Zhuxun Zhang, Jiangqing Zhang. Digital Photogrammetry. Wuhan: Wuhan University Press, 1997, 148-179.

[7] T P Le Bas. An Analytical Correlation and Comparison of High Resolution Side-Scan Sonar Imagery and Multi-beam Bathymetry. The Institute of Electric and Engineers, 1995, 6/1-6/7.

[8] T P Le BAS *et al.* Automatic Registration of TOBI Side-Scan Sonar and Multi-Beam Bathymetry Images for Improved Data Fusion. Marine Geophysical Researches, 1997, 19:163-176.

[9] Behrooz Kamgar-Parsi *et al.* Registration of Multiple Overlapping Range Images Scenes without Distinctive Features[C]. Oceans '89, IEEE Conference Proceedings, 1989, 282-290.

[10] Behrooz Kamgar-parsi *et al.* Toward an Automated System for a Correctly Registered Bathymetric Chart. IEEE JOURNAL OF OCEANIC ENGINEERING, 1989, 14(4):314-325.

[11] Sylvie Daniel *et al.* Side-scan Sonar Image Matching. IEEE JOURNAL OF OCEANIC ENGINEERING, 1998, 23(3):245-259.

[12] Zhuxun Zhang *et al.* Automatic Precision Registration of Multi-resolution Remote Sensing Imagery. Journal of Wuhan Technical University of Surveying and Mapping, 1998, 23(4):320-323.

[13] Mingsheng Liao. Study on Automatic Generation of Interferogram from INSAR Data. Wuhan University, 2000, 30-46.

[14] Yanmei Cui *et al.* Analysis and Evaluation of the Effect of Image Fusion Using Statistics Parameters. Journal of Beijing Institute of Technology, 2002, 20(1):102-106.

[15] Daniel, T Cobra. Estimation of Geometric Distortions in Side-scan Images. IEEE Proc., 1991, 927-934.

[16] Douglas D, Bergersen. A Synopsis of SeaMARC II Side-scan Processing Techniques. IEEE Proc., 1991, 921-926.

[17] Martin C Kleinrock. Overview of Sidescan Sonar Systems and Processing. IEEE Proc., 1991, 77-83.

[18] Pierre Cervenka, Christian de Moustier. Sidescan Sonar Image Processing Techniques. IEEE JOURNAL OF OCEANIC ENGINEERING, 1993, 18(2):108-122.

[19] Donna Johnson. Side Scan Sonar Imagery Analysis Techniques. Oceans '91, IEEE Conference Proceedings, 1991, 935-941.

[20] Zhijun Wang. Research on Wavelet Transforming in Remote Sensing Imagery. Wuhan University, 2000, 53-78.

A Study on Snowstorm Weather in Coastal Area of Western Antarctic

Huang Yaorong (黄耀荣), Xue Zhenhe (薛振和), Xu Cong (许　淙)
National Research Center for Marine Forecasts, Beijing 100081

Abstract In this paper, based on the observational data of 1995 in the Chinese Antarctic Great Wall Station the snowstorm is studied synoptically. It is found that there are two kinds of snowstorms with different physical characteristics and that the happening of snowstorm is always accompanied by a near-ground level inversion layer. The function of the inversion layer is analyzed, too. It is indicated that the strong ESE-wind type snowstorm is mainly caused by katabatic wind and gradient wind together. This idea is new and different from the general concept that there is no katabatic wind in the western Antarctic area.

Keywords Coastal area of west Antarctic, snowstorm weather, inversion layer

1 Introduction

There are different names for snowstorm in China and abroad, and it is called blowing snow in some countries and blizzard in some others; it is called surface drifting snow in Japan and "yanpao heavy snow" in the northeast area of China. In this paper it is called snowstorm in accordance with the definition of the National Meteorological Administration of China: heavy snow blown by strong wind, the horizontal visibility is from less than 1 000 meters to greater than 10 meters, and it is difficult to tell whether the snow is falling from the sky or is blown off the ground.

As early as in 1954, Arisofu[1] mentioned that there are blowing snow, snowstorm, snow tornado, snow spurt and snow quake in the Antarctic, but without details. Schwertfeger[2] mentioned that the statistics by Quinio (1956) shows that blowing-snow days take about one third to half of the total days in a year in Port Marting Station, Antarctica. Budd, Dingle and Radock[3] studied the amount and the transport of blowing snow in Bird Base. A study on the movement and the amount of blowing snow by katabatic was carried out in the Japan National Institute of Polar Researches [4]. A Chinese meteorologist, Zhou Xiuji[5], studied the interaction between Antarctic and global climate. However, those studies deal with neither the mechanism of the creation of snowstorm nor the snowstorm in the coastal area of western Antarctic. Snowstorm is the most common and catastrophic weather in western Antarctic during winter. It damages buildings, hampers sea and air traffic and even causes casualties. There are eight stations, an airstrip and some docks in King George Island. The Drake Passage to the north of the island is an important passage connecting the Pacific Ocean and the Atlantic Ocean. With more and more human activities in western Antarctic it will be necessary to study the forecast of the snowstorm. Based on the data from the Great Wall Station of China and the Bellingshauseng Station of Russia in the year 1995, the mechanism of the creation and extinction of snowstorm is analyzed to find some synoptic ways to forecast it.

Received on November 8, 2002; accepted on February 25, 2003

2 The intermonthly distribution of the snowstorm in the coastal area of western Antarctic

The Great Wall Station, a Chinese Antarctic research station, is situated at 62° 12′ S, 58° 57′ W in King George Island, in the north of the Antarctic Peninsula. As a year-round weather and marine station, the observatory of Great Wall Station is at seashore, 10 m above sea level, suitable for observation and research. Table 1 is the intermonthly distribution of snowstorms from December 1994 to November 1995.

Tab. 1 The intermonthly distribution of snowstorms from December 1994 to November 1995

	Jan	Feb	Mar	Apr	May	June	July	Aug	Sept	Oct	Nov	Dec	Total (day)
BS			3	1	4	3	3	8	10	2	3	0	37
SS				1	1	2	13	5	2	1		0	25

BS blowing snow, the visibility is less than 10 km.

SS snowstorm, the visibility is less than 1km.

It can be seen from the table that there is drifting snow from March to November, and the snowstorms occur from June to September. Since snowstorm is more harmful to mankind, its synoptic features are mainly discussed in this paper.

3 Classification of snowstorm weathers

It has been noticed that there are obviously two kinds of snowstorm weathers in the Great Wall Station, snowstorm with strong northwest wind and snowstorm with strong southeast wind. Table 2 shows the relations between the two kinds[2].

Tab. 2 The relation between snowstorm and wind field

WD	BWS			
	4~5 (5.5 ~ 10.7 m/s)	6 ~ 7 (10.8 ~ 17.1 m/s)	8 (17.2 ~ 20.7 m/s)	Total (day)
NNE		1		1
N		1		1
NNW	1			1
NW	1			1
WNW	1	1		2
SE		1		1
ESE	1	13	2	16
E	1	1		2
Total (day)	5	18	2	25

WD wind direction

BWS Beaufort wind scale

It can be seen from the table that there are two kinds of snowstorms in west Antarctic, the snowstorm with northerly wind and the snowstorm with southeast wind. The former occurs with a wider range of wind directions, lasts a shorter time (1 ～ 2 days), is weaker in strength and fewer in

number. The latter occurs mainly with southeast wind, lasts a longer time (3 ～ 4 days), is stronger (usually with wind of forces 6 ～ 7 on the Beaufort scale and two events of force 8 on the Beaufort scale) and greater in number (19 days in the year); therefore the southeast one is more outstanding.

4 Relations between snowstorm and temperature-humidity field

Table 3 shows the correlation between snowstorm and temperature. It can be seen from the table that all north-wind snowstorms occur when the temperature is above −0.5 ℃, and all south-wind snowstorms occur when the temperature is below −0.5℃. Figure 1 is the element-time profile at the Great Wall Station in July 1995.

Tab. 3 Correlation between the two types of snowstorms and the temperature

WD	T					
	≥0℃	0.1～−5.0℃	−5.1～−10.0℃	−10.0～−15.0℃	−15.0～−20.0℃	−20.0～−25.0℃
NNE		1				
N		1				
NNW	1					
NW		1				
WNW	1	1				
SE			1			
ESE			3	2	7	4
E			1	1		
Total (day)	2	4	5	3	7	4

T air temperature
WD wind direction

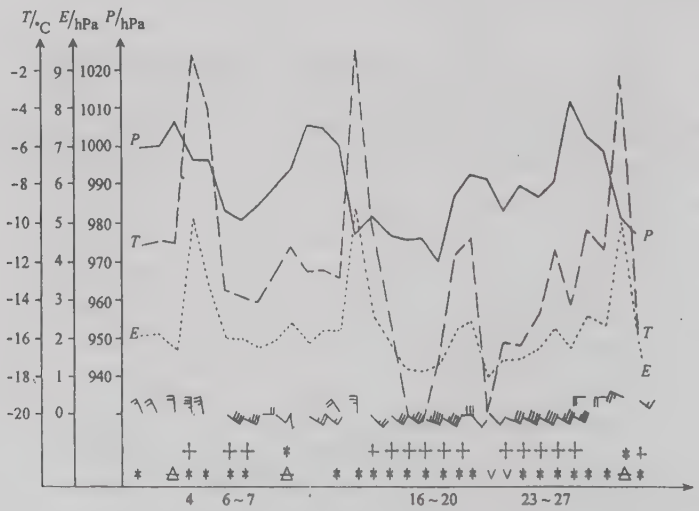

Fig. 1 The element-time profile (July 1st to 31st, 1995)

— pressure, --- air temperature, ··· vapor pressure, ¬ wind, * snow, △ snow grains, ∨ freezing rain, ⚑ blowing snow, ⚑ snowstorm

It can be seen from Figure 1 and Table 3 that the north-wind snowstorm occurs at the stage of high temperature and high humidity, while the south-wind one occurs at the stage of low temperature and low humidity; therefore they are totally different kinds of snowstorms. It has been noticed that the north-wind snowstorm is weak, the weather is calm often with heavy snow, and it is possible, though with some difficulty, to tell the snow fall from the blown snow. The south-wind snowstorm is much more severe with snowflakes blown by strong dry and cold wind, and it is impossible to tell whether there is snow fall or drifting snow.

5 The pressure field in which snowstorm occurs

Snowstorm is a large-scale weather phenomenon with close relations with pressure patterns in polar regions. Statistics show that the two kinds of snowstorms have different pressure patterns. The common characteristic of the north-wind snowstorms (6 events in a year) is the so called "high-east-low-west" pattern, *i.e.* there is a ridge of high to the north of Antarctic Peninsula stretching from the Atlantic subtropical area to Weddell Sea, while a low pressure or a cyclone area is to the west of Antarctic Peninsula and Weddell Sea; and the north-wind snowstorm occurs in the northerly flow in the high-gradient area between the high and the low. The common characteristic of the south-wind snowstorm (19 events in a year) is the "high-west-low-east" pattern or the high-southwest-low-northeast pattern, *i.e.* there is a high controlling the west and the south area of Antarctic Peninsula, and a low in the east and the north area of Antarctic Peninsula; and the southeast-wind snowstorm occurs in the southeast high-gradient area between the high and the low. To explain this in details there is an example as follows.

5.1 The pressure pattern of north-wind snowstorm (high-east-low-west type)

Figure 2 shows the synoptic situation of the snowstorm on July 4th, 1995. It can be seen from the figure that the center of the South Atlantic high is at 38° S and the southern part of the ridge extends as south as 65° S reaching Weddell Sea or the east of Antarctic Peninsula. The area to the west of to the Island Tierra de Fuego and Antarctic Peninsula is controlled by a frontal cyclone, the Great Wall Station is in the high-east-low-west situation and a rather strong high-temperature, high-humidity northerly flow.

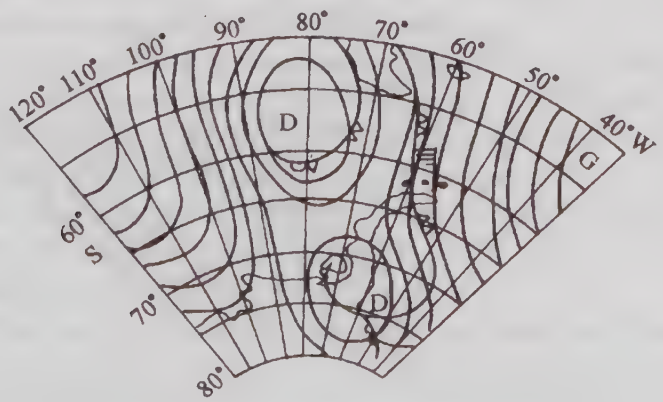

Fig. 2 Surface situation at 14:00 July 4th, 1995

5.2 The pressure pattern of southeast-wind snowstorm

There are two common types.

(1) In type one, or the high-west-low-east type, the high is to the west of Bellingshauseng Sea. As an example Figure 3 shows the synoptic situation of the southeast-wind snowstorm on July 19th, 1995. It can be seen from the figure that the area from the west to Bellingshauseng Sea to Amondson Sea is controlled by a high, which is due to the mergence of the polar high and the southeast Pacific subtropical high. A deep and wide frontal cyclone is to the northeast of Great Wall Station; and the station is in the strong high-west-low-east flow where the gradient is great.

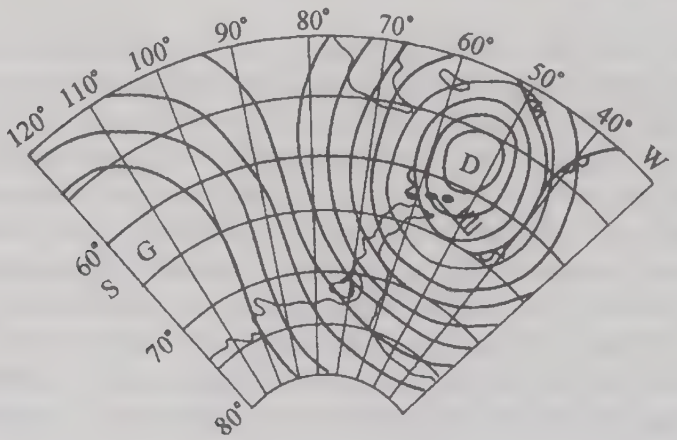

Fig. 3 Surface situation at 14:00 July 19th, 1995

(2) In type two, the high is at Antarctic Peninsula. Figure 4 shows an example of this type. It can be seen from the figure that a high is formed by the extension of the polar high and the southeast Pacific subtropical high; also there is a cyclone passing the Great Wall Station by the north of the station, which, therefore, is in the strong ESE flow.

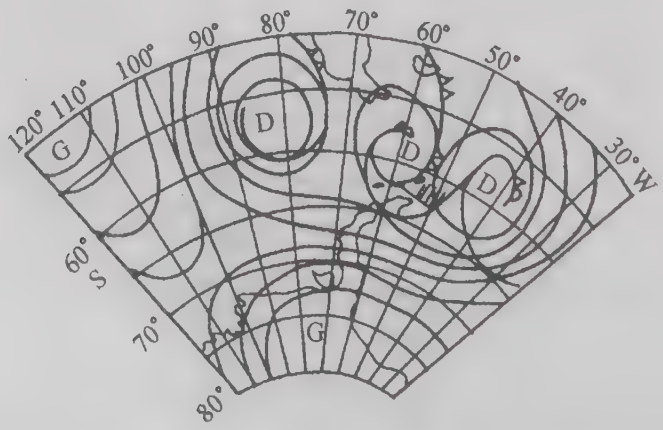

Fig. 4 Surface situation at 14:00 July 26th, 1995

(3) The common character of the two types is that there is extension of the polar high and the southeast Pacific subtropical high in Antarctic Peninsula and the west of it. And the Great Wall Station is in the SE or ESE flow, where the pressure gradient is great. There is some component of katabatic in the snowstorm, since the Antarctic sea ice extends northwards in the winter. The sea ice in Weddell Sea reaches 60° S or further in July, connecting King George Island and Antarctic Peninsula. The katabatic, which is caused by the cold Antarctic high and the slope of Antarctic plateau, can reach the Great Wall Station along Antarctic Peninsula. That makes the ESE wind stronger there (Figure 5).

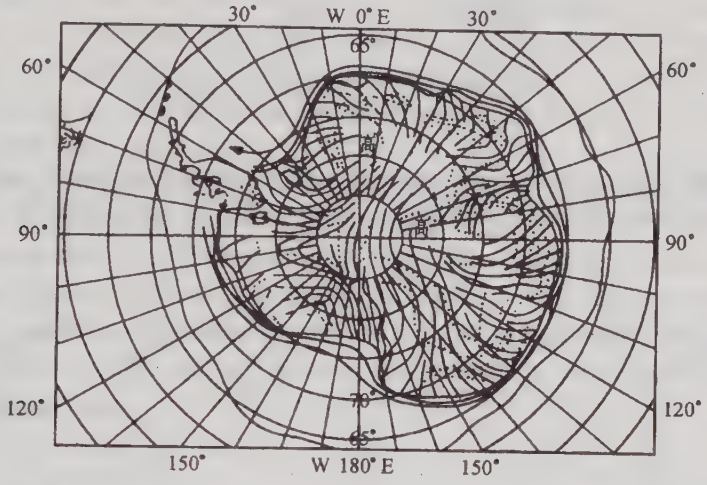

Fig. 5 Antarctic topography, surface stream field (Mather & Miler, 1967), average ice edge in July (Hjaka T, 1983). — isallohypse, → streamline, — the edge of ice

6 High-level stratification of snowstorm

Snowstorm is a catastrophic weather with strong wind, blown snow and thereby low visibility. It can be assumed that snowstorm has strong relation with high-level stratification. Our statistics have proved that. The following is the high-level stratification of the two types of snowstorm.

6.1 High-level stratification of north-wind snowstorm

As an example, the sounding curves of Bellingshausen Station (a Russian station 2 km away from the Great Wall Station) at 00:00 (UTC) July 3rd and 00:00 (UTC) July 4th, 1995 are given in Figure 6. It can be seen from the figure that the temperature lapse rate of the near-ground layer on July 3rd is normal, about 0.8 ℃ per 100 m, but when the snowstorm occurred on July 4th, an inversion layer formed at the near-ground layer (600 m), the temperature rose with the increase of height. When the snowstorm was over, the inversion layer disappeared.

6.2 High-level stratification of south-wind snowstorm

The snowstorm from July 23rd to July 27th, 1995 was an outstanding one of the south-wind type. The temperature lapse rate before the occurrence of the snowstorm, *i.e.*, on July 21st, 22nd, is 0.3 ℃ ~ 0.4 ℃ per 100 m. When the snowstorm occurred at 00:00 (UTC) 23rd July, there was an inversion layer below the height 600 m; its thickness increased to 1 000 m from 24th to 26th; the inversion layer

decreased to less than 200 m when the snowstorm was over on 28th; it disappeared on 29th (Figure 7). The data of July 27th are not available.

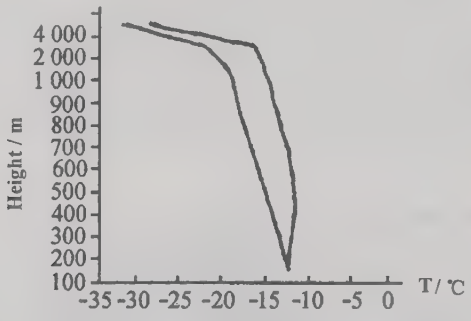

Fig. 6 The sounding curves of a north-wind type snowstorm from July 3rd to 4th 1995. The left is the curve of July 3rd , and the right is the curve of July 4th.

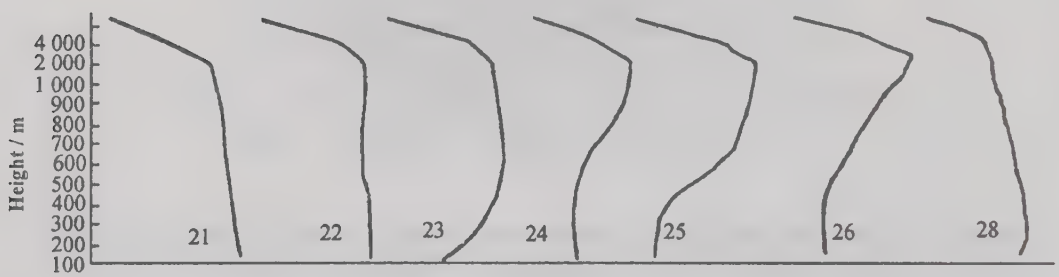

Fig. 7 The sounding curves of a southeast-wind type snowstorm from July 21st to 28th, 1995. From left to right are the curves of July 21st, 22nd, 23rd, 24th, 25th, 26th and 28th.

It can be inferred from the discussion above that a snowstorm is usually accompanied by a near-ground inversion layer. The inversion layer increases the stability of the atmosphere, and blocks the vertical exchange. It works to form and keep the snowstorm weather in the following two aspects.

(1) It restrains the vertical divergence of the kinetic energy in the near-ground layer, and keeps the near ground layer moving in a horizontal direction. It works as the wall of a tube, favorable for the increase of the wind force in the near-ground layer.

(2) It blocks the upward transport of the small snow granules, which are broken snowflakes by strong wind, keeps them in the near-ground layer and makes the visibility low. Therefore an inversion layer is favorable for the forming and the maintaining of a snowstorm weather. Statistics show that there is an inversion layer as long as there is a snowstorm.

7 Conclusions and discussion

The synoptic characteristics of the occurrence and extinction of snowstorm are discussed above in such aspects as stream field, temperature-humidity field, pressure field and high-level stratification.

Here are some conclusions.

(1) Snowstorm is the main catastrophic weather in west Antarctic during the winter.

(2) There are two types of snowstorm weather in west Antarctic, where the Great Wall Station is located, *i.e.*, the north-wind one and the southeast-wind one.

(3) The north-wind snowstorm is weak, lasts short (usually one day), occurs in fewer numbers. The southeast-wind snowstorm is strong, lasts long (usually $3 \sim 4$ days), and occurs in a greater number, hence the main type of snowstorm in west Antarctic.

(4) The north-wind snowstorm usually occurs during the high-temperature-humidity weather, while the southeast-wind snowstorm occurs during the low-temperature-humidity weather.

(5) The pressure field of the north-wind snowstorm is east-high (Weddell Sea is usually controlled by a high) west-low (Drake Passage and the west of it is a low pressure area). The pressure field of the southeast-wind snowstorm is west-high east-low or south-high north-low (*i.e.*, the period of the outbreak of the Antarctic high).

(6) It is interesting that there is always an inversion layer whether there is a north-wind snowstorm or a southeast-wind one. When the inversion layer disappears, the snowstorm is over. The inversion layer in the near-ground level blocks the vertical exchange of the air, favorable for the increase of the horizontal wind and the visibility; so it is an important factor for the forming and the maintaining of snowstorm. Further studies are expected to make sure if there is a certain relation between the snowstorm and the inversion layer. Because of the limited data, it may be assumed that there may exist some other types of snowstorms.

References

[1] Б.П. Альсов. Climatology Course. Beijing: Peoples Education Press. 1958, 552-564.

[2] Schwertfeger W. Weather and Climate of the Antarctic. Developments in Atmospheric Sci., 1984, 15.

[3] Budd W F, Dingle W R J, Radok U. The BYRD Snow Drift Project: Outline and Basic Results. Studies in Antarctic Meteorology, 1966, 71-134.

[4] Xie Simei, Fan Xiaoli. Antarctic Meteorology. Beijing: China Ocean Press. 1996.

[5] Zhou Qiuji, Lu Roonghua. The Study of the Interaction between Antarctic and Global Environment. Beijing: China Meteorology Press. 1996.

[6] Zheng Qinglin, Wang Yunheng. Numerical Study on Influence of Anomaly of Sea ice in the Weddell Sea on Seasonal Transition in East Asia during Early Summer. Acta Oceanologica Sinica, 1999, 21(2): 40-48.

[7] Be Shuzhen, Liao Qipe Study on Circumpolar Current and Fronts at Drake Passage. Acta Oceanologica Sinica, 1997, 19(3): 1-9.

Biochemical Mechanism of the Eutrophication and Its Prevention — the Deep Treatment of Waste Water and Its Denitrification and Dephosphorization

Li Hongshan (李红山), Li Songqiang (黎松强)
Jiaying University, Meizhou, Guangdong 514015

Abstract Biochemical mechanism of forming the red tide is discussed in this paper. The existence of a large number of nitrates and phosphates in the eutrophic water is the prerequisite of explosive increase of algae and the forming of red tide. Reduction of eutrophication is an important approach to preventing the red tide. The method of deep treatment of the waste water and its denitrification and dephosphorization are introduced, and a new opinion on the red tide formation and fundamental prevention is put forward.

Keywords red tide, eutrophication, biochemical mechanism, prevention

1 Introduction

Reason of the red tide fromation is comprehensive, involving chemical factors (eutrophication, proper structure of nutrition salts, *etc.*), biological factors (dynamic mechanism of biological species in red tide formation, competition between biological species, cultivated organisms, *etc.*), hydrologic factors (water temperature, water stability, *etc.*) and meteorological factors (air temperature, rainfall, wind, *etc.*). The frequency of red tide occurrence in our country recently is up rapidly, which is closely related to chemical factors. Eutrophication is the main reason of the red tide occurrence, due to the huge discharge into the sea of industrial and domestic sewage rich in nitrates and phosphates. Analyzing the mechanism of the eutrophication and researching the treatment method of sewage dischgarged into the sea in order to reduce the eutrophication, is an important approach to preventing the red tide.

2 Biochemical mechanism of eutrophication and the formation of red tide

2.1 Eutrophication and the red tide

Eutrophication is a eutrophic state of water when large amounts of industrial or domestic sewage rich in nitrates and phosphates ($N > 0.2 \sim 0.3$ mg/L, $P > 0.01 \sim 0.02$ mg/L) are poured into river, lake or sea. With proper biological, hydrologic and meteorological conditions, planktons such as algae in the eutrophic water reproduce explosively, covering huge area of water, blocking the contact of water with air, and thus resulting in the drop of dissolved oxygen in the water. With the metabolic death of algae, the process of microorganism decomposing the body of algae and other organic substance will also consume a lot of dissolved oxygen, and a huge area of water becomes anaerobic and putrid so that a disaster occurs. Sometimes the red tide becomes rather serious, thus attracting the global attention.

Received on August 12, 2002; accepted on December 5, 2002

The main reason of the red tide is eutrophication caused by the increase of such pollutant substance as nitrates and phosphates in the water. Especially when the content of phosphates (counted by PO_4^{3-}) exceeds 0.3 mg/L, the reproduction speed of algae will increase apparently. Estimation of water eutrophication is described in the following formula suggested by some scholar[1]:

$$IH = \frac{\text{oxygen consumption (mg/L)} \times \text{inorganic nitrogen}(\mu\text{g/L}) \times \text{inorganic phosphorus}(\mu\text{g/L})}{1\,500} \geqslant 1$$

If the measurement result is $IH \geqslant 1$, it shows that the content of nitrates and phosphates in the water reaches the eutrophication condition, and with sufficient sunshine and high temperature, the red tide is easy to occur. Thus a large amount of oxygen is consumed by algae metabolism, causing algae to die due to lack of oxygen. A lot of aquatic organisms also die in the anaerobic water and release a great deal of poisonous gas: H_2S, NH_3, PH_3, CH_4 and so on, and then the water quality becomes worse.

The red tide is a compreheasive result from the interaction of several factors: anaerobic water formed by huge discharge of industrial and domestic sewage into the water, metabolic products and nutrition of organisms, environmental conditions of nature.

2.2 Biochemical mechanism of algae formation

Algae are a big species of lower plants. Because of its tiny body, microscope is needed to see clearly its shape, so it belongs to the scope of microorganism. Most of algae are aquatic organisms existing in freshwater lakes or gulfs. Unicellular algae mainly live in the upper part of water, floating in the water, so it is also called phytoplankton. The algal that results in the red tide is mainly cryptothecodinium cohnii.

The composition of algae protoplasm is $C_{106}H_{263}O_{110}N_{16}P_1$, and except C, H and O, N and P are also included. So the main reason of the red tide occurrence is the water rich in nitrates and phosphates. The foramation mechanism of algae protoplasm is the photosynthesis of carbon, phosphates and nitrates under sunlight in the high temperature season[1]:

$$106CO_2+16NO_3^-+122H_2O+18H^++HPO_4^{2-} \underset{\text{respiratio}}{\overset{\text{photosynthesi}}{\rightleftharpoons}} C_{106}H_{263}O_{110}N_{16}P+138O_2 \quad (1)$$

From the formula above, we should know that a small amount of NO_3^-—N (7.1 g N) and phosphorus (1 g P) can produce a large amount of algae protoplasms (115 g). Due to the thermodynamic action, water is separated into different layers in the high temperature season, the upper layer is warm and has a low specific gravity while the lower layer is cold and has a high specific gravity. If the surface of water is polluted by organic pollutants rich in nitrates and phosphates, judging from the metabolic reaction of algae protoplasm (the reverse reaction of formation of algae protoplasm), decomposing a molecule of algae protoplasm will consume 138 molecules of oxygen. So, the oxygen consumption in algae metabolism is astonishing and the red tide occurs easily.

3 Biochemical mechanism of eutrophication prevention

Prevention of the red tide is still in the stage of research. The authors suggest that the fundamental and effective approach is the deep treatment of industrial and domestic sewage with

denitrification and dephosphorization. So the mechanism of denitrification and dephosphorization is emphatically discussed in this article.

Biochemical degradation treatment of organic waste water mainly includes two processes, *i.e.*, carbon oxidation of organic substances and ammonia oxidation. Carbon oxidation is a process in which aerobic heterotrophic bacteria reproduce in huge quantity with sufficient dissolved oxygen supplied by the aeration tank. Bacteria use organic substances as nutrition and degrade the organic substances in pollutants into small molecule such as CO_2, H_2O through metabolism. Nitrogenous compounds such as protein and fatty acid in organic pollutants are turned into ammonia and amine by ammonifying bacteria in the heterotrophic bacteria. Ammonia oxidation is also called nitrification, in which the ammonia released from protein and fatty acid through nitrification of aerobic autotrophic bacteria is oxidized into NO_2^- and NO_3^-. The denitrification and dephosphorization process is based on the biochemical degradation treatment.

3.1 Carbon oxidation of organic pollutant

During the hypoxia stage, macromolecular, structurally complex and insoluble organic pollutants are aerobic decomposed into small molecule such as organic acids:

hydrolysis of nitrogenous compounds (ammonifying)

$$\mathrm{R\text{-}CHCOOH\text{-}NH_2 + H_2O \xrightarrow{\text{hydrolase}} R\text{-}CH_2COOH + NH_3} \quad (2)$$

hydrolysis of organic substances

$$(C_6H_{10}O_5)_n + H_2O \xrightarrow{\text{hydrolase}} C_{12}H_{22}O_{11} + H_2O \xrightarrow{\text{hydrolase}}$$

$$C_6H_{12}O_6 \begin{cases} \xrightarrow{+O_2} CO_2 + H_2O \\ \xrightarrow{-O_2} \text{butanoic acid} + CO_2 + H_2 \end{cases} \quad (3)$$

hydrolysis of hydrocarbon

$$CH_3(CH_2)_n \cdot CH_2 \cdot CH_2 \cdot CH_3 \xrightarrow[\text{facultative bacteria}]{+H_2O} CH_3(CH_2)_nCOOH + CH_3COOH \quad (4)$$

hydrolysis of olefin hydrocarbon

$$CH_3(CH_2)_n \cdot CH{=}CH_2 \xrightarrow[\text{facultative bacteria}]{+H_2O} CH_3(CH_2)_{n-1}COOH + CH_3COOH \quad (5)$$

During the aerobic stage, through the reproduction of autotrophic bacteria in the aeration tank, NH_3-N is turned into NO_3^--N by nitrification; the small organic molecules produced from hydrolysis are oxidized into CO_2, H_2O, by the growth and reproduction of aerobic bacteria. From that, organic pollutants of COD, BOD, ArOH and oils are degraded. The biochemical process is expressed as follows:

organic acid produced from hydrolysis $CH_3(CH_2)_n COOH \xrightarrow[\text{aerobic bacteria}]{+O_2} n\,CO_2 + n\,H_2O$ (6)

and biochemical degradable organic substances

3.2 Denitrification with ammonia oxidation

3.2.1 Oxidation of organic nitride

Amines in almost all organic nitride chains such as amino-acid, nucleic acid, choline, uarea and so on are changed into NH_3 through decomposition by ammonifying bacteria. Ammonifying of microorganism includes: oxidation, reduction and hydrolysis.

$$RCHNH_2COOH+1/2O_2 \xrightarrow{\text{amino-acid deaminase}} RCOCOOH+NH_3 \quad (7)$$

$$(CH_3)_3NOH(CH_2)_2\,OH+5/2O_2 \xrightarrow[\text{phosphatide oxidation}]{\text{deamination through}} CH_3CH_2COOH+CH_3COOH+CO_2+H_2O+NH_3$$

choline (8)

$$CHN_2CNH_2CNHCNCH+H_2O \xrightarrow{\text{adenosine deaminase}} HOCN_2COHCNHCNCOH+NH_3$$

adenosine uric acid (9)

$$HOOCCH_2CHNH_2COOH \xrightarrow{\text{amino-acid reductase}} HOOCCH=CHCOOH+NH_3 \quad (10)$$

Due to the deamination of proteins and organic acids by microorganisms, not only are many poisonous organic substances degraded, but the toxicants accumulated from metabolism are migrated and converted. So the denitrification is an important step in the organic sewage treatment.

3.2.2 Nitrification of NH_3-N

Nitrogen element in organic pollutants is changed into ammonia in the ammonifying process. It exists in NH_3 and NH_4^+ in water, with a general designation as ammonia nitrogen, indicated as NH_3-N. But ammonia nitrogen is harmful to man and living things, so it must be oxidized into nitrate nitrogen.

It is suggested in the literature[1, 6] that microorganisms degrade NH_3 (with higher toxicity) in nitrification.

$$NH_3+O_2+H_2O \xrightarrow{\text{nitrifying bacteria}} NO_3^-+5H^+ \quad (11)$$

We suggest that the form of ammonia in the water depends on the pH value of water.

$$NH_3+H_2O \rightleftharpoons NH_4^+OH^-,\ K_b = 1.8\times10^{-5},\ so^{[2]}$$

$$\frac{[NH_4^+]}{[NH_3]}\cdot\frac{10^{-4}}{[H^+]} = K_b\text{, therefore:}$$

$$\lg\frac{[NH_3]}{[NH_4^+]} = pH-9.25 \qquad (12)$$

If pH = 9.25, then $[NH_3] = [NH_4^+]$, if pH = 7.25, then $[NH_4^+]/[NH_3] = 10^2$, $[NH_4^+] = 100\,[NH_3]$, the concentration of NH_4^+ is 100 times that of NH_3. It is apparent that ammonia mainly exists in NH_4^+ when pH = 7.25. So the oxidation of NH3-N should go as follows:

$$NH_4^+ + 2O_2 \xrightarrow{\text{nitrifying bacteria}} NO_3^- + H_2O + 2H^+ \qquad (13)$$

It is confirmed by the calculation of reaction enthalpy:

$$\Delta G^0_{\ r} = \Sigma\Delta G^0_{\ f\ resultants} - \Sigma G^0_{\ f\ reactants},$$

from (11): $\Delta G^0_{f(6)} = (\Delta G^0_{fNO_3^-} + 5\Delta G^0_{fH^+}) - (\Delta G^0_{fNH_3} + \Delta G^0_{fH_2O} + \Delta G^0_{fO_2})$

$= [-111.2 + 5\times0] - [-16.7 + (-237.2) + 0]$

$= +142.7\ (kJ/mol)$

from (13): $\Delta G^0_{f(13)} = [(\Delta G^0_{fNO_3^-} + \Delta G^0_{fH_2O}) + 2\Delta G^0_{fNH_3}] - [\Delta G^0_{fNH_3} + \Delta G^0_{fO_2}]$

$\Delta G^0_{r(13)} = [-111.2 + (-237.2) + 2\times0] - [79.3 + 0]$

$= -269.1\ (kJ/mol)$

The calculation shows that the reaction enthalpy in (11) is positive (+ 142.7 kJ/mol), indicating that the reaction can't go spontaneously from left to right. While the reaction enthalpy in (13) is negative (−269.1 kJ/mol) the reaction can go spontaneously from left to right (all data are from literature[2]). So during the process of ammonia nitrification, through the dissimilation of autotrophic bacteria, NH_4^+ is nitrified by microorganism with inorganic carbon (CO_2) as carbon resource.

$$NH_4^+ + 1/2O_2 + 2HCO_3^- \xrightarrow{\text{nitrite bacteria}} NO_2^- + H_2O + 2CO_2 \qquad (14)$$

$$NH_4^+ + O_2 + 2HCO_3^- \xrightarrow{\text{nitrite bacteria}} NO_3^- + H_2O + 2CO_2 + 4H^+ \qquad (15)$$

$$22NH_4^+ + 26O_2 + 4CO_2 + HCO_3^- + 2H_2O \longrightarrow \underset{\text{cellular protoplasm}}{C_5H_7O_2N} + 21NO_3^- + 4H^+ \qquad (16)$$

3.2.3 Denitrification of NO_2^- and NO_3^-

Nitric nitrogen is also harmful to human beings and living things. According to introduction of some material, the combined nitrogens such as NH_3, NO_3^- and NO_2^- reduce the combination ability of aquatic organisms' blood with oxygen, causing the hemoglobinopathy of infants[3, 4]. So the water which highly contains NH_3, NO_3^-, NO_2^- can't be drunk. But the biggest harm done by ammonia and nitric nitrogen is causing eutrophication and forming the red tide by leading to the excessive reproduction of algae. So it is necessary to change ammonia and nitric nitrogen into molecular nitrogen and finish the recycle of nitrogen element.

Biological denitrification includes two processes: one is metabolism of facultative bacteria, through which the organic substrates are dissimilated, NO_3^-, NO_2^- are converted to N_2 and nitrogen resource is supplied to microorganism; the other is assimilation from which the new protoplasm is formed simultaneously. As to organic substrates, methanol is used as carbon resource in several literatures[4].

$$6NO_3^- + 2CH_3OH \longrightarrow 6NO_2^- + 2CO_2 + 4H_2O \quad (17)$$

$$6NO_2^- + 3CH_3OH \longrightarrow 3N_2 + 3CO_2 + 3H_2O + 6OH^- \quad (18)$$

If this method is suitable for the treatment of chemical sewage from production of alcohol[5], for ordinary organic sewage, adding methanol as carbon resource will be unnecessary. Because during the denitrification process, not only can nitrate nitrogen be reduced, but can the organic substances which haven't been degraded in the secondary biolchemical treatment be decomposed further. So, instead of adding carbon resource, the outlet water from the secondary biochemical treatment can be drawn as carbon resource, and the reflux rate should be enhanced. As to the undecomposed COD organic substrates, they are substances not easy to be degraded such as fatty acids, naphthenic acids and phenols. So it is more close to the experimental fact that $C_nH_{2n}O_n$ is the organic substance as carbon resource.

$$2n\ NO_3^- + C_nH_{2n}O_n \xrightarrow{\text{denitrifying bacteria}} 2n\ NO_2^- + n\ CO_2 + n\ H_2O \quad (19)$$

$$2n\ NO_2^- + C_nH_{2n}O_n + n\ H_2O \xrightarrow{\text{denitrifying bacteria}} n\ N_2 + nCO_2 + 4n\ OH^- \quad (20)$$

The energy released can be used in the assimilation of denitrifying bacteria to produce the new protoplasm to fulfill the whole metabolism.

$$n\ NO_3^- + 4C_nH_{2n}O_n + n\ HCO_3^- + 14n\ H^+ \xrightarrow{\text{denitrifying bacteria}} n\ C_5H_7NO_2 + 8n\ H_2O \quad (21)$$

3.3 Dephosphorization

3.3.1 Hypoxic and aerobic dephosphorization

The most common existing forms of phosphorus are phosphide, phosphate and polyphosphate. Polyphosphate is gradually hydrolyzed into phosphate in the water, while phosphide is decomposed by bacteria to phosphate. Biochemical dephosphorization includes two stages.

During the hypoxic stage, organic substances are degraded by reproduction of facultative bacteria, while polyphosphorus bacteria absorb the hydrolyzed products such as methane acid, acetic acid, propionic acid and other acids as nutrition, and release stored phosphate in the form of PO_4^{3-}-P simultaneously in order to obtain energy.

During the aerobic stage, polyphosphorus bacteria oxidize and compose the organic substances stored in its body, release energy, absorb excessively PO_4^{3-}-P in water into its body, and store it in the form of polyphosphate[6~9]. So we can discharge it in the surplus sludge, and then obtain the goal of biochemical dephosphoritation.

3.3.2 Coagulation dephosphorization

At most 20 % ~ 30 % phosphorus can be removed by the primary and secondary biochemical treatment. Other methods should be applied to the full dephosphorization. Coagulation is an effective method, and polyaluminium and polyferrum are suitable coagulants. Coagulants can be added in some stage in sewage treatment: primary settling basin, bio-filter, aeration tank, or before the secondary sedimentation basin. But as to a certain sewage treatment factory, we can choose a certain stage to add the coagulant so as to obtain the best effect. The key factor is that, no matter in what stage the coagulant is added, the dephosphorization effect depends on the removal effect of biological floc and dispersed sediment.

Through the treatment of carbon oxidation and denitrification and dephosphorization of ammonia oxidation, the sewage rich in nitrates and phosphates will be turned into outgoing water that reaches the Chinese national standard about discharge water:

COD_{cr} < 100 mg/L; BOD_5 < 20 mg/L; NH_3-N < 15 mg/L; CN^- < 0.5 mg/L; Oil < 7 mg/L; ArOH < 0.3 mg/L; phosphate (counted by phosphorus) < 0.5 mg/L. The degradation rate of ammonia nitrogen can be more than 80 %. Therefore the quality of the discharged water would be better and the red tide would be prevented.

4 Conclusion

The eutrophication caused by excessively pouring sewage rich in nitrates and phosphates constitutes one of the conditions of the red tide formation, and results in disaster by breaking the ecological balance of sea through deteriotation of water. It is a fundamental method of the red tide prevention that the organic sewage rich in nitrates and phosphates be treated by biochemical denitrification and dephosphorization.

The sewage discharged into the sea can be treated quite well by the deep treatment of waste water. It is an effective approach to reducing eutrophication and preventing the red tide.

References

[1] Wang Jialing *et al.* Environmental Microbiology. Beijing: Higher Education Press, 1998, 170-171.

[2] Inorganic Chemistry Teaching and Research Section of Industral College of Dalian. Inorganic Chemistry. Beijing: People Education Press. 1982, 358-375.

[3] Gu Xiasheng. Mathematical Model of Sewage Biocogical Treatment. Beijing: QingHua University Press. 1993, 194-196.

[4] Gao Tingyao. Control Engineering of Water Pollution (the latter volume). Beijing: Higher Education Press. 1989, 262-265.

[5] Wu Xinping. Research of Ammonia Nitrogen Biological Degradation of Oil Refining Sewage. Oil Refining and Chemical Engineering, 1995, 26(9): 45-51.

[6] Alexarde Martin. Introduction to Siol Microbiology. 2nd ed, 1977, 102-105.

[7] Henze M *et al.* IAWPRC Task Group on Mathematical Modeling for Design and Operation of Biological Wastewater Treatment. London: IAWPRC Scientific and Technical Report No.1.

[8] Henze M *et al.* Activated Sludge Model No.2 IAWQ Task Group on Mathematical Modeling for Design and Operation of Biological Wastewater Treatment. London: IAWQ Scientific and Technical Report No.3,1995.

[9] Henze M *et al.* Wastewater Biological and Chemical Processes. Berlin: Springer Verlag, Second Edition, 1997.

Effect of Temperature on the Fatty Acid Composition of Four Species of Marine Microalgae

Li Wenquan (李文权), Li Qian (李 芊), Liao Qibin (廖启斌), Chen Qinghua (陈清花)
Department of Oceanograghy / Institute of Subtropical Oceanograpghy, Xiamen University, Xiamen 361005

Abstract The GC analysis of fatty acid of four species of marine microalgae cultured at different temperature shows that the temperature has distinct effects on the composition and unsaturated degree of fatty acid of microalgae. The percentages of TPUFA in TFA and the number of mean double-bond of fatty acids of *Isochrysis galbana*, *Dunaliella salina* and *Phaeodactylum tricornutum* decrease with the ascending temperature, while those of TMUFA and TSFA increase under the conditions of the present experiment. The content of TPUFA and the number of mean double-bonds of *Chlorella* sp. first decrease and then increase, with the minimum occurring at 20℃.

Keywords temperature, microalgae, fatty acids

For most aquacultured animals, the unsaturated fatty acids of marine microalgae have the effects of raising their rates of hatchability, survival and growth and the essential nutrients for the cultured animals such as fish and shrimp. Japanese and ROK scholars have reported that the algal powder added into the fish and shrimp bait may act as coagulating and anti-collapsing agents, and is especially effective if it is used in the water lacking minerals and vitamins[1]. Japanese scholars have prepared the bait for *Penaeus monodon* with EPA from marine algae and achieved very good results[2]. The composition and content of fatty acids of marine algae are affected to a large extent by environmental factors and, among the many environmental effects, temperature is a most important factor. The paper studies the effect of temperature on the composition and content of fatty acids of marine algea.

1 Materials and methods

1.1 Samples and reagents

The algal species selected for the experiment are *Phaeodactylum triconutum*, *Dunaliella salina*, *Chlorella* sp. and *Isochrysis galbana*. The culture solution is prepared with the F/2 formula, and the samples are cultured in the Model SPX-250 biochemical incubator with a photodarkening period of 12 h / 12 h. Three temperature groups of 12, 20 and 26 ℃ are set for *Isochrysis galbana*, *Dunaliella salina* and *Chlorella* sp. and four temperature groups of 8, 12, 16 and 20 ℃ for *Phaedactylum tricornutum*. Each microalgal is cultured for several days under different temperatures and the liquid algae are collected respectively when the exponential growth stage is reached. Two parallel samples are taken for each experimental temperature. The standard samples of fatty acid are purchased from the US SIGMA Co..

1.2 Hydrolysis of samples and preparation of fatty acid methylester

Take 50 m^3 experimental algal liquid (cell number: 1.2×10^5 ind./cm^3), place it in a drier after

Received on February 23, 2003; accepted on March 10, 2003

filtration to be dried and put it together with the filter membrane into a hydrolyzer with nut, add 0.3 cm^3 ortho-nonadecanoic acid internal standard solution (content: 0.2 mg/cm^3) and 2 cm^3 $CHCl_3$-CH_3OH mixed solution (volume ratio : 2 : 1), and seal the hydrolyzer after it has been filled with nitrogen gas for 1 min; ultrasonically extract for 30 min with the Model SCQ-250 ultrasonic cleaner (33 kHz, 250 W), remove the supernatant and repeat the procedure 3 ~ 4 times (The ultrasonic action time may be reduced to 10 min); Merge the extract liquids, add 2 mol/dm^3 HCl-CH_3OH solution after the liquids are condensed and dried up with nitrogen gas, and enclose the hydrolytic tube after it is filled with nitrogen gas. (To ensure good airtightness, first the polytetrafluoroethylene material may be used to seal up the tube mouth and then the nut is tightened.) Let the solution react in a 100 ℃ water bath for 40 min, extract twice after it cools down with 2 cm^3 n-hexane, merge the extract liquids in a centrifugal tube with plug and fill it with nitrogen gas to 20 ~ 50 mm^3 for chromatographic analysis.

1.3 Gas chromatographic analysis

The experiment uses the Model SP-3420 gas chromatograph (produced by the Beijing Analytical Instruments Plant) and the 30 m × 0.22 mm × 0.25 μm SE-54 elastic quartz capillary chromatographic column (Australia International Sales). The programmed hyperthermic treatment is carried out in four phases. For the first phase, the column temperature is 50 ℃ ~ 120 ℃ with a temperature rise rate of 20 ℃/min, and is kept constant at 120 ℃ for 1 min; For the second phase, the column temperature is 20 ℃ ~ 180 ℃ , with a temperature rise rate of 6 ℃/min, and kept constant at 180 ℃ for 1 min; For the third phase, the column temperature is 180 ℃ ~ 210 ℃, with a temperature rise rate of 6 ℃/min, and kept constant at 210 ℃ for 10 min; and for the fourth phase, the column temperature is 210 ℃ ~ 280 ℃, with a temperature rise rate of 3 ℃/min, and kept constant at 280 ℃ for5 min. The sampler temperature is 300 ℃; the FID temperature, 300 ℃; the carried gas, highly pure N_2; the column head temperature, 0.42 MPa, constant-current controlled; the flow of N_2, 30 cm^3/min; the air flow, 300 cm^3/m; the flow dividing ratio, 1 : 18; and the amount of sampling, 1 mm^3. The qualitative and quantitative gas chromatographic analyses of the fatty acid of marine algae are conducted according to Ref. [3].

2 Results and discussion

2.1 Effect of temperature on the growth rate of microalgae

The results of measurement are shown in Tables 1 and 2. The temperature conditions of the experiment are all within the range of preferential temperatures for the growth of experimental algal species. The constants of the microalgal growth rate increase with temperature. The optimum growth temperature for *Isochrysis galbana*, *Dunaliella salina* and *Chlorella* sp. is about 26 ℃ and that for *Phaeodactylum tricornutum* is about 16 ℃. The experimental results are consistent with those reported by Ref. [4].

2.2 Effect of temperature on the fatty acid composition of microalgae

It can be seen from Table 1 that with the increase of temperature, the percentage content of TPUFA, C18 : 3, EPA, DHA of *Isochrysis galbana* decreases while the percentage content of TMUFA, saturated fatty acid (C14 : 0, C16 : 0) and TSFA presents an increasing tendancy with temperature. The research findings of Fan Yunzhen *et al.* (1998) on *I. galbana* 3011 indicate that

Tab. 1 Fatty acid composition of *Isochrysis galbana*, *Dunaliella salina* and *Chlorella* sp. at different temperatures

Temperature (℃)	12			20			26		
Microalgae	*Isochrysis galbana*	*Dunaliella salina*	*Chlorella sp.*	*Isochrysis galbana*	*Dunaliella salina*	*Chlorella sp.*	*Isochrysis galbana*	*Dunaliella salina*	*Chlorella sp.*
C14 : 0	13.62	0.52	3.50	14.58	0.59	4.45	16.94	0.64	4.23
C15 : 0	0.30	0.20	0.32	0.30	0.40	0.41	0.21	0.40	0.38
C16 : 4	0.39	14.15	0.22	0.42	12.93	0.43	0.16	12.03	0.24
C16 : 3	0.31	1.79	0.95	0.27	1.91	0.36	0.13	1.44	0.10
C16 : 2	0.35	0.76	0.26	0.57	1.35	0.40	0.04	3.19	0.32
C16 : 1	2.51	3.63	18.80	3.05	3.09	20.15	3.43	1.84	17.84
C16 : 0	11.83	14.54	20.00	15.23	15.18	32.63	13.43	18.39	23.89
C18 : 4	15.97	3.38	0.33	12.12	2.56	0.10	15.48	1.89	0.19
C18 : 3	18.53	48.47	1.13	16.14	45.79	0.45	16.53	40.25	1.10
C18 : 2	5.46	5.33	3.86	5.32	8.68	3.41	4.12	10.13	3.72
C18 : 1	18.37	6.32	7.18	20.54	6.37	5.84	21.14	9.28	9.92
C18 : 0	1.18	0.91	0.49	1.10	1.13	1.05	0.87	0.51	0.67
C20 : 4	1.96	nd	6.81	0.70	nd	2.45	0.36	nd	5.74
C20 : 5	1.99	nd	33.93	1.51	nd	26.92	1.06	nd	30.74
C20 : 1	0.76	nd	1.29	1.95	nd	0.41	0.48	nd	0.24
C22 : 6	6.47	nd	0.92	6.21	nd	0.55	5.61	nd	0.68
TSFA	26.93	16.17	24.31	31.20	17.31	38.54	31.45	19.94	29.17
TMUFA	21.63	9.95	27.27	25.54	9.46	26.40	25.05	11.13	28.00
TPUFA	51.43	73.88	48.42	43.26	73.23	35.06	43.50	68.93	42.83
K (d^{-1})	0.063	0.086	0.048	0.114	0.110	0.068	0.158	0.128	0.101
MDB	2.12	2.43	2.46	1.84	2.53	1.86	1.86	2.19	2.22

Note: The percentage composition of fatty acids is counted by the content of total fatty acid; K is the constant of growth rate (d^{-1}), $K=(\ln N-\ln N_0)/T$, N_0 is the initial cell density of the algal liquid (ind./cm^3); N is the cell density of algal liquid at the time T (ind./cm^3); T is the experimental time (d); MDB= $\sum D_i \times \eta_i$ /100, D_i is the double bond number in the fatty acid molecule, η_i is the percentage of a certain fatty acid molecule in the total fatty acid. nd means "not detected".

Tab. 2 Fatty acid composition of *Phaeodactylum tricornutum* at different temperatures

Temperature (℃)	8	12	16	20
C14 : 0	6.03	7.10	7.50	9.16
C15 : 0	0.26	0.29	0.27	0.40
C16 : 4	6.45	6.33	3.08	2.77
C16 : 3	8.22	6.08	5.19	4.83
C16 : 2	8.52	9.41	9.16	7.33
C16 : 1	14.17	16.41	23.86	28.84
C16 : 0	12.70	13.27	14.20	14.15
C18 : 4	1.54	1.22	0.88	0.46
C18 : 3	1.30	1.25	1.34	1.49
C18 : 2	2.97	2.53	2.66	2.54
C18 : 1	3.61	5.07	5.56	8.68
C18 : 0	0.53	0.61	0.59	0.79
C20 : 4	1.78	1.25	0.77	0.80
C20 : 5	28.86	27.24	22.87	18.00
C20 : 1	0.31	0.26	1.00	0.73
C22 : 6	2.73	1.69	1.06	0.89
TSFA	19.53	21.27	22.56	22.62
TMUFA	18.09	21.74	30.42	38.25
TPUFA	62.38	56.99	47.01	39.13
K (d^{-1})	0.069	0.076	0.089	0.082
MDB	2.69	2.49	2.13	1.89

Note: The percentage composition of fatty acid is counted by the content of total fatty acid.

with the rise of the culture temperature, its proportion of the total fat and DHA in the total fatty acid tends to drop[5]. Observations made by Grima *et al.* (1993) show that when *I. galbana* is cultured at 15 ℃, the percentage composition of the polyunsaturated fatty acids such as EPA, DHA in its body is the maximum and begins to drop remarkably when the temperature rises to 20 ℃[6]. These research reports are consistent with the results of this experiment.

With the increase of temperature, TPUFA and C18 : 3 of *Dunaliella salina* somewhat drop and the percentage content of TMUFA increases slightly while the percentage contents of TSFA, C14 : 0 and C16 : 0 increase with temperature. Temperature has greater effect upon the composition of fatty acids of *Phaeodactylum tricornutum*. With the rise of temperature, the percentage contents of TPUFA, EPA and DHA drop, and TMUFA, TSFA, C14 : 0 and C16 : 0 increase while the percentage content of C18 : 3 shows little change. As compared with the aforementioned three microalgae, the change pattern of the percentage composition of fatty acid in *Chlorella* sp. is obviously different, and the percentage contents of TPUFA of *Isochrysis galbana*, *Dunaliella salina* and *Phaeodactylum tricornutum* tend to decrease with rise of temperature; The percentage contents of TPUFA, TMUFA, EPA, DHA and C18 : 3 in the body of *Chlorella* sp. first drop and then rise with the increase of temperature, with the minimum value occurring at 20℃; while those of TSFA, C14 : 0 and C16 : 0 show an opposite change tendancy, *i.e.*, first rise and then drop with the increase of temperature, with the maximum value at 20℃.

The change in the unsaturated degree of fatty acids of microalgae is manifested in the fact that the percentage contents of polyunsaturated fatty acids drop with the rise of temperature while the saturated fatty acids and the mono-unsaturated fatty acids rise with temperature. Besides, the number of mean double-bond of fatty acids is also a parameter reflecting the degree of unsaturation of fatty acids of microalgae. From the data of the number of mean double-bond of four fatty acids of microalgal in Tables 1 and 2, we can easily find that the rise of the unsaturated degree of the four microalgae fatty acids with temperature exhibit different change patterns: That for *Isochrysis galbana*, *Dunaliella salina* and *Phaeodactylum tricornutum* rises with temperature and the MDB value and the percentage content somewhat drop; while those of *Chlorella* sp. first decrease and then increase. The general trend is: with the decrease of temperature, the degree of unsaturation of microalgal fatty acids increases, the percentage content of TPUFA increases, the percentage contents of EPA and DHA rise obviously and the percentage content of C18 : 3 in both *Isochrysis galbana* and *Dunaliella salina* also increases. This is in consistency with the phenomenon observed in the higher plants and other organisms. Patternson (1970) found that, for *Chlorella sorlkiniana* growing at 22 ℃, the degree of unsaturation of its fatty acid is much higher than that for the cells growing at 30 ℃[7]. Lynch and Thompson (1982) reported that the degree of unasturation of fatty acid in the particle body phospholipid of the chloroplast of *Dunaliella salina* in lower temperature is higher than that in higher temperature [8]. Yang Qingxiao has measured the fatty acid composition of the microalga *Ochrosphaera cricosphaera*, suggesting that the maximum value of DHA percentage content occurs at 15℃, and when the temperature rises to 20℃ , the DHA percentage content drops dramatically and again rises slightly at 23 ℃ while the saturated fatty acid C14 : 0 emerges as the minimum at 25 ℃, the maximum at 20 ℃ and again drops slightly at 23 ℃[9]. The drop of temperature and the rise of degree of unsaturation may increase the flowability of cell membrane lipid, which is the physiological need of the organism itself so as to maintain its normal physiological functions, thus improving its tolerance to low temperature. With the rise of temperature, the rate of metabolism in the consumption

of unsaturated fatty acid would increase and the relative content of polyunsaturated fatty acid within its cells is lower. Therefore, in the culture of microalgal baits for aquaculture, it is necessary, as appropriate, to control the temperature so as to raise the content of unsaturated fatty acid in the microalgae.

3 Concluding remarks

Temperature is one of the most important factors in the growth of marine organisms. The effects of temperature on the composition of fatty acids and their degree of unsaturation in different microalgae vary greatly. Under the conditions of the present experiment, with the rise of temperature, the percentage content of TPUFA in *Isochrysis galbana* drops while the percentage contents of TMUFA and TSFA increase; in *Dunaliella salina*, the percentage content of TPUFA decreases, that of TMUFA slightly increases and that of TSFA increases; The change in the content of unsaturated fatty acids in *Phaeodactylum tricornutum* is greater. With the rise of temperature, the percentage content of TPUFA decreases significantly and the percentage content increases of TMUFA and TSFA are more obvious. The number of mean double-bond (MDB) of fatty acids of *Isochrysis galbana*, *Dun aliella salina* and *Phaeodactylum tricornutum* decreases with the ascending temperatures while the percentage content of TPUFA and TMUFA and the number of mean double-bond of *Chlorella* sp. first decrease and then increase, with the minimum occurring at around 20℃. The percentage content of TSFA, on the contrary, first increases and then decreases.

References

[1] Jin Jun and Lin Meijiao. Utilization and Processing of Marine Algae. Beijing: Beijing Science Press, 1993, 301-306.

[2] Yu Fucai. A Brief Account of the Research on Biologically Active Matter in Marine Animals and Plants. Marine Science, 1994, 18(4): 20-22.

[3] Cai Agen, Zheng Airong, Li wenquan *et al.* Gas Chromatographic Analysis of Marine Algal Fatty Acids. Ocean Technology, 1998, 17(4): 64-68.

[4] Liang Ying, Sun Shichun and Wei Jiangong. Bait Culture Technologies for Marine Organisms. Qingdao: Ocean University of Qingdao Publishing House, 1998, 16-29.

[5] Fan Yunzhen, Liu Fayi, Li Hefang *et al.* Research on Highly Unsaturated Fatty Acids in Marine Microalgae Ⅱ. Effect of Environmental Factors on the Content of the Highly Unsaturated Fatty Acid in *Isochrysis galbana* 3011. Collected Papers of Marine Science, 1998, (40): 155-160.

[6] Grima M E, Perez S J A, Camacho G F *et al.* N-3 PUFA Productivity in Chemostat Cultures of Microalgae. Appl Microbiol Biotechnol, 1993, 38(5): 599-605.

[7] Patterson G W. Effect of Culture Temperature on Fatty Acid Composition of *Chlorella sorlkiniana.* Lipids, 1970, 5(3): 597-600.

[8] Lynch D V, Thompson G A J. Low Temperature-induced Alterations in the Chloroplast and Microsomal Membranes of *Dunaliella salina.* Plant Physiol, 1982, 69(6): 1 369-1 375.

[9] Yang Qingxiao. Effect of Temperature on the Fatty Acid Composition in Some Phytoplankton. Oceanologia et Limnologia Sinica, 1988, 19(5): 439-446.

Reanalysis of the Atmospheric Flux of Nutrient Elements to the Southern Yellow Sea and the East China Sea

Wan Xiaofang (万小芳), Wu Zengmao (吴增茂), Chang Zhiqing (常志清)
Institute of Physical Oceanography, Ocean University of China, Qingdao 266003

Abstract Based on the recent research results on dry and wet deposition of nutrient elements and sulphate, we estimate the atmospheric flux of nutrient elements and sulphate to the southern Yellow Sea and the East China Sea in each season. The results suggest that the concentrations of nutrient elements and sulphate in aerosol and precipitation show an apparent seasonal cycle with the maximum values in winter and the minimum values in summer. Depositions of nitrate and sulphate are dominated by wet deposition, while the deposition for phosphate is mainly dry deposition. Moreover, compared with the riverine inputs, the atmospheric deposition may be the main source of dissolved inorganic nutrients in the southern Yellow Sea and the East China Sea.

Keywords the southern Yellow Sea, the East China Sea, nutrient elements, atmospheric flux

1 Introduction

The chemical material flux from atmosphere to ocean plays an important role in biogeochemical cycling, and the view on atmospheric deposition as an important source of nutrients, particularly to oligotrophic oceans, is received widely now. Previous works have suggested that in certain oceanic region biological productivity may be influenced by direct input of inorganic nutrients from atmospheric deposition[1, 2]. Eutrophication related to the land drainages and atmospheric deposition of nutrients in the marginal sea is believed to be the major cause of frequent toxic plankton blooms (red tide). Moreover, the impact of atmospheric deposition of nutrients on new productivity in the central waters of the Yellow Sea was also studied[3, 4].

However, there still lacks a whole knowledge of the atmospheric deposition in the Yellow Sea and the East China Sea for the data limit to date. In China, a National Basic Key Research Program entitled Ecosystem Dynamics and Sustainable Utilization of Living Resources in the East China Sea and the Yellow Sea is performed. Therefore, it is necessary to deeply analyze the flux of nutrient elements via atmosphere to ocean. Based on the recent studies on dry and wet deposition, and the field survey data (2000—2001) in Shenshi provided by Prof. Zhang Jing, we estimate the atmospheric flux of nutrient elements and sulphate in each season. Special interest is focused on the southern Yellow Sea and the East China Sea because of the data limitation and the emphasis of our ecosystem study.

2 Estimation of atmospheric flux of nutrients in each season

2.1 Estimation of dry deposition flux

The dry deposition velocity of particles depends on many factors, such as the size of particles,

Received on December 20, 2002; accepted on April, 10, 2003

wind speed, relative humidity and the stability of the surface layer atmosphere. So there exist a lot of difficulties to estimate the dry deposition velocity accurately. In this paper, we would take the dry deposition velocity of nutrient elements as 2.0 cm/s according to the research results[5~7]. As to sulphate, its dry deposition velocities of 0.224 cm/s, 0.226 cm/s, 0.237 cm/s and 0.228 cm/s are chosen, respectively, for spring, summer, autumn and winter, given by Mao Jietai[8].

Concentrations of aerosols in each season, which are shown in Table 1, are estimated by weighted average of data from representative stations. Silicate aerosol isn't taken into account here, since silicate concentration observed in aerosol is too low in the northeastern China[9] and the Yellow Sea[10]. Cheju Island (33° 17′ N, 126° 10′ E)[11~13] is taken as the representative station in the southern Yellow Sea, but for lack of information on phosphate aerosol, we have to estimate its concentration using observation data from its vicinity. The concentration of phosphate in aerosol is about 0.06 μg/m^3 over Xiamen area[14], and about 0.307 μg/m^3 in the northeastern China[9]. Estimated is the phosphate concentration in the southern Yellow Sea in each season with weighted average according to the transport distance by prevailing wind. In contrast, studies on aerosol concentration in the East China Sea are focused on the joint region with the Kuroshio[15]. The ammonium concentration is also obtained by weighted average of data over Tsushima area[16], Xiamen Sea[17] and north of the South China Sea[18].

Tab. 1 Average concentrations (μg/m^3) and dry deposition fluxes (mg • m^{-2} • month^{-1}) (the values under the oblique line) of nutrient elements and sulphate in the southern Yellow Sea and the East China Sea in different seasons

Sea areas	Season	NO_3^-	NH_4^+	PO_4^{3-}	SO_4^{2-}	Reference
The Southern Yellow Sea	Spring	1.54 / 79.8	1.37 / 71.0	0.0681 / 3.53	7.63 / 44.3	Carmichael *et al.* (1997), (1996); Kim *et al.* (1998)
	Summer	0.82 / 42.5	1.17 / 60.7	0.0519 / 2.69	6.33 / 37.1	
	Autumn	1.01 / 52.4	1.34 / 69.5	0.0938 / 4.85	6.56 / 40.3	
	Winter	1.19 / 61.7	1.06 / 55.0	0.1133 / 5.87	6.15 / 36.4	
	Average	1.14 / 59.1	1.24 / 64.3	0.0818 / 4.24	6.68 / 39.5	
The East China Sea	Spring	0.11 / 5.7	1.79 / 92.6	0.0377 / 1.95	2.70 / 15.7	Chen Liqi *et al.* (1992), (1993); Wakamatsu *et al.* (1996); Wu Dui (1995)
	Summer	0.16 / 8.3	1.11 / 57.3	0.0287 / 1.49	3.70 / 21.7	
	Autumn	0.10 / 5.2	1.57 / 81.2	0.0518 / 2.68	3.10 / 19.0	
	Winter	0.20 / 10.4	1.90 / 98.5	0.0626 / 3.25	4.70 / 27.8	
	Average	0.14 / 7.3	1.59 / 82.5	0.0452 / 2.34	3.55 / 21.0	

As is found in Table 1, all substances in this region show a similar seasonal cycle. Basically, the concentration is highest in spring and lowest in summer in the southern Yellow sea. Distinguished seasonal variability of nutrients and sulphate in this region is due to its characteristic geological position, which, as is known, is under the control of the eastern Asian monsoon. In late winter the prevailing wind is from the north, and the southern Yellow Sea is influenced by the air coming from the Korea Peninsula. In the spring the air flows are mainly from northern China under the influence of the anthropogenic activities and Asian dust storms. In summer the flows are from southern China and

Japan, Pacific maritime conditions. In addition, summer is the wettest season and rain scavenging also contributes to the summer minimums. For example, sulphate concentration shows a strong seasonal cycle with peak values in the spring, reflecting the transport of dust particles from northern China during this season. It tends to be minimum in the summer time. Nitrate also shows the similar cycle. According to the concentration of nutrients and sulphate described above, we can also get the dry deposition fluxes in each season (also in Table 1). The seasonal variability of dry deposition fluxes of each substance is similar to that of its concentration. The dry deposition flux of nitrate in the southern Yellow Sea is with the maximum in spring and reaches its minimum in summer. Other nutrient elements in the southern Yellow Sea have similar seasonal cycles to that of nitrate.

However, the concentrations in aerosol over the East China Sea are slightly different from those over the southern Yellow Sea. The concentrations of nutrient elements in the East China Sea show a pronounced winter maximum and summer minimum. The seasonal variation of sulphate is like that of nutrients. Compared with those in the southern Yellow Sea, concentrations of nitrate, phosphate and sulphate in the East China Sea are relative lower, except for ammonium, which is mostly affected by temperature. It is mainly due to terrain difference, that is, the Yellow Sea is a semi-enclosed sea and is more influenced by land, while the East China Sea is an open sea that is less affected by land. On the other hand, the rainfall in the East China Sea is much higher and will more effectively reduce the concentrations of elements in aerosol. The dry deposition fluxes have the same trend as the concentrations, so their values tend to be higher in winter and lower in summer. Certainly, the dry deposition fluxes to the southern Yellow Sea are higher than those in the East China Sea.

2.2 Estimation of wet deposition fluxes

The basic concentration data in precipitation in the southern Yellow Sea is obtained from Qianliyan Island (36° 16′ N, 121° 23′ E) and Maidao Island (36° 03′ N, 120° 25′ E)[3,19,20] in the west part of Yellow Sea and Ansan, Korea (37° 17′ N, 126° 50′ E)[4] in the east part of Yellow Sea. Contrasting to that in the western Yellow Sea, the average concentrations and annual rainfall in eastern Yellow Sea are much higher. The concentration of nitrate is more or less the same in both parts of Yellow Sea, phosphate and ammonium are also the same, but the silicate concentration shows a big difference for both areas. Based on the above studies, we get the concentrations in the southern Yellow Sea by weighted average, as listed in Table 2. The concentrations in the East China Sea are given from the observations in Shenshi Island, China (30° 43′ N, 122° 48′ E) from May 2000 to April 2001, and the precipitations in the southern Yellow Sea and the East China Sea are provided by Southampton Oceanography Centre (SOC) surface flux climatology (version 1.1). As can be seen from Table 2, the peak rainfall in the southern Yellow Sea occurs only in summer, while the precipitation in the East China Sea reaches its maximum in both spring and summer. The rainfall in the East China Sea is nearly twice as much as that in the southern Yellow Sea.

Similar to the spatial distribution of aerosol concentrations, the element concentrations in precipitation in the southern Yellow Sea are a bit larger than those in the East China Sea. In details, the phosphate concentration is extremely low in precipitation, because there are no significant vapor phase forms of phosphorus in the atmosphere[6]. The concentration of silicate is also low resembling ph osphate. It still displays a seasonal cycle of the concentration in precipitation. In fact, their values in winter are higher than in other seasons in the southern Yellow Sea, but the seasonal variability in the East China Sea of the concentration is much more complicated.

Tab. 2 The monthly average precipitation (mm) and the concentrations ($\mu mol \cdot L^{-1}$) of nutrient elements and sulphate in precipitation in the southern Yellow Sea and the East China Sea

Sea areas	Season	Precipitation	NO_3^-	NH_4^+	PO_4^{3-}	SiO_3^{2-}	SO_4^{2-}	Reference
The Southern Yellow Sea	Spring	48.52	9.8	41.5	0.50	4.90	57.3	Zhang J *et al.* (1994), (1999); Chung *et al.* (1998); Zhang Jinlia *et al.* (2000)
	Summer	122.74	17.4	35.7	0.53	3.51	31.9	
	Autumn	60.80	21.6	41.8	0.76	5.17	54.9	
	Winter	36.25	34.4	52.4	0.81	5.35	69.8	
	Average	67.08	20.9	44.8	0.65	4.14	53.5	
The East China Sea	Spring	146.17	13.24	9.67	0.18	3.26	22.1	Observations in Shenshi (provided by Zhang Jing)
	Summer	144.75	8.89	9.00	0.06	5.13	24.3	
	Autumn	126.71	7.23	2.54	0.21	3.37	51.2	
	Winter	90.59	8.16	15.07	0.15	4.56	37.2	
	Average	127.05	9.38	9.07	0.15	4.08	33.7	

Note: Precipitation data taken from SOC (Version 1.1).

Tab. 3 The monthly average wet deposition fluxes of nutrient elements and sulphate towards the southern Yellow Sea and the East China Sea in different seasons ($mg \cdot m^{-2} \cdot month^{-1}$)

Sea areas	Season	NO_3^-	NH_4^+	PO_4^{3-}	SiO_3^{2-}	SO_4^{2-}
The Southern Yellow Sea	Spring	29.48	44.3	2.27	18.0	266.9
	Summer	132.4	96.4	6.11	32.7	375.8
	Autumn	81.5	55.9	4.34	23.9	320.4
	Winter	77.3	41.8	2.76	14.7	242.9
	Average	86.9	59.6	4.10	27.3	384.1
The East China Sea	Spring	120.0	31.1	2.46	36.2	310.1
	Summer	79.8	28.7	0.81	56.4	337.7
	Autumn	56.8	7.1	2.49	32.5	622.8
	Winter	45.8	30.0	1.29	31.4	323.5
	Average	73.9	25.4	1.80	39.4	411.0

From the concentrations in precipitation and monthly rainfall data in Table 2, we can easily calculate the monthly average wet deposition fluxes in the southern Yellow Sea and the East China Sea (Table 3). The seasonal variability of wet deposition fluxes in the southern Yellow Sea is contrary to those of dry deposition fluxes. It tends to reach maximum in summer and minimum in winter. Though the concentrations are relatively low in summer, the wet deposition fluxes are still the greatest in the whole year due to enormous rainfall. While there is a big difference in seasonal cycle in the East China Sea, where the wet deposition flux for different elements shows a different seasonal cycle. By comparing dry and wet deposition fluxes, we can also find that the wet deposition fluxes are greater

than dry deposition fluxes in the summer time. Depositions of nitrate and sulphate are dominated by wet deposition, while deposition of phosphate is mainly dry deposition because of its low concentration in precipitation. The total deposition fluxes decrease from the southern Yellow Sea to the East China Sea, in other words, the farther away from the mainland, the lower the total deposition fluxes are.

3 Comparison between the total atmospheric fluxes and riverine inputs

The total atmospheric fluxes to the southern Yellow Sea and the East China Sea are, respectively, calculated based on the results as we discussed above. In order to account for the importance of air to sea fluxes in both areas, the values are compared with the riverine inputs (Table 4). Changjiang River flows into the southern Yellow Sea and the East China Sea in different ratio for each season, but in winter, the riverine input nearly gets into the East China Sea[21]. Additionally, Minjiang and Jiulongjiang rivers both discharge into the East China Sea. Based on the drainage areas and concentrations of nutrient elements[22], we can obtain the riverine inputs of nutrient elements to the southern Yellow Sea and the East China Sea.

Tab.4 The comparison between annual atmospheric and riverine inputs of nutrient elements to the southern Yellow Sea and the East China Sea ($\times 10^{10}$ g/a)

Sea areas	Source	NO_3^-	NH_4^+	PO_4^{3-}	SiO_3^{2-}
The southern Yellow Sea	Atmospheric Input	49.1	41.6	2.8	9.2
	Riverine Input	85.2	13.4	2.3	301.6
The East China Sea	Atmospheric Input	75.0	99.7	3.8	36.4
	Riverine Input	127.9	17.0	3.2	485.6

As the southern Yellow Sea (being to the south of 37° N) has a smaller area ($2.8\times10^{11}m^2$) than that of the East China Sea ($7.7\times10^{11}m^2$), the annual atmospheric input to the southern Yellow Sea is smaller than that to the East China Sea. Rivers are obviously the major source of nitrate and silicate, especially for the latter, as about 90% of them is supplied by rivers. However, the atmospheric input of ammonium is about six times the riverine input to the East China Sea. Comparing atmospheric inputs with riverine inputs, it is found that although the atmospheric inputs of phosphorous are smaller, they are still greater than riverine inputs in both sea areas, and the nutrient elements inputs via the atmosphere may be important for new productivity.

4 Summary

By synthesis and reanalysis of recent research results on dry and wet deposition of nutrient elements and sulphate in the Yellow Sea and the East China Sea, presented here are the estimations of the atmospheric fluxes of nutrient elements and sulphate to the southern Yellow Sea and the East

China Sea in each season. The results are as follows:

(1) The concentrations of nutrient elements and sulphate in aerosol and precipitation show an apparent seasonal cycle with the maximum values in winter and the minimum values in summer, which is closely related with the seasonal variations in prevailing winds and precipitation.

(2) Depositions of nitrate and sulphate are dominated by wet deposition, while the deposition of phosphate is mainly dry deposition.

(3) The dry and wet deposition fluxes in the East China Sea are both smaller than those in the southern Yellow Sea, but owing to its large area, the annual atmospheric input to the East China Sea is greater than that to the southern Yellow Sea.

(4) Rivers are obviously the major source of silicate, as they supply about 90% of the total silicate, while the atmospheric inputs of ammonium and phosphate are greater than that from rivers. The nutrient elements inputs via atmosphere play an important role in controlling new productivity in the southern Yellow Sea and the East China Sea.

Just as pointed out at the beginning of the paper, for lack of observation data, conclusions presented in this paper are rather elementary and more thorough work need to be done in this direction. Exchange of views and comments is sincerely asked for.

Acknowledgments

This work is supported by the State "973" basic research program under contract (G19990437) and the international cooperation program under contract (2001CB711004). We also sincerely thank Prof. Zhang Jing & Dr. Liu Sumei for providing data and helpful comments.

References

[1] Paerl H W. Enhancement of Marine Primary Production by Nitrogen Enriched Acid Rain. Nature, 1985, 315: 747-749.

[2] Knap A H, Jickells T D, Pszenny A *et al.* Significance of Atmospheric-derived Nitrogen on Productivity of the Sargasso Sea. Nature, 1986, 320: 158-160.

[3] Zhang J, Liu M G. Observations on Nutrient Elements and Sulphate in Atmospheric Wet Depositions over the Northwest Pacific Costal Oceans-Yellow Sea. Marine Chemistry, 1994, 47: 173-189.

[4] Chung C S, Hong G H, Kim S H *et al.* Shore Based Observation on Wet Deposition of Inorganic Nutrients in the Korean Yellow Sea Coast. The Yellow Sea, 1998, 4: 30-39.

[5] GESAMP (Group of Experts on Scientific Aspects of Marine Pollution) Working Group 14. The Atmospheric Input of Trace Species to the World Oceans. Rep Stud 38. Geneva: World Meteorol Organ, 1989, 106.

[6] Duce R A, Liss P S, Merrill J T *et al.* The Atmospheric Input of Trace Species to the World Ocean. Global Biogeochemical cycles, 1991, 5(3): 193-259.

[7] Patterson C C, Settle D M. Review of Data on Eolian Fluxes of Industrial & Natural Lead to the Land & Seas in Remote Regions on a Global Scale. Marine Chemistry, 1987, 22: 137-162.

[8] Mao Jietai and Li Jianguo. Seasonal Variations of Wet Deposition Velocities of SO_2, SO_4^{2-} and HNO_3 (g) in the East Parts of China. Acta Meteorologica Sinica, 1997, 55(5): 545-561.

[9] Dong Jinquan and Yang Shaojin. Characteristics of the Aerosol and Study of Their Sources in Huabei Clean

Area. Environmental Chemistry, 1998, 17(1): 38-44.

[10] Dai Shugui, Zhu Tang, Zeng Yousheng, *et al.* Judge the Characteristics and Sources of Aerosols over the Bohai Sea and the Yellow Sea Areas Based on the Element Composition. Marine Environmental Science, 1987, 6(3): 9-13.

[11] Carmichael G R, Zhang Y, Chen L-L *et al.* Seasonal Variation of Aerosol Composition at Cheju Island, Korea. Atmospheric Environment, 1996, 30(13): 2 407-2 416.

[12] Carmichael G R, Hong M S, Ueda H *et al.* Aerosol Composition at Cheju Island, Korea. Journal of Geophysical Research, 1997, 102(D5): 6 047-6 061.

[13] Kim Y P, Lee J H, Baik N J *et al.* Summertime Characteristics of Aerosol Composition at Cheju Island, Korea. Atmospheric Environment, 1998, 32(22): 3 905-3 915.

[14] Shang Shaoling and Hong Huasheng. Atmospheric Flux of Phosphorous to the Ocean in Xiamen Region. Journal of Xiamen University (Natural Science), 1997, 36(1): 106-109.

[15] Chen Liqi, Yang Xulin, Tang Rongkun *et al.* The Chemical Characteristics of Aerosols over the Kuroshio Area. Transactions of Kurshio Research (4), Ocean Press, Beijing, 1992, 295-307.

[16] Wakamatsu S, Utsunomiya A, Han J S *et al.* Seasonal Variation in Atmospheric Aerosols Concentration Covering Northern Kyushu, Japan and Seoul, Korea. Atmospheric Environment, 1996, 30(13): 2 343-2 354.

[17] Chen Liqi, Gao Pengfei, Zhang Yuanhui *et al.* The Characteristics of Aerosols over the Xiamen Region. Acta Oceanologica Sinica, 1993, 15(2): 24-32.

[18] Wu Dui. The Distribution Characteristics of Water-soluble Composition of Atmospheric Aerosol over North of the South China Sea. Scientia Atmospherica Sinica , 1995, 19(5): 616-622.

[19] Zhang J, Chen S Z, Yu Z G *et al.* Factors Influencing Changes in Rainwater Composition from Urban Versus Remote Regions of the Yellow Sea. Journal of Geophysical Research, 1999, 104(D1): 1 631-1 644.

[20] Zhang Jinliang, Yu Zhigang, Zhang Jing *et al.* Wet Deposition (Precipitation) of Major Elements at Two Sites of Northwestern Yellow Sea. Environmental Chemistry, 2000, 19(4): 352-356.

[21] Wang Baodong. On the Extension and Nutrient Transportation of the Changjiang River Diluted Water. Journal of Oceanography of Huanghai & Bohai Seas, 1998, 16(2): 41-47.

[22] Zhang J. Nutrient Eelements in Large Chinese Estuaries. Continental Shelf Research, 1996, 16(8): 1 023-1 045.

Chemical Associations of Heavy Metals in the Sediments near Bailonggang Sewage Discharge Outlet of Shanghai

Bi Chunjuan (毕春娟), Chen Zhenlou (陈振楼), Xu Shiyuan (许世远)
Department of Geography, College of Resource and Environmental Science, East China Normal University, Shanghai 200062

Abstract The five chemical associations of heavy metals have been extracted continuously using the *Tessier* extracting method. Results show that Cu, Pb, Fe, Zn and Cr in the sediments are mainly distributed in residual fraction, while the major chemical association of Mn is carbonates. Carbonate heavy metals are converted into Fe-Mn oxides in autumn. And in the low tidal flat, after carbonates have changed into ionic heavy metals, some of the elements are transported to the overlying water. Cu, Pb, Fe and Mn have good correlations with each other, and Zn, Cr also show their similarity of chemical behavior in the sediments.

Keywords heavy metals, chemical associations, Bailonggang sewage discharge outlet, tidal flat

The study of the geochemical associations of heavy metals, which have different chemical behavior and bioavailability, has received much attention at home and abroad[1~3]. As a crossing region of the river and the ocean, the estuary is subjected to extremely complex physical, chemical and biological actions due to the interaction of run-off and tidal current[4, 5], which make heavy metals deposit and accumulate continuously in the tidal flat. Attention has been focused on the total concentrations of heavy metals in the tidal flat of Shanghai[6, 7], with little information available on the geochemical associations and seasonal variation of heavy metals within the estuary. This paper reports the seasonal variation of each chemical association concentrations of heavy metals in the sediments of the high, middle and low tidal flats near Bailonggang sewage discharge outlet. By comparing the metal concentrations between the chemical associations in different seasons, the transport and conversion of heavy metals between chemical associations is preliminarily discussed.

1 Sample collection and methods

The sampling transect is located in the tidal flat, about 1km south of the Bailonggang sewage discharge outlet of Yangtze estuary (Fig. 1). Surface sediments between 0 ~ 5 cm in depth are sampled respectively with a small plastic shovel from the high, middle and low tidal flats in January, April, July and October, 2000. Samples are returned to the laboratory and dried to constant weight below 40 ℃. Then the sediment material is grounded and homogenized, and subsequently passes through a 63 μ m size nylon mesh.

One gram of homogenized sediments is analyzed according to the sequential extraction proposed by Tessier *et al.* and Zhang Hui *et al.*[1, 8]. The five chemical associations of heavy metals, that is, the

Received on December 11, 2002; accepted on February 25, 2003

exchangeable, carbonates, Fe-Mn oxides, organic matter and residual are extracted continuously. In addition, about 0.5 g of homogenized sediments are hot digested with HNO_3-HF-$HClO_4$ (GR), and then diluted to 50 mL volume with 1:1 (v / v) HNO_3. Concentrations of heavy metals (Cu, Pb, Zn, Fe, Mn and Cr) in the solutions are determined by atomic absorption spectrophotometer (Zeeman-5000) in flame mode. The detection limits of Cu, Pb, Zn, Fe, Mn and Cr are 0.006×10^{-6}, 0.010×10^{-6}, 0.002×10^{-6}, 0.008×10^{-6}, 0.003×10^{-6} and 0.03×10^{-6} respectively.

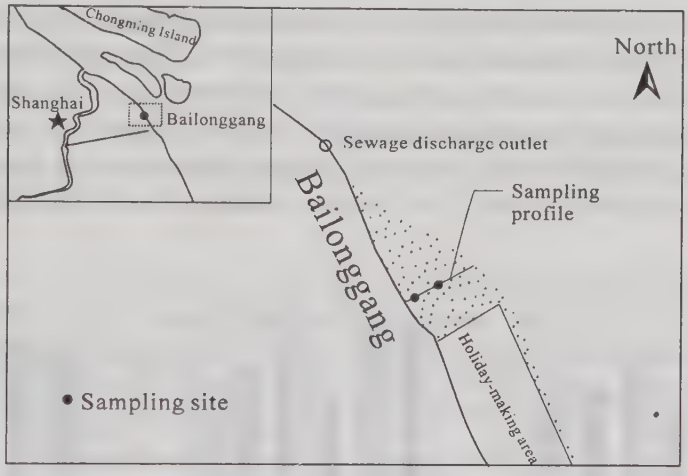

Fig. 1 Location of sampling sites

2 Results and discussion

2.1 Total concentrations and seasonal variation of heavy metals

Average concentrations of the total five metal chemical associations and the total tested heavy metal concentrations are presented in Table1. For each element, sum of the five chemical associations

Tab. 1 Average concentrations of the total five chemical associations and the tested heavy metal concentrations (μg/g)

	Cu	Pb	Fe	Mn	Zn	Cr
Sum of the chemical associations	41.5	30.8	36 514	844	155	25.0
Tested heavy metal concentrations	43.4	33.7	38 257	886	175	32.9
Relative deviation / %	4.0	7.5	4.4	4.9	11.8	15.8
Background value[7]	17	20	/	/	49	28

Relative deviation $\delta=[\sum(|c1-c2|/c1)]/n$. c1: tested heavy metal concentrations, c2: sum of the chemical associations, n: sample number

is comparable to the total concentration digested by HNO_3-HF-$HClO_4$, which shows that the error is very low in the process of sequential extraction. Compared with the background values of these metals in the tidal flat of Shanghai[7], Cu, Pb, Zn and Cr are all characterized by high concentrations, especially the concentrations of Cu and Zn, which are 2.6 and 3.6 times more than the background values respectively. The concentrations of Cu, Pb, Zn and Cr in the intertidal sediments near Bailonggang sewage discharge outlet in 1990 are 17.1×10^{-6}, 16.0×10^{-6}, 105.1×10^{-6} and 59.5×10^{-6} separately[9], compared with which, the concentrations of Cr in the sediments decrease largely, while Cu, Pb and Zn show a steep rise in concentration.

The seasonal variation of total heavy metals in the intertidal sediments is illustrated in Figure 2. In the sediments of high tidal flat, the concentrations of Mn and Zn in spring and summer are lower than in autumn and winter, while seasonal variation of the concentrations of Cu, Pb and Fe are quite different from Mn and Zn, no trend being observed. In the sediments of middle tidal flat, the concentrations of Cu, Pb, Fe, Mn and Zn are lower in spring and summer, but higher in the sediments of low tidal flat in the same seasons. This seasonal variation of metal concentrations may result

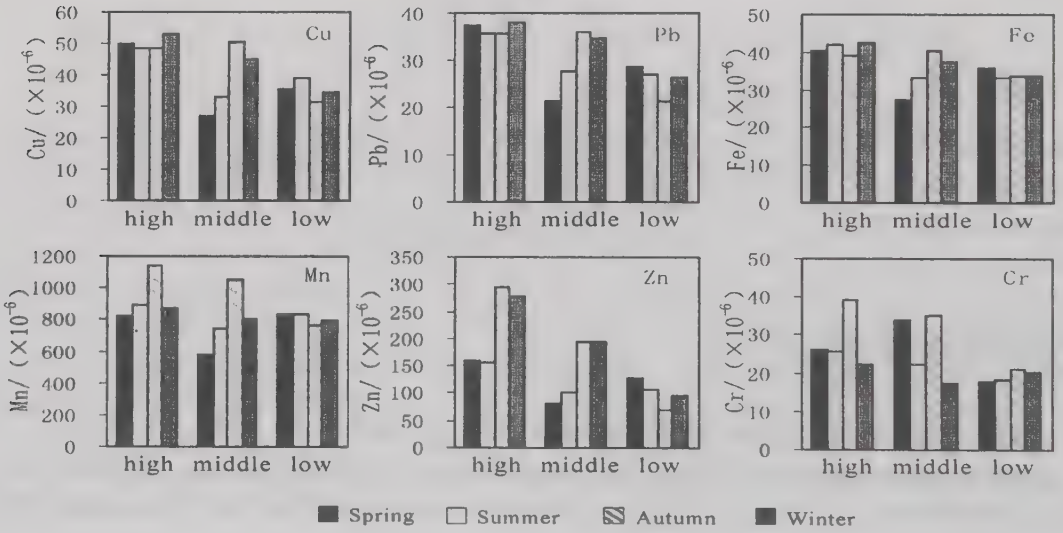

Fig. 2 Seasonal variation of heavy metals in the sediments

principally from the discharged sewage and the plant uptake. About 70 % of waste water discharged by Bailonggang sewage outlet is domestic sewage, and, therefore, with the increasing domestic water consumption in spring and summer, which leads to the increasing sewage discharging volume, part of the metal elements in the sewage would be deposited and accumulated in the sediments. Spring and summer are the growing seasons of *Phragmites australis* and *Scirpus mariqueter*, which mainly live in the high and middle tidal flats as dominant species. Large numbers of heavy metals are absorbed by the roots and subsequently accumulated in the plant body[10], resulting in the decrease of heavy metal concentrations in the sediments. Different from the other heavy metals, Cr is characterized by low

concentrations in the sediments of high, middle and low tidal flats in summer, but relatively high concentrations in autumn. The reason is that in the Yangtze estuary, Cr mainly exists in the dissolved and trihydic patterns in summer, but in other seasons, Cr is characterized by particulate Cr. When the physical and chemical conditions change from summer to autumn, particulate Cr would be transported and accumulated in the sediments in autumn[11].

2.2 Chemical associations of heavy metals

Concentrations of the chemical associations of heavy metals in the sediments, averaged for each season, are given in Table 2, together with the relatively standard deviations. Copper, Pb, Fe, Zn and Cr in the sediments are preferentially linked to the residual fraction, secondly distributed among the carbonate and Fe-Mn oxide fractions. The organic matter of Cr also has relatively high concentration in the sediments. Mn is mainly distributed in carbonate fraction, with the percentage concentration reaching or surpassing 50 %, and secondly are the residuals and Fe-Mn oxides. All the concentrations of exchangeable heavy metals are the lowest among the five chemical associations.

Tab. 2 The average percentage and standard deviation of each chemical association of heavy metals in the sediments (%)

chemical association	Cu±SD	Pb±SD	Fe±SD	Mn±SD	Zn±SD	Cr±SD
exchangeable	1.4±0.8	0.4±0.5	0	3.9±2.9	0.1±0.4	1.3±0.8
carbonates	18.7±2.9	29.1±12.0	3.5±2.2	48.8±9.0	27.8±9.6	4.6±1.5
Fe-Mn oxides	17.0±3.7	29.7±9.7	12.8±1.3	18.7±12.5	19.3±7.7	19.7±6.5
organic matter	10.9±2.0	9.4±1.8	2.6±0.4	3.3±2.7	4.9±1.0	12.4±3.4
residuals	52.1±2.6	31.3±4.1	81.1±1.8	25.3±3.5	47.9±14.0	61.9±9.7

2.3 Seasonal variation of heavy metal chemical associations

Seasonal variation of the five chemical association concentrations of heavy metals in the intertidal sediments is similar in the high, middle and low tidal flats, so Figure 3 only gives the seasonal variation of each chemical association in the sediments of the middle tidal flat. For all heavy metals, the concentrations of exchangeable and organic matter fractions show less distinct seasonal variation. Higher concentrations of Fe-Mn oxide Cu, Pb, Fe and Mn in surface sediments are recorded in autumn, while the concentrations of carbonates are lower in autumn. Lead and Mn are mainly distributed in carbonate fraction, whereas Cu and Fe are preferentially linked to the residual fraction in the sediments, and, therefore, the seasonal fluctuations are larger for carbonate and Fe-Mn oxide Pb and Mn than for Cu and Fe. The concentrations of Fe-Mn oxide Zn and Cr in the sediments increase substantially in autumn as well and their carbonate metal concentrations are higher in autumn than in spring and summer. This is because Zn is the most abundant element absorbed by plant. In spring and summer, lots of carbonate Zn is absorbed by the plant roots, resulting in the decrease of the concentration in the sediments of the high and middle tidal flats. Being similar to Zn in the metal

chemical behavior[12], Cr shows similar seasonal variation. Being absorbed by plant, non-residual heavy metals decrease in the plant growing season, which makes the percentage concentrations of residual Cu, Pb, Fe, Mn, Zn and Cr in the sediments in spring and summer usually higher than in autumn and winter. This result shows that the carbonate heavy metals have been converted into Fe-Mn oxides in the sediments of tidal flat near the Bailonggang sewage discharge outlet in autumn.

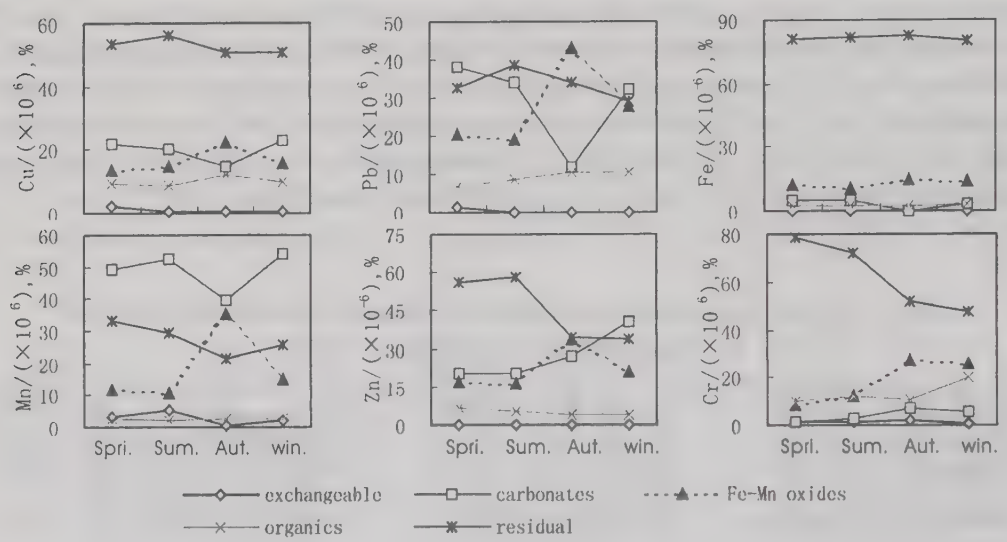

Fig. 3 Seasonal variation of the chemical associations of heavy metals in the sediments

In the sediments of low tidal flat, due to the powerful hydrodynamics and active chemical behavior of Zn and Cr[12], the seasonal variations of carbonate and Fe-Mn oxide Zn and Cr are extremely complex. In addition, the residual heavy metals in the low tidal flat show higher concentrations in autumn, indicating that only part of the carbonate heavy metals has been oxidized, others have been transported and diffused to the overlying water.

2.4 Correlation between carbonate and Fe-Mn oxide heavy metals

Studies on the correlation between carbonate and Fe-Mn oxide heavy metals show that the correlation coefficients between Cu, Pb, Fe and Mn are high, with the value up to 0.70, while low correlation coefficients exist between Zn, Cr and Fe, Mn. High correlation coefficients only exist between Zn and Cr. The result suggests that when the carbonate and Fe-Mn oxide heavy metals have been transported and converted in the sediments, the behaviors of Cu, Pb, Fe and Mn show no difference, and similar behaviors exist between Zn and Cr. If calculated according to all the chemical associations of heavy metals, the correlation coefficients between Cu and Fe, Pb and Mn, Zn and Fe, Cr and Fe are respectively 0.95, 0.76, 0.77 and 0.96, showing that the circulation of Fe and Mn is one of the major mechanisms controlling the behavior of heavy metals in the intertidal sediments of Shanghai.

3 Results

(1) All the concentrations of Cu, Pb, Zn and Cr in the intertidal sediments near the Bailonggang sewage discharge outlet surpass the background values in the tidal flat of Shanghai. And concentrations of Cu, Pb, Fe, Mn and Zn in spring and summer are low in the sediments of high and middle tidal flats, but high in the sediments of low tidal flat. Lower concentrations of Cr in summer are found in all the high, middle and low tidal flats.

(2) Cu, Pb, Fe, Zn and Cr in the sediments are preferentially linked to the residual fraction, whereas Mn is mainly distributed in carbonate fraction, with the percentage concentration reaching 50%. The concentrations of exchangeable and organic heavy metals show less distinct seasonal variation, and, otherwise, the concentrations of other chemical associations of heavy metals show large fluctuations in autumn.

(3) Seasonal variation of the residual heavy metals in the sediments of high and middle tidal flats is related to the growing process of plant in the tidal flat. In the sediments of low tidal flat, part of the carbonate heavy metals is oxidized, while others have been transported and diffused to the overlying water.

(4) The correlation analysis shows that Cu, Pb, Fe and Mn in carbonate and Fe-Mn oxide fractions behave similarly in the transporting and converting process, and high correlation coefficient is found between Zn and Cr. The correlation analysis on all the chemical associations of heavy metals shows that the circulation of Fe and Mn is one of the major mechanisms controlling the behaviors of heavy metals in the intertidal sediments of Shanghai.

Acknowledgements

This work is supported by the National Natural Science Focal Projects Foundation of China (Grant No.40131020), the National Natural Science Foundation of China (Grant No.49833030), the Venus Program Foundation for Young Scientists of Shanghai (Grant No. 97QA14023) and its Tracking Program (Grant No. 01QMH1406), and the Dawn Program of Shanghai Ecucational Development Foundation.

References

[1] Zhang Hui, Ma Dongsheng. Fractionation of Heavy Metals in Soils from Nanjing. Acta Scientiae circumstantiae, 1997, 17(3): 346-351.

[2] Gambrell R P. Trace and Toxic Metals in Wetlands — a Review. Journal of Environment Quality, 1994, 23: 883-891.

[3] Shao Mihua, Wang Zhengfang. A Study on the Distributive Characteristics of Chimical form of Cu, Pb and Cd in Suspended Particulate in Chang Jiang River Estuary. Oceanologia Et Limnologia Sinica, 1992, 23(2): 144-149.

[4] Shen Huanting, He Songlin, Pan Dingan *et al.* A Study of Turbidity Maximum in the Changjiang Estuary. Acta Geographica Sinica, 1992, 47(5): 272-279.

[5] Yang S L. The Role of *Scirpus* Marsh in Attenuation of Hydrodynamics and Retention of Fine Sediment in the Yangtze Estuary. Estuarine, Coastal and Shelf Science,1998, 47: 227-233.

[6] Chen Zhenlou, Xu Shiyuan, Liu lin *et al.* Spatial Distribution and Accumulation of Heavy Metals in Tidal Flat Sediments of Shanghai Coastal Zone. Acta Geographica Sinica, 2000, 55(6): 641-651.

[7] Xu Shiyuan, Tao Jing, Chen Zhenlou *et al.* Dynamic Accumulation of Heavy Metals in Tidal Flat Sediments of Shanghai. Oceanologia Et Limnologia Sinica, 1997, 28(5): 509-515.

[8] Tessier A, Campbell PGC, Bisson M. Sequential Extraction Procedure for the Speciation of Particulate Trace Metals. Analytical Chemstry, 1979, 51(7): 844-851.

[9] Dai Weiming, Gu Youzhi. Analysis on the Accumulation of Heavy Metals in the Sediments of West and South Sewage Outlets in Shanghai. Shanghai Environmental Sciences, 1990, 9(7): 38-40.

[10] CaCador I, Vale C, Catarino F. Seasonal Variation of Zn, Pb, Cu and Cd Concentrations in the Root-sediment System of *Spartina maritima* and *Halimione portulacoides* from Tagus Estuary Salt Marshes. Marine Environmental Research, 2000, 49:279-290.

[11] Huang Huarui, Pang Xuezhong. Chromium Behaviour in the Changjiang River Estuary and its Adjacent Sea Area. Oceanologia Et Limnologia Sinica, 1990, 21(6): 571-577.

[12] Luo Shuyi, Zang Xiwen, Fan Jinghui. Inorganic Geochemistry. Beijing: Peking university publishing house, 1990.

Accumulation and Cycle of Heavy Metals in *Sonneratia apetala* and *S. caseolaris* Mangrove Community at Futian of Shenzhen, China

Wang Bosun (王伯荪)[1], Zan Qijie (昝启杰)[1, 2], Zhang Weiyin (张炜银)[3], Wang Yongjun (王勇军)[2]

1 *School of Life Sciences, Zhongshan University, Guangzhou* 510275

2 *Neilingding-Futian National Nature Reserve of Guangdong, Shenzhen* 518040

3 *Institute of Forest Ecology, Environment and Protection, Chinese Academy of Forestry, Beijing* 100091

Abstract This paper reports the absorption, accumulation, distribution and cycle of Cu, Pb, Zn, Cr and Ni in *S. apetala* + *S. caseolaris*, mangrove community at Futian Mangrove Nature Reserve of Shenzhen. The Cu, Pb, Zn, Cr and Ni contents in forest soil increase from bottom to surface layers, and the storage of the five heavy metals in the surface layer (depth 0 ~ 30 cm) is Zn > Pb > Ni > Cr > Cu. The concentration ability is *S. caseolaris* > *S. apetala* > *K. candel*. The existing accumulation of Cu, Pb, Zn, Cr and Ni in the community is 23 019.63 μ g/m^2, 23 429.66 μ g/m^2, 117 870.42 μ g/m^2, 6 835.80 μ g/m^2, and 12 995.22 μ g/m^2, respectively. The annual absorption is 6 592.57 μ g/m^2, 2 664.80 μ g/m^2, 23 123.56 μ g/m^2, 853.24 μ g/m^2, and 1 990.95 μ g/m^2, respectively. The annual return is 3 179.50 μ g/m^2, 1 300.65 μ g/m^2, 7 401.31 μ g/m^2, 398.99 μ g/m^2, and 646.20 μ g/m^2, respectively. The annual net retention accumulation of Cu, Pb, Zn, Cr and Ni in the community is 3 413.07 μ g/m^2, 1 364.15 μ g/m^2, 15 722.25 μ g/m^2, 454.25 μ g/m^2, and 1 344.75 μ g/m^2, respectively. The turn over periods of Cu, Pb, Zn, Cr and Ni are 8,19,15,18 and 21 years, respectively.

Keywords *Sonneratia apetala*, *S. caseolaris*, heavy metal, accumulation, cycle

Wetland ecosystem in the Shenzhen Bay is one of the internationally important ecosystems in South China Region. Its core, with the Mai Po Mangrove Nature Reserve in Hong Kong on the one side and the Futian Mangrove Nature Reserve in Shenzhen on the other side, provides habitats for many rare and endangered wild birds, especially for migratory birds[1, 2]. With the economic development in Hong Kong and Shenzhen, a large mount of silt and untreated waste water are poured into the Shenzhen Bay, causing the depositation and pollution. To increase the biodiversity in the Futian Mangrove Natural Reserve, to improve the environmental quality, and to ensure the stable and sustainable development of Shenzhen Bay wetland ecosystem, *Sonneratia apetala* Buch.-Ham and *S. caseolaris* (L.) Engl. were introduced into the Futian Mangrove Naturel Reserve in the early 1990s[3]. We studied the absorption, accumulation, distribution and cycle of Cu, Pb, Zn, Cr and Ni in *S. apetala* + *S. caseolaris* mangrove community, revealing the accumulation of pollutants and the dynamics of absorption of heavy metals in plants and providing the baseline for conservation and management of the Futian Mangrove Nature Reserve.

1 Materials and methods

Received on December 29, 2002; accepted on March 2, 2003

1.1 Study site

The research is conducted at the Shenzhen Futian Mangrove Nature Reserve (22° 32′ N, 114° 03′ E). The reserve area is of lower tropical monsoon climate with a mean annual temperature of 22 ℃, the highest temperature (July) of 38.7 ℃ and the lowest temperature (January) of 0.2 ℃. The mean annual rainfall is 1 927 mm, but it is not uniform. The annual relative moisture is 79 %. The physical and chemical feature of soil in the community are presented in Table 1. The density of *S. apetala*, *S. caseolaris* and *K. candel* is 457 ind./hm^2, 319 ind./hm^2 and 5 050 ind./hm^2, respectively. Two layers of trees can be recognized: the upper layer consisting of *S. apetala* and *S. caseolaris*, and the lower layer of *K. candel*[3].

Tab. 1 Physical and chemical features of soil in forest

Depth of soil (cm)	pH	Salinity (%)	Volume weight /g • cm^{-3}	Organic matter (%)	Total N (%)	Total P (%)	Total K (%)
Surface layer (0 ~ 30)	6.01	2.553	0.784	2.748	1.27	0.90	23.16
Mid-layer (30 ~ 60)	7.94	0.837	0.817	1.113	0.54	0.50	24.82
Bottom-layer (60 ~ 90)	8.29	0.815	0.912	0.750	0.41	0.31	27.87

1.2 Sampling and analysis

In November 1999, a 40 m × 40 m plot was established in the community[4]. Soil samples are taken from three layers at regular intervals (0 ~30 cm, 30 ~ 60 cm and 60 ~ 90 cm). The studied samples are divided by species and parts of plant, then all the samples are dried at 60℃. The samples are passed through a sieve with 0.15 mm size. All samples are treated with $HClO_4$ and HNO_3. Cu, Pb and Zn are determined by the ICP spectrum method. Cr and Ni are measured by the graphite stove method. Soil salinities are measured by the $AgNO_3$ titration method, and soil pH values (soil : water = 1 : 5) determined by the electrometric method[5].

2 Results

2.1 Contents of Cu, Pb, Zn, Cr and Ni and accumulation index in the soil of the community

The sequence of concentrations of the five heavy metals in three layers of soil in the community is surface layer > mid-layer > bottom layer (Table 2). The contents of heavy metals are the highest in the surface layer due to pollution. The contents of the five heavy metallic elements are higher in the community than those in an *Avicennia marina* forest of fifty-six years old in Futian, Shenzhen[6]. They are also higher than those in a *Kandelia candel* forest in Fugong, Fujian and those in a *Rhizophora stylosa* forest in Yinluogan, Guangxi[7, 8].

On the basis of the contents of the elements and the volume weight, we could get the storages for 5 heavy metallic elements in the community. The storages of the five heavy metals in the soil of surface layer (depth 0 ~ 30 cm) are Zn > Pb > Ni > Cr > Cu.

Tab. 2 The content and pod amount of 5 elements in soil

Depth of soil (cm)	Elements Contents ($\mu g \cdot g^{-1}$)					Pod amount of elements ($g \cdot m^2$)				
	Cu	Pb	Zn	Cr	Ni	Cu	Pb	Zn	Cr	Ni
(0 ~ 30) Surface layer	45.58	69.92	125.08	58.04	62.80	10.72	16.45	29.42	13.65	14.77
(30 ~ 60) Mid-layer	25.14	56.41	95.41	34.20	49.94	6.16	13.83	23.29	8.38	12.24
(60 ~ 90) Bottom-layer	10.69	51.92	81.76	23.81	33.58	2.92	14.02	22.37	6.51	9.19

Accumulation indexes of five heavy metallic elements are presented in Table 3. Table 3 shows that accumulation indexes vary both from species to species and from organs to organs. Accumulation indexes of Cu, Pb, Zn and Cr are higher in fine roots and mid-roots, but those in trunk, perennial branch and bark are low. The organs with the highest or the lowest accumulation indexes of Ni in 3 populations are different. Comparing accumulation indexes and weight average values, we could know that accumulation capacity in *S. caseolaris* is the highest, followed by that in *S. apetala* and in *K. candel*. Sequence of accumulation index of 5 elements in 3 populations is Zn > Cu > Pb > Ni > Cr. It is suggested that the accumulation capacities of Zn and Cu are high, while those of Ni and Cr are low.

2.2 Contents of 5 elements in different fractions of mangrove plants

Contents of 5 elements in different fractions of mangrove plants are presented in Table 4. Table 4 shows that the contents of heavy metallic elements in different organs in the same specie are distinct. The contents of the same element in the same organ of different species are distinct. The contents of Cu in different fractions in the *S. apetala* from high to low are recognized in the fine roots, pneumatophore, leaves, flowers and fruits, dead branches, twigs, mid roots, barks, big roots, perennial branches, trunks; those in *S. caseolaris* are in fine roots, dead branches, twigs, barks, flowers and fruits, leaves, mid-roots, pneumatophore, perennial branches, trunks and big roots; and those in *K. candel* are in fine roots, mid-roots, leaves, twigs, big roots, hypocityl, barks, perennial branches, dead branches and trunks. The sequences of contents of Ni and Zn in 3 populations from high to low are *S. apetala* > *S. caseolaris* > *K. candel* and *K. candel* > *S. caseolaris* > *S. apetala*, respectively.

In the 3 populations, the contents of 5 heavy metallic elements are all the highest in the fine roots. The contents in the roots of the 3 populations decrease sequentially in the fine root, mid-root and big root. Because the fine root is the absorbing organ and most of the absorbed heavy metallic elements maintain in the outer cortex of the root, the contents of heavy metallic elements are fairly higher in the fine root than in any other organ. The contents of the 5 elements in the pneumatophore of *S. apetala* and *S. caseolaris* are higher than those in above ground organs, probably because the pneumatophore absorbs heavy metallic elements from sea water due to the flood tide. The contents of 5 elements in the trunks and perennial branches are low, a phenomenon similar to what is observed in the study of 56 a old *Avicennia marina* in Futian[16]. Because the mechanical constituents are high in the trunks, it is not easy to accumulate heavy mental elements in the trunks. In *S. apetala*, by weight average, the sequence of contents of 5 elements from high to low is Pb > Zn > Cu > Ni > Cr, in *S. caseolaris*, that is Zn > Cu > Pb > Ni > Cr, and in *K. candel*, that is Zn > Pb > Cu > Ni > Cr. Therefore, it may be suggested that the contents of heavy metallic elements are distinct in the organs of different species.

Tab. 3 Accumulation indexes in 3 species (soil depth 0 ~ 30 cm)

Species	Fraction	Cu	Pb	Zn	Cr	Ni
S. apetala	Leaf	0.104	0.056	0.164	0.018	0.052
	Twig	0.070	0.031	0.093	0.009	0.025
	Perennial branch	0.042	0.018	0.047	0.008	0.025
	Dead branch	0.078	0.031	0.118	0.009	0.032
	Trunk	0.027	0.025	0.058	0.009	0.007
	Bark	0.068	0.048	0.114	0.025	0.074
	Flower and Fruit	0.097	0.042	0.125	0.017	0.044
	Pneumatophore	0.122	0.060	0.231	0.025	0.064
	Big-root	0.059	0.041	0.115	0.024	0.024
	Mid-root	0.069	0.057	0.236	0.027	0.040
	Fine-root	0.217	0.338	0.637	0.050	0.062
	Average	0.087	0.068	0.176	0.020	0.041
S. caseolaris	Leaf	0.147	0.048	0.268	0.017	0.038
	Twig	0.211	0.042	0.135	0.017	0.031
	Perennial branch	0.101	0.030	0.065	0.008	0.025
	Dead branch	0.216	0.043	0.113	0.009	0.039
	Trunk	0.079	0.019	0.047	0.009	0.013
	Bark	0.188	0.074	0.124	0.026	0.071
	Flower and Fruit	0.182	0.041	0.144	0.017	0.037
	Pneumatophore	0.130	0.089	0.168	0.036	0.073
	Big-root	0.083	0.056	0.101	0.017	0.026
	Mid-root	0.148	0.114	0.203	0.045	0.066
	Fine-root	0.273	0.313	0.310	0.078	0.058
	Average	0.160	0.079	0.153	0.025	0.043
Kandelia candel	Leaf	0.076	0.024	0.411	0.017	0.038
	Twig	0.071	0.035	0.100	0.008	0.024
	Perennial branch	0.044	0.035	0.061	0.008	0.024
	Dead branch	0.048	0.041	0.078	0.008	0.036
	Trunk	0.031	0.012	0.055	0.009	0.019
	Bark	0.058	0.028	0.138	0.016	0.059
	Hypocotyl	0.058	0.017	0.127	0.012	0.018
	Big-root	0.064	0.044	0.194	0.018	0.039
	Mid-root	0.091	0.097	0.507	0.026	0.057
	Fine-root	0.089	0.260	0.674	0.061	0.052
	Average	0.063	0.059	0.240	0.018	0.037

Tab. 4 The content of 5 elements in different fractions of mangrove plant ($\mu g \cdot g^{-1}$)

Species	Fraction	Cu	Pb	Zn	Cr	Ni
S. apetala	Leaf	4.76	3.92	20.55	1.02	3.27
	Twig	3.20	2.13	11.57	0.50	1.60
	Perennial branch	1.90	1.24	5.85	0.49	1.55
	Dead branch	3.55	2.13	14.73	0.50	2.00
	Trunk	1.23	1.75	7.29	0.51	0.41
	Bark	3.11	3.32	14.20	1.45	4.67
	Flower and Fruit	4.42	2.94	15.68	0.98	2.75
	Pneumatophore	5.56	4.16	28.86	1.46	3.99
	Big-root	2.70	2.83	14.38	1.42	1.52
	Mid-root	3.13	3.98	29.52	1.55	2.49
	Fine-root	9.88	23.61	36.63	2.91	3.88
	Average	3.95	4.72	18.12	1.16	2.56
S. caseolaris	Leaf	6.72	3.35	33.49	0.98	2.36
	Twig	9.63	2.92	16.88	0.98	1.96
	Perennial branch	4.59	2.10	8.12	0.49	1.58
	Dead branch	9.84	3.04	14.16	0.51	2.44
	Trunk	3.61	1.30	5.83	0.51	0.81
	Bark	8.56	5.16	15.46	1.51	4.43
	Flower and Fruit	8.30	2.86	18.04	0.96	2.30
	Pneumatophore	5.94	6.22	21.03	2.08	4.60
	Big-root	3.78	3.88	12.57	1.01	1.62
	Mid-root	6.77	7.99	25.35	2.59	4.16
	Fine-root	12.43	21.91	38.71	4.52	3.62
	Average	7.29	5.52	19.06	1.45	2.72
Kandelia candel	Leaf	3.46	1.710	51.410	0.999	2.40
	Twig	3.24	2.453	12.457	0.478	1.53
	Perennial branch	2.02	2.422	7.619	0.472	1.51
	Dead branch	2.20	2.848	9.812	0.476	2.29
	Trunk	1.43	0.859	6.824	0.502	1.21
	Bark	2.62	1.965	17.277	0.919	3.69
	Hypocotyl	2.65	1.174	15.867	0.465	1.12
	Big-root	2.93	3.078	24.217	1.028	2.47
	Mid-root	4.14	6.807	63.453	1.492	3.59
	Fine-root	4.04	18.194	84.310	3.545	3.25
	Average	2.87	4.151	27.325	1.038	2.31

2.3 Pod amount and distribution of 5 heavy metallic elements

According to the contents of elements in each organ and the biomass of the community, by using the method of statistics, the pod amount and distribution of 5 elements in the community could be calculated. The results are presented in Table 5. Table 5 shows that the pod amount of Cu, Pb, Zn, Cr and Ni in the community is 23 019.63, 23 429.66, 117 870.42, 6 835.80, 12 995.22 $\mu g/m^2$, respectively. Followed by those in the branches and trunks, the distributions of Cu, Pb, Zn, Cr and Ni in the roots are the largest, making up 39.3 %, 54.8 %, 57.8 %, 58.6 % and 47.8 % respectively in the pod amount of the 5 elements in the community. The distributions of 5 elements in the leaves, flowers and fruits, and twigs are very small. Cu, Pb, Zn, Cr and Ni are stored in the organs, such as the roots, trunks and perennial branches that are not eaten easily by second consumers, a process that reduces the possible pollution effects on the consumers and thus purifies the environment.

Tab. 5 Pod amount and distribution of 5 heavy metallic elements ($\mu g \cdot m^{-2}$)

Species	Fraction	Cu	Pb	Zn	Cr	Ni
S. apetala	Leaf	718.11 (9.48)	590.83 (7.53)	3 098.19 (7.37)	153.51 (5.95)	492.36 (9.45)
	Branch	2 136.93 (28.21)	1 412.96 (18.01)	7 185.96 (18.02)	428.30 (16.62)	1 372.38 (26.33)
	Trunk	1 265.88 (16.71)	1 703.43 (21.71)	7 101.18 (17.18)	497.98 (19.32)	399.55 (7.66)
	Bark	678.91 (8.97)	724.33 (9.23)	3 099.86 (7.77)	317.41 (12.31)	1 018.59 (19.54)
	Flower and Fruit	5.300 (0.07)	3.52 (0.04)	18.82 (0.05)	1.18 (0.05)	3.30 (0.06)
	Root	2 769.08 (36.56)	3 412.34 (43.48)	19 374.82 (48.58)	1 179.17 (45.75)	1 926.95 (36.96)
	Total	7 574.21 (100)	7 847.41 (100)	39 878.83 (100)	2 577.55 (100)	5 213.13 (100)
S. caseolaris	Leaf	462.94 (4.85)	231.09 (3.24)	2 307.32 (10.7)	67.52 (3.93)	162.47 (4.92)
	Branch	3 681.42 (38.57)	1 353.55 (19.02)	6 477.23 (30.04)	381.68 (22.19)	962.73 (29.14)
	Trunk	1 728.35 (18.11)	2 246.86 (31.54)	2 792.47 (12.95)	242.32 (14.09)	388.87 (11.77)
	Bark	432.38 (4.53)	260.33 (3.65)	780.93 (3.62)	76.05 (4.42)	223.72 (6.77)
	Flower and Fruit	89.64 (0.94)	30.88 (0.43)	194.79 (0.91)	10.31 (0.59)	24.81 (0.75)
	Root	3 149.70 (33.00)	2 999.90 (42.12)	9 009.75 (41.78)	942.26 (54.78)	1 541.23 (46.65)
	Total	9 544.43 (100)	7 122.61 (100)	21 562.49 (100)	1 720.14 (100)	3 303.83 (100)
Kandelia candel	Leaf	582.65 (9.87)	287.62 (3.40)	8 647.16 (15.32)	168.03 (6.62)	404.35 (9.03)
	Branch	1 326.49 (22.48)	1 095.63 (12.95)	3 972.64 (7.04)	196.26 (7.73)	632.06 (14.11)
	Trunk	814.38 (13.80)	625.57 (7.40)	3 880.81 (6.88)	285.49 (11.25)	687.59 (15.35)
	Hypocotyl	41.14 (0.70)	18.20 (0.24)	245.94 (0.44)	7.21 (0.28)	17.36 (0.39)
	Root	3 136.33 (53.15)	6 432.62 (76.04)	39 682.55 (70.32)	1 881.12 (74.12)	2 736.90 (61.12)
	Total	5 900.99 (100)	8 459.64 (100)	56 429.10 (100)	2 538.11 (100)	4 478.26 (100)
Sum of forest		23 019.63 (300)	23 429.66 (300)	117 870.42 (300)	6 835.80 (300)	12 995.22 (300)

In Table 5, it is shown that the accumulations of the 5 elements vary among the species. Cu in *S. caseolaris*, Cr and Ni in *S. apetala*, Pb and Zn in *K. candel* are the highest, respectively making up 41.5 %, 37.7 %, 40.1 %, 36.1 %, 47.9 % of the pod amount of the 5 elements in the community, while Cu in *K. candel*, Pb, Zn, Cr and Ni in *S. caseolaris* are the lowest. It may be suggested that the accumulations of heavy metallic elements in various species are distinct.

2.4 Biological cycle of five heavy metallic elements

2.4.1 Annual retention of 5 elements in the community

Annual retention is the total amount of elements in annual net production of plants[4]. It can be calculated by measuring annual increasing of the biomass and the concentrations of elements. Annual retentions of 5 elements are presented in Table 6 and the annual retentions of Cu, Pb, Zn, Cr, and Ni are 3 413.07, 1 364.15, 1 5722.25, 454.25, 1 344.75 μ g/m^2 respectively. The retentions of Cu and Pb

Tab. 6 The yearly net retention accumulation of 5 elements in the community (μ g . m^{-2})

Species	Fraction	Cu	Pb	Zn	Cr	Ni
S.apetala	Leaf	101.19 (9.68)	37.00 (8.38)	379.64 (7.84)	10.30 (5.85)	46.25 (8.95)
	Twig	268.36 (25.66)	78.56 (17.79)	755.96 (15.61)	28.89 (16.4)	129.52 (25.07)
	Trunk	157.18 (15.03)	48.94 (11.08)	766.72 (15.83)	29.44 (16.71)	33.07 (6.40)
	Bark	140.11 (13.40)	66.43 (15.04)	556.27 (11.49)	31.19 (17.70)	140.25 (27.14)
	Flower and Fruit	0.22 (0.02)	0.07 (0.01)	0.68 (0.02)	0.02 (0.01)	0.09 (0.02)
	Root	378.67 (36.21)	210.66 (47.7)	2 382.90 (49.21)	76.34 (43.33)	167.52 (32.42)
	Total	1 045.73 (100)	441.66 (100)	4 842.17 (100)	176.18 (100)	516.70 (100)
S. caseolaris	Leaf	89.70 (5.65)	19.90 (4.30)	388.75 (11.35)	6.23 (4.22)	20.99 (5.20)
	Twig	559.72 (35.28)	100.60 (21.74)	858.16 (25.05)	27.99 (8.94)	110.04 (27.27)
	Trunk	336.36 (21.20)	53.85 (11.64)	472.56 (13.79)	22.46 (15.19)	50.45 (12.50)
	Bark	84.34 (5.32)	22.57 (4.88)	132.45 (3.87)	7.06 (4.78)	29.09 (7.21)
	Flower and Fruit	17.43 (1.10)	2.67 (0.57)	32.94 (0.96)	0.96 (0.64)	3.22 (0.79)
	Root	498.88 (31.45)	263.14 (56.87)	1 540.78 (44.98)	83.10 (56.23)	189.78 (47.03)
	Total	1 586.43 (100)	462.73 (100)	3 425.64 (100)	147.80 (100)	403.57 (100)
Kandelia candel	Leaf	55.08 (7.06)	12.08 (2.63)	710.80 (9.54)	7.56 (5.81)	25.48 (6.00)
	Twig	103.48 (13.25)	49.27 (0.72)	341.61 (4.58)	10.31 (7.91)	46.30 (10.91)
	Trunk	86.85 (11.12)	23.16 (5.03)	359.89 (4.83)	14.50 (11.31)	48.88 (11.52)
	Hypocotyl	5.44 (0.69)	1.07 (0.23)	28.29 (0.38)	0.45 (0.34)	1.53 (0.36)
	Root	530.06 (67.88)	374.18 (81.39)	6 013.85 (80.67)	97.45 (74.81)	302.29 (71.21)
	Total	780.91 (100)	459.76(100)	7 454.44 (100)	130.27 (100)	424.48 (100)
Sum		3 413.07 (300)	1 364.15 (300)	15 722.25 (300)	454.25 (300)	1 344.75 (300)

are the highest in *S. caseolaris*, while those of Zn, Cr and Ni are the highest in *S. apetala*. The retentions of Cu and Cr are the lowest in *K. candel*, the lowest of Zn and Ni in *S. caseolaris* and Pb in *S. apetala*. It is also shown in Table 6 that the retentions of 5 elements are the highest in the roots, followed by those in the branches and trunks, and the retentions of 5 elements are relatively low in other organs.

2.4.2 Annual return of the 5 elements in the community

Annual return is the content of the elements that enter the soil by litter fall in one year[4]. According to the contents of each element in the monthly litter fall and the total weigh of litter fall, the returns of 5 elements are calculated and shown in Table 7. The returns of Cu, Pb, Zn, Cr and Ni in the community are 3 179.5, 1 300.65, 7 401.31, 398.99 and 646.20 $\mu g/m^2$ respectively (Table 7). Table 7 shows that the returns of the 5 elements in the three species are distinct. For Cu, the sequence of return from high to low is *S. caseolaris*, *S. apetala* and *K. Candel*; for Pb and Cr, the sequences of return are *S. apetala*, *S. caseolaris* and *K. Candel*; and for Zn and Ni are *K. candel*, *S. caseolaris* an d *S. apetala*.

Tab. 7 The yearly return of 5 heavy metal elements in the community ($\mu g \cdot m^{-2}$)

Species	Cu	Pb	Zn	Cr	Ni
S. apetala	1 141.66	638.12	2 565.27	149.45	189.99
S. caseolaris	1 389.38	461.11	1 881.64	134.21	210.11
K. candel	648.46	201.42	2 954.40	115.33	246.10
Sum	3 179.50	1 300.65	7 401.31	398.99	646.20

2.4.3 Annual uptake and turnover period of the 5 elements in the community

Uptake equals the retention plus the return[9]. On the basis of Table 6 and Table 7, we could get the uptakes of the 5 elements in the community. The annual uptakes of Cu, Pb, Zn, Cr and Ni are 6 592.57, 2 664.80, 23 123.56, 853.24 and 1 990.95 $\mu g/m^2$ respectively. Proportions of the annual retention of Cu, Pb, Zn, Cr and Ni in the community are 51.8 %, 51.2 %, 68.0 %, 53.2 % and 67.5 % respectively, and those of the annual return of the 5 elements are 48.2 %, 48.8 %, 32.0 %, 46.8 % and 32.5 % respectively. So the retentions are larger than the returns.

Turnover period is the ratio of the total amount of an element in a standing crop to the amount of the homologous element in the annual litter fall in the community[10]. The turnover periods of Cu, Pb, Zn, Cr and Ni in the community are calculated to be 8 a, 19 a, 15 a, 18 a and 21 a respectively. The sequence of turnover periods from long to short is Ni, Pb, Cr, Zn and Cu. Compared with those in the 56 a old *Avicennia marina* community[6], and in the *Kandelia candel + Aegiceras corniculatum* community in Futian[11], the turnover periods of the heavy metals in this studied community are shorter. Because the studied community is young in age, the turnover periods of the elements are related to the age of the community. The older the community is, the longer turnover periods of the elements would be[12].

2.4.4 Absorption coefficient, ultilization coefficient and cycle coefficient of the 5 elements in the community

Absorption coefficient, utilization coefficient and cycle coefficient of 5 heavy metallic elements in the community may be calculated according to the standing crop, uptake, return and pod amount in the surface soil[13, 14]. From that, we could know some cycling characteristics in the community, such as the element utilization and return ratio. Absorption coefficients, utilization coefficients and cycle coefficients of the 5 elements in the community are presented in Table 8. It is shown in Table 8 that the sequence of absorption coefficients of the 5 heavy metal elements is Zn > Cu > Pb > Ni > Cr, that of utilization coefficients is Cu > Zn > Ni > Pb, Cr, and that of cycling coefficients is Cu, Pb > Cr > Ni, Zn. Sequences of the three coefficients of the 5 elements are distinct.

Tab. 8 Absorption coefficient, utilization coefficient and cycle coefficient of 5 heavy metals in the community

Elements	Absorption coefficient	Utilization coefficient	Cycle coefficient
Cu	0.000 62	0.284 6	0.482 3
Pb	0.000 16	0.113 7	0.488 1
Zn	0.000 82	0.204 7	0.348 3
Cr	0.000 06	0.124 8	0.476 7
Ni	0.000 13	0.153 2	0.324 6

3 Conclusion

S. apetala + *S. caseolaris* artificial forest communities in Futian, Shenzhen Bay are able to absorb and accumulate heavy metal elements such as Cu, Pb, Zn, Cr, Ni and so on. Among the plants, *S. caseolaris* absorbs the five elements most effectively, followed by *S. caseolaris*, and the least does *Kandelia candel*. As a result of the accumulation of heavy metal pollutants in the mangrove plants, in a way, the pollution on the secondary consumers and ecological environment decreases. The mangrove estuary bay and the mangrove wetland ecosystem have been looked as the convenient place for discharging the polluted domestic and industrial water. However, it is, in fact, still a problem needed to be tackled whether the discharging of the polluted water does good to the mangrove plants or what effects of the discharging are on the other creatures (birds and bottom animals) living in the same ecosystem [15~18]. Shenzhen Bay is located between the two big cities, Shenzhen and Hong Kong. Therefore, arising from the liquid and solid waste pollution, the pressure on and threat to the bay become more and more serious. The pollution of heavy metals in the Shenzhen Bay becomes more and more critical because of the city construction, industrial development and population growth. To maintain the Shenzhen Bay as an important global wetland, and especially an important habitat of migratory birds in the world, we should make full use of the purifying function of the mangrove forest. At the same time, in order to ensure the stable state and sustainable development of wetland ecosystem of the Shenzhen Bay, the discharging of the domestic and industrial wastes without any proper

treatment should be forbidden and controlled strictly.

Acknowledgments

This study is supported by the Key Program of National Natural Science Foundation of China (39830310), and Science and Technology Department of Shenzhen (99-1-33).

References

[1] Wang Yongjun, Lin Peng, Song Xiaojun. Annual Dynamics of Water Birds at Futian Mangrove Zone, DeepBay, Shenzhen, China. Journal of Xiamen University (NaturalScience), 1998,37(1):122-129.

[2] Wang Yongjun, Zan Qijie.The Changes of Land Birds' Species and Its Protection in Futian Mangroves, Shenzhen, China. Journal of Xiamen University (NaturalScience),1999, 38(1):137-144.

[3] Zan Qijie, Wang Yongjun, Liao Baowen *et al.* The Structure of *Sonneratia apetala* + *S. caseolaris-Kandelia candel* Mangrove Plantations of Futian, Shenzhen. Forest Research, 2001, 14(6):610-615.

[4] Zan Qijie, Wang Yongjun, Liao Baowen *et al.* Biomass and Net Productivity of *Sonneratia apetala*, *S. caseolaris* Mangrove Man-made Forest. Journal of Wuhan Botanical Research, 2001, 19(5):391-396.

[5] Institute of soil science , Chinese Academy of Science. Analysis of Physical and Chemical Property of Soil. Shanghai: Shanghai Science Press. 1978, 62-72.

[6] Zheng Wenjiao, Lin Peng. Accumulation and Distribution of Cu, Pb, Zn and Cd in *Avicennia marina* Mangrove Community of Futian in Shenzhen. Oceanologia et Limnologia Sinica, 1996, 27(4):386-393.

[7] Zheng Wenjiao, Zheng Feng, Lian Yuwu *et al.* Accumulation and Dynamics of Cu, Pb, Zn and Mn Elements in *Kandelia candel* L. Druce Mangrove Community of Jiulong River Estuary of Fujian. Acta Botanica Sinica, 1996, 38(3):227-233.

[8] Zheng Wenjiao, Lian Yuwu, Zheng Fengzhong *et al.* Accumulation and Dynamic of Heavy Metal Elements in *Rhizophora stylosa* Community at Yingluo Bay in Guangxi. Acta Phytoecologica, 1996, 20(1):20-27.

[9] Biology department of Yunnan University. Plant Ecology. Beijing: Science Press. 1980, 310-316.

[10] Golley F B. Production and Elements Cycles (Li Wenhua translated, 1982), Translations Selection of Plant Ecology (Vol. 4), Beijing: Science Press. 1975, 124-134.

[11] Zhang Jinhong, Li Mei, Pan Nanming. Absorption, Accumulation and Cycle of Several Heavy Metals by Mangrove.Environment Science of Yunnan, 2000, 19(Supp):53-56.

[12] Zhang Hongda, Chen Guizhu, Liu Zhipin *et al.* Study on Futian Mangrove Wetland Ecosystems, Shenzhen. Guangzhou: Guangdong Sci & Tech Press. 1998, 46-47.

[13] Chen Lingzhi, Lindley D K. Nutrient Cycling Hampsfell Bracken Grassland Ecosystem England. Acta Botanica Sinica, 1983, 25(1):67-74

[14] Larcher W. Physiological Plant Ecology (Li Bo *et al* translated. 1982) (2 st Edn), Beijing: Science Press. 1975, 159-161.

[15] Nedwell D B. Sewage Treatment and Discharge into Tropical Coastal Waters. Ecology, 1974, 5(5):187-190.

[16] Clough B F, Boto K G, Attiwill P M. Mangrove and Sewage: a Re-evaluation. In: Teas HJ ed. Biology and Ecology of Mangrove. Vol. S. Lancaster: Dr Junk W Publicshers. 1983, 151-161.

[17] Boto K G. Nutrients and Mangrove. In: Connell D W, Hawker D W ed. Pollution in Tropical Aquatic Systems. Ann Arbor, London: CRC Press Inc. 1992, 129-145.

[18] Breaux A, Farber S, Day J. Using Natural Coastal Wetland Systems for Wastewater Treatment: an Economic Benefit Analysis. J Envir Mgmt. 1995, 44:285-291.

Effect of $NaNO_3$ Concentrations on the Growth and Fatty Acid Compositions of *Nitzschia closterium* and *Chaetoceros gracilis**

Liang Ying (梁 英), Mai Kangsen (麦康森), Sun Shichun (孙世春)
Key Laboratory of Mariculture, Ministry of Education, Ocean University of Qingdao, Qingdao 266003

Abstract Fatty acid compositions of two strains of marine diatoms *Nitzschia closterium* (MACC B222) and *Chaetoceros gracilis* (MACC B13) have been examined. The microalgae have been grown at different initial $NaNO_3$ concentrations (75, 375, 750, 1 125, 1 500, 1 875 mg/L) and harvested at the late exponential phase. The results by one factor analysis of variance show that the $NaNO_3$ concentrations have no significant influence on the relative growth rate of two strains of marine diatoms; the influence of $NaNO_3$ concentrations on the fatty acids differs from species to species. The major fatty acids of two diatom strains are 14:0, 16:0, 16:1n−7 and 20:5n−3 (EPA), B13 also has high percentage of 20:4n−6 (6.0 ~ 9.1%).

Keywords *Nitzschia closterium*, *Chaetoceros gracilis*, $NaNO_3$, relative growth rate, fatty acid

1 Introduction

It has long been recognized that culture conditions play a major role in determining the quantity and quality of lipids produced by microalgae. The fatty acid compositions of a certain algal strain are not only determined by its heredity, but can also be modified by different growing conditions (water temperature, salinity, light intensity, medium compositions *etc.*)[1~8]. Nitrogen source and concentration often have dramatic effect on the biochemical profile of microalgae[2, 3, 9]. Studies have been carried out on the effects of different initial $NaNO_3$ concentrations on growth and fatty acid compositions of two strains of marine diatoms (*Nitzschia closterium* and *Chaetoceros gracilis*), and the results are presented in this report.

2 Materials and Methods

2.1 Microalgal strains

The following two strains of marine diatoms are obtained from the Microalgae Culture Center (MACC), Ocean University of Qingdao.

Nitzschia closterium MACC /B222

Chaetoceros gracilis MACC/B13

2.2 Culture conditions

Cultures are carried out using 3-L flasks with f/2 medium except initial $NaNO_3$ concentration[10] at (22 ± 1) ℃. The initial $NaNO_3$ concentrations are 75, 375, 750, 1 125, 1 500 and 1 875 mg/L,

Received on July 5, 2002; aceepted on April 10, 2003
* Project supported by the Hi-Tech "863" programs of the Ministry of Science and Technology, China (863-819-02-01)

respectively. Cultures are repeated in triplicate for each $NaNO_3$ concentration. The salinity of all culture media is adjusted to 28 with distilled water before sterilization. Successive aeration is supplied. The light intensity is 5 000 lx (using fluorescent tubes as light source). Relative growth rate K is calculated during the logarithmic phase as:

$$K = (\log_{10} N_1 - \log_{10} N_0) / T_1 - T_0$$

Where N_1 = cell density at time 1 (T_1) and N_0 = cell density at time 0 (T_0).

2.3 Harvest

The cell density for each microalgal culture is determined every day with a haemocytometer. The cultures are centrifuged (4 000 rev/m) at the late exponential phase. Vacuum dried samples are preserved at −40 ℃ in test tubes filled with nitrogen until analysis.

2.4 Fatty acid analysis

A modified method of Volkman *et al.*[11] is used to analyze fatty acids with an HP5890II gas chromatograph fitted with a carbowax capillary column (30 m × Φ0.25 mm). High purity N_2 is used as the carrier gas at a flow rate of 2 ml • min^{-1}, injector and detector temperature is 280 ℃. The oven is programmed from 150 ℃ to 200 ℃ at 15 ℃ • min^{-1}, then to 250 ℃ at 2 ℃ • min^{-1} and held at 250 ℃ until all peaks have appeared. Fatty acid methyl esters are identified by comparing the retention times of experimental samples to those of known standards.

2.5 Statistical analysis

Means and standard deviation are calculated by Excel software. All experimental data are analyzed using a one factor ANOVA followed by a post hoc Tukey test to determine differences between specific means.

3 Results

3.1 Relative growth rate

The effect of $NaNO_3$ concentrations on the relative growth rate of two strains of diatoms is shown in Table 1.

Tab. 1 The relative growth rate of two strains of marine diatoms

Initial $NaNO_3$ concentrations(mg/L)	Relative growth rate (X±S)	
	Nitzschia closterium (MACC/ B222)	Chaetoceros gracilis (MACC/ B13)
75	0.39±0.02	0.36±0.01
375	0.40±0.02	0.38±0.01
750	0.41±0.00	0.37±0.00
1 125	0.40±0.00	0.34±0.01
1 500	0.42±0.01	0.35±0.03
1 875	0.41±0.01	0.36±0.02

When the initial $NaNO_3$ concentrations increase from 75 mg/L to 1 875 mg/L, the relative growth rate of B222 and B13 are 0.39 ~ 0.41 and 0.34 ~ 0.38, respectively. The results by one factor analysis

of variance show that the $NaNO_3$ concentrations have no significant influence on the relative growth rate of two strains of marine diatoms ($P > 0.05$).

3.2 Fatty acid compositions

The fatty acid compositions of B222 and B13 cultured at different initial $NaNO_3$ concentrations are shown in Tables 2 ~ 3. The results in Tables 2 ~ 3 indicate that the influence of $NaNO_3$ concentrations on the fatty acid compositions differs from species to species.

Tab. 2 Effect of initial $NaNO_3$ concentrations on the fatty acid compositions of *Nitzschia closterium* MACC /B222 [Expressed in percentage of total fatty acids, % (X±S)]

Fatty acids	$NaNO_3$ concentrations (mg/L)					
	75	375	750	1 125	1 500	1 875
Saturates						
14:0	4.9 ± 0.1^{abc}	4.4 ± 0.4^{b}	5.6 ± 0.6^{c}	4.6 ± 0.2^{b}	4.5 ± 0.1^{b}	6.5 ± 0.1^{d}
15:0	0.2±0.2	0.3±0.1	0.3±0.0	0.3±0.1	0.3±0.1	0.3±0.0
16:0	25.7±1.3	23.8±0.8	22.8±3.6	23.4±0.2	23.0±2.1	24.4±0.8
18:0	0.7±0.1	0.6±0.1	0.4±0.0	0.5±0.1	0.5±0.1	0.6±0.1
Sum / %	31.5	29.1	29.1	28.8	28.3	31.8
Monounsaturates						
16:1 n−9	1.1±0.2	0.4±0.1	1.1±0.1	1.1±0.6	0.6±0.0	0.5±0.1
16:1 n−7	42.6 ± 1.7^{a}	42.7 ± 0.6^{a}	38.5 ± 0.4^{b}	40.5 ± 1.7^{ab}	34.3 ± 0.8^{c}	39.4 ± 0.2^{b}
18:1 n−9	3.5±0.7	3.3±0.1	3.4±0.1	3.6±0.0	4.0±0.3	3.3±0.2
18:1 n−7	1.1 ± 0.0^{a}	0.9 ± 0.1^{ac}	0.5 ± 0.2^{b}	1.0 ± 0.3^{ac}	0.9 ± 0.1^{abc}	0.7 ± 0.1^{bc}
Sum / %	48.3	47.2	43.5	46.2	39.8	43.9
Polyunsaturates						
16:2 n−7	0.5±0.0	0.6±0.1	0.7±0.1	0.7±0.1	0.7±0.2	0.6±0.4
16:2 n−4	0.7±0.0	0.8±0.0	0.7±0.1	0.7±0.0	0.6±0.1	0.8±0.1
16:3 n−4	1.3 ± 0.1^{a}	1.6 ± 0.1^{b}	1.8 ± 0.1^{bc}	1.6 ± 0.1^{b}	1.6 ± 0.1^{b}	2.0 ± 0.1^{c}
16:4 n−1	0.6±0.1	0.8±0.0	0.5±0.0	0.7±0.1	0.8±0.2	0.7±0.4
18:2 n−6	1.0 ± 0.1^{a}	1.0 ± 0.0^{a}	1.1 ± 0.0^{ab}	1.4 ± 0.1^{bc}	1.4 ± 0.2^{bc}	1.5 ± 0.1^{c}
18:3 n−6	0.6±0.1	0.6±0.0	0.6±0.0	0.6±0.0	0.6±0.0	0.6±0.0
18:3 n−3	0.1±0.1	0.2±0.1	0.3±0.1	0.2±0.1	0.3±0.1	0.2±0.1
18:4 n−3	0.5 ± 0.1^{a}	0.7 ± 0.1^{ac}	0.6 ± 0.1^{a}	0.7 ± 0.1^{ac}	0.9 ± 0.0^{b}	0.9 ± 0.1^{bc}
20:4 n−6	0.5 ± 0.1^{a}	0.5 ± 0.0^{a}	0.5 ± 0.1^{a}	0.8 ± 0.1^{a}	1.4 ± 0.5^{b}	0.2 ± 0.3^{a}
20:4 n−3	0.5±0.1	0.4±0.0	0.5±0.1	0.4±0.1	0.6±0.3	0.7±0.2
20:5 n−3	8.4 ± 0.4^{a}	10.5 ± 0.1^{b}	10.8 ± 0.4^{b}	10.6 ± 0.4^{b}	12.6 ± 0.6^{c}	12.8 ± 1.5^{c}
22:6 n−3	0.4±0.1	0.7±0.1	0.5±0.1	0.9±0.0	0.9±0.1	1.1±0.7
Sum / %	15.1	18.4	18.6	19.3	22.4	22.1

The major fatty acids of B222 are 14:0 (4.4 % ~ 6.5 %), 16:0 (22.8 % ~ 25.7 %), 16:1n−7 (34.3 % ~ 42.7 %) and 20:5n −3 (EPA) (8.4 % ~ 12.8 %). The results by one factor analysis of variance show that the $NaNO_3$ concentrations have extremely significant influence ($P < 0.01$) on the 14:0, 16:1n−7, 16:3n−4 and EPA fatty acids; have significant difference ($P < 0.05$) on the 18:1n−7, 18:4 n−3 and 20:4n−6 fatty acids; and have no significant difference on other fatty acids ($P > 0.05$). The EPA content increases with the increase of $NaNO_3$ concentrations and maximizes at 1 875 mg/L (12.8 %).

Tab. 3 Effect of initial $NaNO_3$ concentrations on the fatty acid compositions of *Chaetoceros gracilis* MACC/B13 [Expressed in percentage of total fatty acids, % (X±S)]

Fatty acids	$NaNO_3$ concentrations (mg/L)					
	75	375	750	1 125	1 500	1 875
Saturates						
14:0	26.9±2.0	30.9±2.3	29.1±3.9	32.6±0.3	26.6±3.1	28.3±1.7
15:0	0.6±0.1	0.6±0.1	0.7±0.1	0.5±0.1	0.4±0.1	0.6±0.0
16:0	7.9±0.8	10.5±4.4	11.9±2.1	8.9±0.1	10.4±2.5	10.6±1.1
18:0	0.7±0.3	0.6±0.1	0.5±0.1	0.9±0.4	0.8±0.1	0.5±0.1
Sum%	36.1	42.6	42.2	42.9	38.2	40.0
Monounsaturates						
16:1 n−9	0.8±0.0	0.7±0.2	0.7±0.2	1.2±0.5	1.5±0.1	0.8±0.1
16:1 n−7	28.1±2.8	28.6±2.6	30.7±2.2	26.2±2.6	28.8±2.7	30.0±2.5
18:1 n−9	1.1±0.1	0.9±0.1	0.9±0.5	1.2±0.0	0.8±0.0	1.0±0.1
18:1 n−7	0.5±0.1	0.7±0.1	0.6±0.1	0.7±0.4	0.7±0.4	0.4±0.0
Sum%	30.5	30.9	32.9	29.3	31.8	32.2
Polyunsaturates						
16:2 n−7	1.0±0.1	1.0±0.3	0.9±0.3	1.1±0.1	1.6±0.4	1.1±0.4
16:2 n−4	1.3±0.1	1.3±0.1	1.3±0.3	1.4±0.4	0.8±0.3	1.0±0.3
16:3 n−4	2.0±0.1	1.6±0.4	1.5±0.2	1.7±0.6	2.1±0.2	1.7±0.1
16:4 n−1	0.1±0.1	0.6±0.1	0.5±0.1	-	0.2±0.3	-
18:2 n−6	$2.3±0.0^{a}$	$1.9±0.1^{ab}$	$2.0±0.3^{a}$	$2.1±0.3^{a}$	$1.3±0.1^{b}$	$2.1±0.4^{a}$
18:3 n−6	$2.5±0.0^{a}$	$1.9±0.4^{ab}$	$2.0±0.1^{ab}$	$1.4±0.1^{b}$	$1.2±0.1^{b}$	$2.4±0.5^{a}$
18:3 n−3	-	-	0.1±0.1	-	0.2±0.1	0.2±0.0
18:4 n−3	$0.4±0.1^{ac}$	$0.4±0.1^{abc}$	$0.4±0.1^{abc}$	$0.1±0.1^{b}$	$0.3±0.0^{ab}$	$0.6±0.1^{c}$
20:4 n−6	8.1±0.6	7.2±1.7	6.0±2.6	9.1±0.4	6.5±0.1	7.7±0.4
20:4 n−3	0.1±0.1	-	-	-	-	-
20:5 n−3	10.0±0.6	7.0±1.6	6.5±1.1	7.8±1.1	9.5±1.1	8.1±0.5
22:6 n−3	1.5±0.4	1.4±0.1	1.3±0.6	1.5±0.1	1.5±0.1	1.0±0.1
Sum / %	29.3	24.3	22.5	26.2	25.2	25.9

Notes: "-" not detectable; Values with different superscripts in the same row indicating significant differences ($P < 0.05$)

The major fatty acids of B13 are 14:0 (26.6 % ~ 32.6 %), 16:0 (7.9 % ~ 11.9 %), 16:1n−7 (26.2 % ~ 30.7%), 20:4n −6 (6.0 % ~ 9.1%) and EPA (6.5 % ~ 10.0 %). The results by one factor analysis of variance show that the $NaNO_3$ concentrations have significant influence ($P < 0.05$) on the 18:2n−6 and 18:4n−3 fatty acids; and have no significant influence on other fatty acids ($P > 0.05$). The $NaNO_3$ concentrations have no significant influence on the EPA content, the EPA content shows a decrease tendency with the increase of $NaNO_3$ concentrations and maximizes at 75 mg/L (10.0 %).

4 Discussion

A wide range of fatty acid content has been reported for different diatoms[2,6,8,11,12~14]. The results indicate that almost all diatoms contain high proportions of 14:0, 16:0, 16:1(n−7) and 20:5(n−3) fatty acids. C_{18} and C_{22} PUFAs are minor constituents[11]. This paper shows that the two diatoms both contain high proportions of 14:0, 16:0, 16:1(n−7) and 20:5(n−3) fatty acids. This result is consistent with that of other authors. But the fatty acids profiles of B13 are different from that of B222, B13 contains higher 14:0 (26.6 % ~ 32.6 %) and 20:4n−6 (6.0 % ~ 9.1%) but lower16:0 (7.9 % ~ 11.9 %). The difference may be resulted from different species.

Nutrient concentration often has a dramatic effect on the biochemical profile of microalgae with variations dependent on the species and the nutrients provided. Nitrogen content of the medium has been reported to affect the proportion of saturated to unsaturated fatty acids in many microorganisms. Under nitrogen stress, *Dunaliella bardawil* and *D. salina* produce a higher percentage of EPA[15]. In contrast, the proportion of PUFAs in the freshwater algae *Chlorella* and *Phaeodactylum tricornutum* increases at high nitrogen concentrations[16]. Grima[17] reported that for concentrations below 2 mmol/L $NaNO_3$, the PUFAs and EPA content of the total fatty acids increases with increasing $NaNO_3$ concentration. The results of Yongmanitchai and Ward (1991) indicate that EPA production in *Phaeodactylum tricornutum* UTEX640 increases from 9.1 % to 32.1 % of the total fatty acids when nitrate concentration increases from 0.25 g/L to 1.5 g/L, but nitrate levels in excess of 1.5 g/L reduce biomass dry weight and EPA production[4].

Our results indicate that the effect of $NaNO_3$ concentration on the fatty acid profiles differs from one species to the other. $NaNO_3$ concentration has significant influence on most fatty acids of B222 ($P < 0.05$) but only significant influence on the 18:2 n−6 and 18:4 n−3 fatty acids of B13. This may result from different microalgal species. The EPA content of B222 has an increase tendency with the increase of $NaNO_3$ concentration, while the EPA content of B13 has a decrease tendency with the increase of $NaNO_3$ concentration. The diatoms often have a lower DHA content (often below 2 %); the $NaNO_3$ concentration has significant influence ($P < 0.05$) on the DHA content of B222 but no significant influence on the DHA content of B13.

In conclusion, the biochemical properties of microalgae change when the culture conditions change. The effect of nitrogen concentration on the microalgal fatty acid compositions depends on the range of nitrogen concentration and different microalgal species. Our aim is to select the culture conditions to produce microalgal feeds of the appropriate nutritional value for bivalves, penaeid prawns, rotifers, brine shrimps and shrimps under culture.

References

[1] Alonso D L, Grima E M, Sanchez Perez J A *et al.* Isolation of Clones of *Isochrysis galbana* Rich in Eicosapentaenoic Acid. Aquculture, 1992, 102: 363-371.

[2] Ben-Amotz A, Tornabene T G, Thomas W H. Chemical Profile of Selected Species of Microalgae with Emphasis on Lipids. J Phycol, 1985, 21: 72-81.

[3] Brown M R, Dunstan G A, Norwood S J *et al.* Effects of Harvest Stage and Light on the Biochemical Composition of the Diatom *Thalassiosira pseudonana.* J Phycol, 1996, 32: 64-73.

[4] Chen Mingyao. Living Food Culture. Beijing: Agriculture Publishing Company. 1995, 65-71.

[5] Grima E M, Sanchez Perez J A, Garcia Sanchez J L *et al.* EPA from *Isochrysis galbana*: Growth Conditions and Productivity. Process Biochem, 1992, 27: 299-305.

[6] Kayama M, Araki S, Sato S. Lipids of Marine Plants. In Marine Biogenic Lipids, Fats, and Oils. Volume II (ed. R G, Ackman) CRC Press, Florida, 1989, 4-21.

[7] Piorreck M, Baasch K, Pohl P. Biomass Production, Total Protein, Chlorophylls, Lipid and Fatty Acids of Freshwater Green and Blue-green Algae under Different Nitrogen Regimes. Phytochemistry, 1984, 23: 207-216.

[8] Reitan K I, Rainuzzo J R, Olsen Y. Effect of Nutrient Limitation on Fatty Acid and Lipid Content of Marine Microalgae. J Phycol, 1994, 30: 972-979.

[9] Renaud S M, Parry D L, Thinh L V *et al.* Effect of Light Intensity on the Proximate Biochemical and Fatty Acid Composition of *Isochrysis sp.* and *Nannochloropsis oculata* for Use in Tropical Aquaculture. J Appl Phyco, 1991, 3: 43-53.

[10] Tan C K and Johns M R. Screening of Diatoms for Heterotrophic Eicosapentaenoic Acid Production. J Appl Phycol, 1996, 8: 59-64.

[11] Teshima Shin-ichi, Yamasaki S, Kanazawa A *et al.* Effects of Water Temperature and Salinity on Eicosapentaenoic Acid Level of Marine *Chlorella.* Bull Jpn Soc Sci Fish, 1983, 49(5): 805.

[12] Thompson P A, Harrison P J, Whyte J N C. Influence of Irradiance on the Fatty Acid Composition of Phytoplankton. J Phycol, 1990, 26: 278-288.

[13] Viso A C and Marty J C. Fatty Acids from 28 Marine Microalgae. Phytochemistry, 1993, 34(6): 1 521-1 533.

[14] Volkman J K, Jeffrey S W, Nichols P D *et al.* Fatty Acid and Lipid Composition of 10 Species of Microalgae Used in Mariculture. J Exp Mar Biol Ecol, 1989, 128: 219-240.

[15] Yongmanitchai W and Ward O P. Growth and Omega-3 Fatty Acid Production by *Phaeodactylum tricornutum* under Different Culture Conditions. Appl Envir Microbiol, 1991, 57: 419-425.

[16] Zhou Hongqi, Renaud S M, Parry D L. Effect of Temperature on Growth, Total Lipid Content and Fatty Acid Composition of the Microalgae, *Nitzschia closterium, Nitzschia paleacea* and *Pavlova sp.* J Fish China, 1996, 20: 235-240.

[17] Zhukova N V and Aizdaicher N A. Fatty Acid Composition of 15 Species of Marine Microalgae. Phytochemistry, 1995, 39(2): 351-356.

Characteristics of Heavy Minerals Composition and Distribution in Jiulong River Estuary Sediment *

Xu Maoquan (徐茂泉), Li Chao (李超), Xu Wenbin (许文彬), Sun Meiqin (孙美琴)
Institute of Subtropical Oceanography, Xiamen University 361005

Abstract The bottom sediment samples were gathered during island investigation in 1994 and in the period of carrying out the natural science fund project of Fujian in 1999. The composition, distribution and assemblage characteristics of heavy minerals which granularity distributes from 0.063 to 0.125 mm in the sediment from Jiulong River estuary are studied in the paper. The results show that there are 49 kinds of heavy minerals and the average content of them is 9.38 %. The dominant and characteristic minerals are magnetite, hematite, epidote, ilmenite, limonite, hornblende, zircon, andalusite, biotite and so on. 4 mineral assemblage zones (Ⅰ.The watercourse gateway of Jiulong River mineral zone, Ⅱ. The northern estuary of Jiulong River mineral zone, Ⅲ. The southern estuary mineral zone, Ⅳ. The eastern estuary of Jiulong River mineral zone), can be divided based on the heavy mineral contents and the distribution characteristics, which not only relates to the matter sources but also is controlled by hydrodynamic condition and the sedimentary environment in the Jiulong River estuary.

Keywords Jiulong River estuary, heavy mineral distribution characteristics, mineral assemblage, sedimentary environment

1 Introduction

Jiulong River is the second largest river in Fujian. Its drainage area covers 1.47×10^4 km^2 and consists of the north, west and south streams flowing into the sea, which becomes the Jiulong River estuary on the southern beach of Haicang Taiwan Business Area of Xiamen. According to the observation and the statistics from the Pu'nan and Zhendian hydrological stations, annual runoff volume reaches 15 Gm^3 and the total silt input is 2.23 Mt, with a maximum of 6.47 Mt. A great deal of silt being taken by Jiulong River mostly deposit inside the estuary by mechanical sedimentary differentiation and form the subaquatic delta of Jiulong River estuary.

The subaquatic delta of Jiulong River estuary is a violent silting region and processes eastward 28 m every year between 1958 and 1976. It annually deposits 3～4 m with a sedimentation rate of 17 cm/a. Although the sedimentation rate slows down now, it slowly processes toward the gateway of Jiulong River. It seriously affects inland river shipping and threats the shipping safety of Xiamen West Port and the new-built Haicang Port. Therefore the source, diffusion , deposition of silt and the rush-silting change of surmarine geomorphy have been followed with great interest[2~7].

The study of mineral composition in submarine deposits is very important to clarifying the process of sedimentation. It not only shows the composition, distribution pattern and matter source of the sediments, but also makes out further the source of eroded zone and transformation regularities of

Received on December 10, 2002; accepted on March 15, 2003
*The natural science fund of Fujian (Numbering item: D9910006)

transported minerals. In the past, although some authors had done many different researches of deposited detrital minerals in this region[5, 6], the conclusions were not unanimous and the special research work on heavy minerals of very-fine sand (0.063 ~ 0.125 mm) has not been done. So, to further reveal the matter source and diffusion regularities, the composition, distribution and assemblage sediments of Jiulong Estuary are studied in this paper, so as to explore the relationship between estuary sediment environment and hydrodynamics, which can supply the scientific basis for channel protection and port-building in the Xiamen Special Economic Zone.

2 Sampling and analytical methods

2.1 Sampling

34 deposited samples were obtained in December, 1994 and in October, 1999 by the grab dredger machine (0.025 m^2) and stored in lab. Sampling stations are shown in Fig. 1.

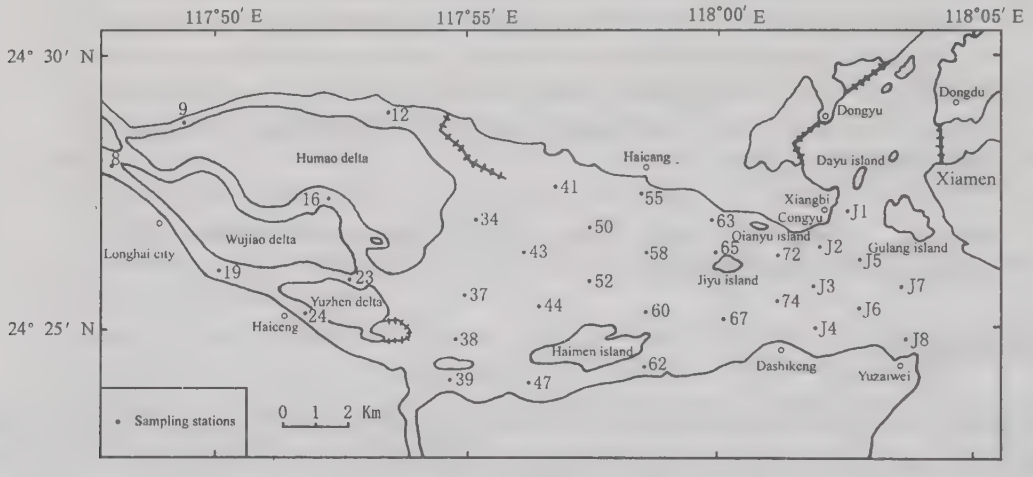

Fig. 1 Distribution of sampling stations

2.2 Analytical methods

According to marine survey standards[1], 1.5 g of sample is cleaned with 2×10^{-3} oxalate sodium and analyzed in each station, then the samples are separated with diluted tribromo methane ($CHBr_3$, with a specific gravity of 2.85 at 20℃). The light and heavy minerals are separately washed with industrial alcohol and distilled water, then the weight percentage content of light and heavy minerals are obtained. Light and heavy minerals are identified with a high resolution binocular entity microscope and 500 grains of them are counted with the stripped-band method. Some transparent minerals (10 %) are examined with immersion-oil under a petrographic microscope, and some minerals are also tested with chemical analysis. Finally the percentage content of each kind of minerals is calculated respectively.

1) Book IV of the Marine Survey Standards of the State Oceanic Administration, 1975

3 Results

3.1 Composition characteristics of heavy minerals

The results show that there are 49 heavy minerals (0.063 to 0.125 mm) in the surface sediments of Jiulong Estuary (Tab. 1), and most of them are terrigenous detrital minerals while a few are marine anthigenic minerals. Among them, silicate minerals occupy 51 %, oxide and hydroxid occupy 26.53 %, carbonate and phosphate minerals are 8.16 % and 6.12 %, sulfide minerals own 4.08 % and sulphate and halide exist occasionally, only 2.04 % respectively.

Tab. 1 Heavy mineral composition

Content	Mineral name
Major	magnetite, hematite, epidote, ilmenite, limonite, hornblende, zircon
Secondary	leucoxene, andalusite, apatite, zoisite, clinoisite, biotite, muscovite, granet, xenotime, monatime, tiurmaline, sphene, anatase, rutile, actinolite, topar, variant zircon, dolomite
Minor	augite, diopside, hyperthene, fluorite, corundum, fergusonite, phlogopite, chlorite, staurolite, cyanite, sillimanite, wollastonite,thorite, broohite, barite, cassiterite, piedmontite, allanite, siderite, rhodochrosite, goethite, chalcopyrite, pyrite, malachite

3.2 Distribution characterstics of heavy minerals

3.2.1 Distribution characterstics of heavy mineral content

The content percentage of heavy minerals with granularity of 0.063 to 0.125 mm is 1.12～22.98 and its average is 9.38 (Fig. 2).

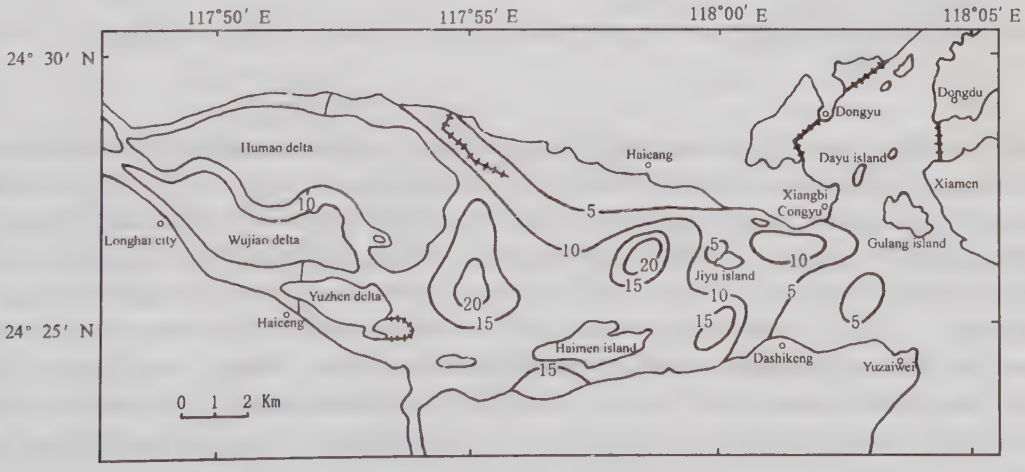

Fig. 2 Weight percentage content distribution of heavy minerals

There are 4 regions where the heavy minerals' content exceeds 15 % as shown in Fig. 2, distributing in the west of Jiulong River estuary, the west of Jiyu Island, the south of riffle region and the inshore zone in western watercourse of Haimen. The regions with an extremely high content of more than 20 % locate at the No.37 and No.58 stations respectively and the region with a low content of less than 5 % locates at the inshore of the southern Haicang and the eastern deep water zone between Xiangbi and Dashikeng Bay. As a whole, the variation gradient isoline of heavy minerals content of Jiulong River estuary changes acutely and decreases from west to east and from south to north.

3.2.2 Distribution characteristics of major dominant minerals

Tab.2 lists the grain percentage content and appearance odds of 7 major heavy minerals in the surface sediments of Jiulong Estuary which are magnetite, hematite, epidote, ilmenite, limonite, hornblende and zircon. It can be figured out that the content of 7 major heavy minerals is 82.59 %. The magnetite and epidote can be found in each sample station and their contents are 36.92 % and 11.45 %, so they can be regarded as the major dominant minerals in the study area.

Tab. 2 Percentage content of major heavy minerals

Mineral name	Content	Average content	Occurrence probability
Magnetite	16.51～60.22	36.92	100
Hematite	7.31～23.94	12.03	97
Epidote	3.01～21.45	11.45	100
Ilmenite	1.54～17.94	8.13	91
Limonite	1.72～24.18	7.78	85
Hornblende	0.92～8.21	4.36	82
Zircon	0.19～5.38	1.92	76

Fig. 3 and Fig. 4 show the distribution of grain percentage contents of magnetite and epidote, in which there are 4 high-value regions of magnetite which content is greater than 40 %: ① the north, middle and south branch stream riverbeds of Jiulong River and the eastern estuary fan-shaped zone; ② the underwater riffle region to the west of Jiyu Island; ③ Haimen watercourse and its east and west sides; ④ the north watercourse of Jiyu Island (also named Qianyu pool). The very-high-value region of magnetite (> 50 %) locates at the western 58th and the southern 67th stations of Jiyu Island. However, the low value region (< 30 %) mainly locates at Haicang inshore (the 41th and 55th stations) and the area nearby the bay mouth. So the distribution characteristics of magnetite is very similar to that of heavy minerals. Their high and low value regions are quite anastomosed and the isoline change gradient is great. There also exits an obvious change trend of decreasing from north to south and from west to east. However, the content distribution characteristics of epidote (Fig. 4) is simpler and its high value region (> 15 %) locates in the northwest estuary, but the low value region

(< 5 %) only locates in the small area near the western Jiyu Island (the 58th station), showing an obvious change trend of decreasing from west to east and from north to south.

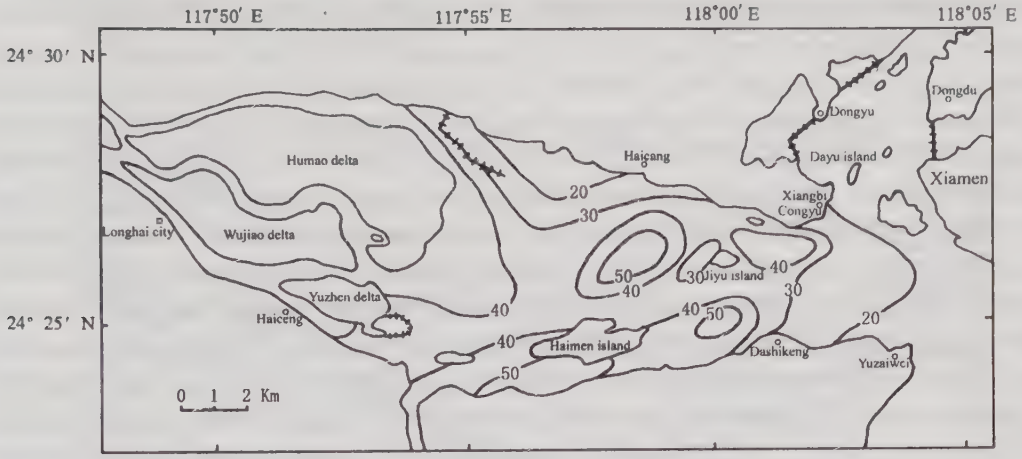

Fig. 3 Distribution of grain percentage content of magnetite

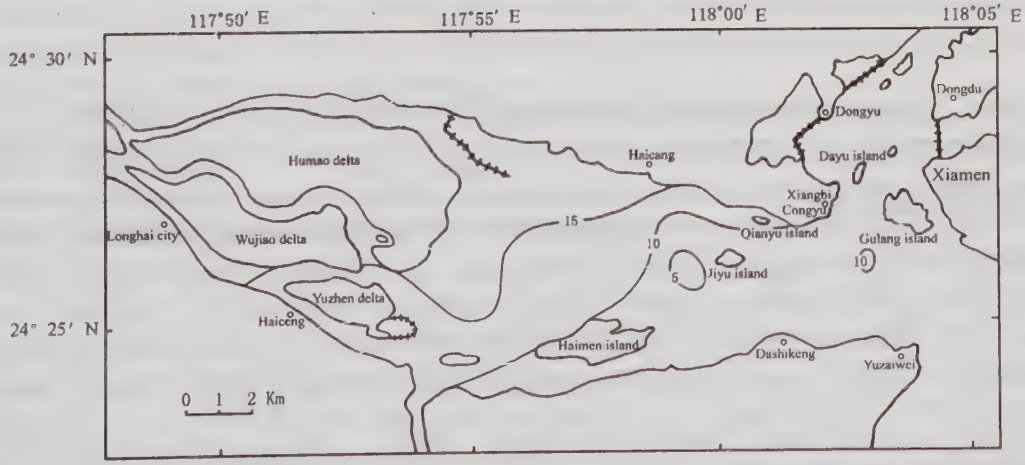

Fig. 4 Distribution of grain percentage content of epidote

The isoline of other five major heavy minerals (hematite, ilmenite, limonite, hornblende, zircon) suggests that the distribution characteristic of ilmenite and zircon is quite similar to that of magnetite, and those of hematite, limonite, hornblende is similar to that of epidote.

3.3 Assemblage zones of heavy minerals

Based on the content and dominance of heavy metals as well the distribution features of characteristic minerals and in the light of hydrodynamic factors and bottom types, the Jiulong estuary is divided into 4 mineral assemblage zones (Fig. 4). Each mineral assemblage type and its dominance, and the mean grain percentage content of characteristic minerals are shown in Tab. 3.

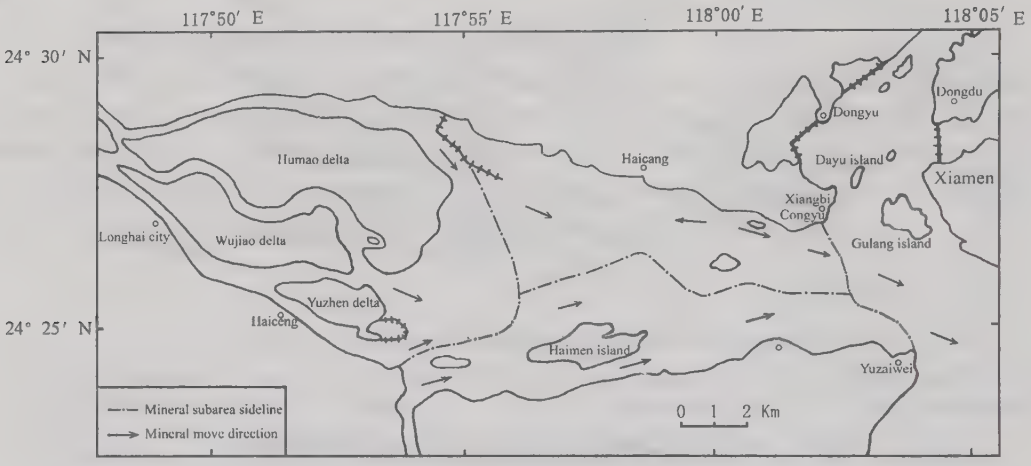

Fig. 5 Assemblage zones and removal direction of heavy minerals

Tab. 3 Grain percentage contents of main mineral in the heavy mineral assemblage region

Mineral subarea	Sample number	Heavy mineral	Mineral name								
			Magnetite	Hematite	Epidote	Ilmenite	Limonite	Hornblende	Zircon	Andalusite	Biotite
I	10	12.66	43.66	11.58	16.26	8. 92	7.93	4.05	1.65	0.63	0.42
II	9	6.02	31.52	12.75	10.83	4.04	8.55	4.34	1.23	1.05	1.16
III	10	12.18	42.47	9.67	8.92	11.92	6.50	3.63	2.93	1.98	0.39
IV	15	3.25	22.04	16.32	8.01	6.33	8.65	6.47	1.68	1.72	3.51

I The watercourse gateway of Jiulong River mineral zone: The assemblage zone of magnetite-epidote-hematite-ilmenite which distributes in the north, middle and south branch streams and the outlet of Jiulong River estuary. Major minerals consist of magnetite, epidote, hematite and ilmenite, and subordinate minerals are limonite, zircon, *etc.* Their shapes are granular or columnar with intact crystal, for example, zircon has graved cylindrical surface and double-tetragonal pyramid combinate;

but the magnetite is mostly an octahedron or is granular in shape and a few are rhombic dodecahedrons. The content of major medium-coarse grit in the sediments is greater than 50 %, the value of Md ϕ is 0.8 ϕ and it is well-sorted or very well-sorted. Probability curve shows two-sect type and there exits mainly saltation and suspension transport. This indicates that there are a strong fluviatile action and a high-energy sedimentary environment subjected to the tidal current action.

II The northern Jiulong River estuary mineral assemblage zone: The assemblage of magnetite-hematite-epidote-hornblende is scattered over the northern out-riffle region of Jiulong River estuary. Major minerals consist of magnetite, hematite, epidote, limonite and hornblende and the subordinate minerals are ilmenite, zircon, biotite and so on. The sediment mainly consists of medium-fine sand (86.54 %[2]) and a few medium-coarse grit, grit and gravel sand. However, the silt-mud is dominant in the nearshore and the grain is coarser in the tidal passageway. The probability cumulative curve presents a three-sect type. They are traction, saltation and suspension transport, but saltation is more important. The sedimentation includes fluviation, tide and wave actions. The distribution of surface sediments shows that the tidal current action strengthens gradually from estuary inside to seashore outlet and there exists a coarse-fine interphase and interbed apprearance of sediments in the deposit section; however, sea-way action happens mainly inshore and produces an obvious winnowing action to nearshore sediments.

III The southern estuary mineral assemblage zone: The assemblage of magnetite-ilmenite-zircon - andalusite is scattered over the southern out-riffle region of Jiulong River estuary. Major minerals consist of magnetite and ilmenite; the characteristic mineral contents of zircon and andalusite are obviously higher than those of I and II mineral regions. Sediment types and sedimentation are similar to that of II mineral region. The only difference lies in the fact that tractional load granulites taken by the south branch stream of Jiulong River spread eastwardly in the south of Haimen watercourse up to the north of Dashikeng and form a zone of deposition with medium-coarse grit parallel to the coastline. This shows the violent river dynamic action.

IV The eastern Jiulong River estuary mineral assemblage zone: The combination of hematite-limonite-hornblende-biotite distributes the eastern bay mouth of Jiulong River estuary (the southern sea areas of Gulang Island) where there are wider sea areas, even submarine relief, sloping towards the southeast slightly with the gradient within 1/1000. But the water depth ranges from 14 to 18 m and the deepest point can be up to 25 m. Major minerals consist of magnetite, hematite, limonite, hornblende and biotite; subordinate minerals are epidote, ilmenite, andalusite, zircon, *etc.* Silt-mud is major sediment type and the average value of Md ϕ is 8.92 ϕ . It is well-sorted and the percentage content of mud is greater than 60 %. However, the content of coarser sand (Md $\phi < 4\ \phi$) is smaller than 10 %. Sedimentation gives priority to the suspended particles carried by tidal current. This suggests that the hydrodynamic action is weaker and it belongs to the low energy sedimentary environment.

4 Discussion

4.1 Sources and diffusion of matters

On the basis of the above research, 49 heavy minerals (Tab. 1) are examined from surface sediments of Jiulong River estuary which mainly come from terrigenous detrital minerals. But the weight percentage content of magnetite (Fig. 3) and their isolines take on an obvious change trend of

decreasing gradually from west to east (from inside to outside). This indicates fully that the matter sources are middle and upper reaches of the Jiulong River and the estuary peripheral region. In terms of regional geology, different periods of the Yanshanian acid and medium-acid intrusive rock, igneous rock and dynamometamorphic rock are widely distrubuting in the drainage area of Jiulong River and its debouch peripheral region. Rock type is mainly common kali-type which belongs to calc-alkaline series. Lithology mainly consists of granodiorite (K_1Y), moyite (K_1M, K_1G, J_3N), biotite-adamellite (K_1X, T_3N), dacitic or rhyolite tuff, welded tuff, tuff lava, rhyolite (Je^2, Jx^d), *etc.* These rock mass or rocks mostly have porphyritic or porphyroid granitic texture and their phenocryst is potash feldspar and quartz; but the matix commonly contains potash feldspar, plagioclase, quartz, hornblende, pyroxene, biotite, *etc.* So the accessory mineral has high content and many species, which different peridical intrusive rock accessory minerals mainly have magnetite, titanite, zircon, monazite *etc.* However, igneous rock accessory minerals mainly have allanite, xenotime, thorianite, granet, fluorite, andalusite *etc.* It has very developed epidotization between every rock mass and the surrouding rock exocontacts. Invariable mineral and accessory mineral of rock mass or rock mentioned above are basically intercorresponding to heavy minerals in the surface sediments of Jiulong River estuary. This indicates further that the Jiulong River sediments mainly come from the drainage area of Jiulong River and the weathering or erosion products originating from the bedrock of the debouch peripheral region.

Due to people's weak consciousness of ecological conservation, the destruction of forests for land reclamation is getting out of control, accelerating damage to the earth's surface and the serious erosion. The silt content of Jiulong River increased sharply from 12 g/m^3 in the 1950s to 33 g/m^3[3] in the 1980s. Even so the suspended silt in the Jiulong River estuary and outport has 42.1 g/m^3 on average content which can reach 1 462.5 g/m^3[1] by testing the bottom layer content. According to the statistics, the silt coming from the upper reaches of Jiulong River has increased sharply 3~5 times in recent forty years from 1.13 Mt in 1952 to 3.60 Mt in 1988 and largely can be up to 5.65 Mt[3]. A large mass of silt has filled up the river bed near the inlet of Jiulong River estuary and most of the sand is carried to the estuary riffle. That can fasten its rate of sedimentation. However, suspended fine-grained matters (fine silt and clay of $d > 6\ \phi$) continue to diffuse eastwardly and so enhance the sedimentation of seashore outlet.

It can be figured out from Fig.5 that the migration and diffusion trend of very fine-silt matters can be drawn in the light of content change of heavy minerals (0.063～0.125 mm) and distribution and assemblage characteristics of major standard minerals. The results suggest that the immigration of deposit detrital minerals is identical to the diffusion of silt which is influenced by hydrodynamic condition and marine bottom configuration. All can be seen as follows.

4.2 Factors influencing distribution and assemblage of heavy minerals

4.2.1 Hydrodynamic conditions

Hydrodynamics not only plays an important role in transporting and changing sediment detrital matters, but also is a primary agent of affecting and controlling distribution and combination of heavy minerals. A great amount of terrestrial detrital matters carried into sea by Jiulong River come into the unique estuary environment and consequentlly undergo transfer, change, group selection, redistribution and combination, so as to adapt to the sediment environment formed by different hydrodynamic conditions which fits for their particle diameter and specific gravity.

1) Runoff

Jiulong River runoff mostly affects recent deposition of Jiulong River estuary and can influence Jiyu Island nearby. As the Jiulong River estuary region is a drowned estuary shaped like an overturned ampulla with a big belly but small mouth, which is completely different from the classic funnel-shaped or infundibuliform estuary, e.g., Hangzhou Estuary, its tidal effect is not so intense as the latter and only forms an estuarine riffle controlled by runoff and tidal current to the west of Jiyu Island. And because the north, middle and south branch streams are different in the declined flow rate at respective outgate, for example, flowing rate of north branch stream decelerates very soon after flowing into sea and the runoff action rapidly dwindles; but the south breach stream still keeps a stiff torrent and a strong runoff action; the middle stream is between the two, the eastward extending scopes and distances of the medium-coarse grid deposited in the river beds of the three branch streams are different: the north one extends for a short distance and on a small scope; the middle one becomes a typical fan to the east of the mouth and extends 2.5 km toward sea; but the south one extends eastwardly far along nearshore to Dashikeng and Yuzaiwei vai the Haimen watercourse. This pattern is more prominent in the flood period: the total estuary silt content can surpass 0.3 g/m^3 and reaches 0.8 g/m^3 in the south, so the high concentration turbid water obviously deviates south during the flood; the whole estuary turbidity is very small after the flood period; but the asymmetric phenomenon is still obvious between south and north, the northern Congyu-Haicang region is a "limpidity water" region with a lower content of silt. This fully suggests that the estuarine south is a main passage between the runoff of Jiulong River and the silt flowing into sea; at the same time, this is the primary reason why the content isoline of heavy minerals and the content distribution of characteristic minerals with very big specific gravity (magnetite, ilmenite, zircon *etc.*) present a trend of being high in the south and low in the north and of decreasing gradually from west to east.

The runoff action of south stream is very small and weakens promptly after having flowed into sea. And it flows eastward through the Haimen watercourse after converging with the south branch stream. It is mainly a transport canal for some minerals such as andalusite, hornblende, *etc.* The former originates from metamorphic igneous rock and the latter comes from the granodiorite in the south stream area, but its acidic intrusive rock is the source rock of magnetite. Therefore, it plays an important role in forming the southern estuary mineral zone.

2) Tidal current and residual current

Jiulong River estuary is an important part of Xiamen harbour, and its tide belongs to the regular semidiurnal tide. The tidal range is 2.85 m during the neap tide, the maximum tidal range is 6.42 m and the mean tidal range is 4.95 m (according to the record, 1962—1982), and the highest tidal range may have reached 7.77 m in history (1933.10. 23). The tidal current is a reciprocal current, and also has the character of a standing wave. At flood-tide, it flows into the gulf, and flows out of the gulf at ebb tide. Because of the influence of the topography, the flowing direction varies with place. Vertically the rate of surface layer is usually bigger than that of bottom; Horizontally, in general the deep waterway current velocity is bigger than the riffle one. For the narrow waterway, the current velocity is the maximum, and in the broad riffle, the current velocity is the minimum. It is shown by the observed data that in each place the current velocity at ebb tide is bigger than that at flood- tide, except to the north of Jiulong River[1]. During the spring tide, the maximum current velocity of the bottom layer can exceed 1.5 m/s, and those of the middle, and upper layers can exceed 2.0 m/s[3]; The residual current velocity is smaller, in general ranging between several cm/s and 10 cm/s, and its

flowing direction is different because of topography, with each sea region forming an independent system, while the residual current forms a counterclockwise circulation at the Jiulong River estuary[1].

Tidal current and residual current are the main force of transporting harbour sediment, and the periodical water fluctuation with not quite big energy can winnow and sort debris in the intertidal riffle, which can be partly carried away by ocean current. The tidal current plays a more prominent role in the tidal passageway or similar landform unit, where its velocity is 10 times more than the residual current, and at the same time, to the submarine sediment it has very strong erosion and transportation ability; the energy of residual current is little, but its flowing direction is stable relatively. Therefore, residual current, especially that of the bottom layer also plays an important role in the migration of sediment[5]. According to observation and analysis, in most cases, in the Jiulong River, the flowing directions of the residual current and the tidal current in the same layer are coincidental with aech other[4]. It is shown in this paper that there is a close relationship among heavy mineral, tidal current and residual current according to the heavy mineral distribution characteristics. For example, the bottom residual current is NWW with moderate energy all the year to the south and north of Jiyu Island in Jiulong River, and the corresponding sediment is just magnetite and zircon with greater specific gravity, *etc.*, which is the weathering and erosion material of moderate acid tuff lava in Jiyu Island (the 58th station of zone III). At the same time, the epidote and hornblende in the monzonitic granite are mainly deposited in the nearby sea areas, and controlled by runoff and granodiorite from Jinshan to Haicang. Therefore, there forms the combination of magnetite-hematite-epidote-hornblende in this sea area (zone II). In addition, there is a zone where heavy minerals and magnetite are enriched between Haimen Island and Haicang to the west of Jiyu Island, and at the outlet of the north waterway to the northeast of Jiyu Island (Fig.2 and Fig.3). The location of the former is just the zone which is affected by the counterclockwise circulation, and also the zone where bottom residual currents converge[4], while the latter lies in the riffle of channel in Haicang. According to survey data[10], in this riffle the velocity of tidal current diminishes gradually from the surface to the bottom layers with a maximum current velocity of only 1.06 ~ 1.37 m/s, appearing frequently in the subsurface layer. Because of topography, the tidal current is bifurcated and diffused in this place, and the current velocity slows down obviously, forming a tranquil flow zone in the riffle, which is helpful for silt sediment action. The general trend of residual current is that the surface layer is outward (SE) in this riffle (SE), with a current velocity of 10 cm/s; while the bottom layer is inward (NW), with a current velocity of 5 ~ 10 cm/s. For the horizontal distribution of residual current, the calculated results from using the two-dimensional variable boundary tidal current mathematic model indicate[7] that the northeast sea area of Jiyu Island and the southeast sea area of Xiangbi (riffle region) have greater counterclockwise circulations. This kind of distribution of residual current is also helpful for sedimentation there. According to hydraulics equivalent principle[12], the heavy minerals (0.063 ~ 0.125 mm) are transported in suspension or saltation. Such distribution characteristics of tidal current and residual current in the riffle region weaken the water power, which is helpful for the heavy minerals with very fine sand equivalent to precipitate, while the smaller tidal and residual current velocity can't again trigger the subsided heavy mineral. Therefore, the Jiulong River estuary riffle region often is also the high value region of heavy mineral.

3) Wave

Xiamen region belongs to the subtropical marine monsoon climate, with the constant wind direction of northeaster, but mainly southeaster or southwester in summer. The typhoon season

prevails in the months from July to September annually and the wind power ranges from force 7 to 10 , the maximum of which can reach more than force 12[1]. Jiulong River estuary is dominated by wind waves, the frequency of which is 88 %[1]. The region has been shielded by many islands nearby, and has a shorter distance of wind transport, but at climax, under forces 4～5 winds, the inshore riffle along bank above −2 m and the coast around still lie within the effective influence of the wind waves. If there is a typhoon or strong northeaster, the influence of wind waves will strengthen, and the sediment nearby the bank will be susceptible to tilt, and the magnitude of sand in waters will increase dramatically. Driven by wave and longshore current, one part of the silt falls and deposits in the bank beach bottom, while the other part transports into the underwater riffle and the channel along with the current and diffusion. The isobath of the riffle with small depth to the west of Jiyu Island mostly is within 5 m, and, with the winnowing of strong wave, it is helpful for sorting and enriching of the heavy mineral with different specific gravities. That is perhaps the reason why the isoline with the content of the heavy mineral > 10 % mainly distributes in the sea area to the west of Jiyu Island (Fig. 2).

4.2.2 Submarine geomorphy

As mentioned above, Jiulong River estuary has a big belly but a small mouth , and it is a drowned estuary like an overturned ampulla. The gulf inside width is 7 km, the gulf mouth width is 4 km, and the submarine topography inclines from west to east (from gulf inside to gulf mouth), sloping nearly 2/1000[1]. The water depth in the gulf inside usually is 5 m, the underwater riffle is well-developed, and they extend like finger from gulf inside to gulf mouth, between which the tidal ditch waterway zigzags and forms complex submarine geomorphy.

Underwater riffle region is the main sediment part of front bed in Jiulong River estuary subaquatic delta and its sediment is medium-coarse and medium-fine sand containing clay, with an average diameter of 1~1.5 Φ larger than Cha River district. Here is the shallow sedimentary environment where river and seawater exchange frequently, tidal current and wave play the role together, so large amounts of terrigenous clastic matter piled up here, and transported by runoff from the Jiulong River estuary, are once again subjected to tilting, sorting, removal and deposition, thus resulting in a different distribution of various heavy minerals; At the same time, because the rate of sedimentation is rapid here, most of the riffle region locates over the low-water line. Though the water depth of several tidal current grooves is greater, making them the major passageway of the estuary transport, with underwater riffle silt constantly rising and moving down, its navigation ability is lower than in the past. Fifty ～ sixty years ago, for example, the south channel of Jiyu Island from Xiamen to Shima can allow the 500 t class steam ship with a draft of 3.5 m to pass through without being influenced by the tidal level, now only ships with less than 100 t, and a draft of 1.5～1.8 m, must navigate following tide; the riffle in Haicang channel at the outlet of north waterway in Jiyu Island is an obstruction to navigation, where the landform is slightly protruding, the top is flat, and the slope is gentle, inclining to the east like a covex bank. The present water depth is 7～8 m, and that in the shallowest place is only 6.7 m[7]. It lies across the deep channel of north waterway in Jiyu Island and the Xiamen harbour waterway, it is also the channel to Haicang new harbour that ships will have to go through, which has an obvious debris barrier feature. The research of heavy minerals in this paper shows that here is just the high value region for the average content of magnetite and heavy minerals (Fig. 2 and Fig. 3). According to Ref. [7], from 1974 to 1986, this riffle generally silted up and it total siltation thickness was up to 20~30 cm, with an average silting rate of 1.6～2.5 cm/a. Given unceasing supply of silt from the Jiulong River, it has become an unrefutable fact that the entire Jiujing

River estruary riffle zone is now still slowly silting up. Therefore, it is important to desilt and dredge the south and north channels of Jiyu Island. Otherwise, there will be serious threats to shipping in Jiulong River downstream and the new harbour that has been built recently in the Haicang investment zone, and directly affect the sustained development of Xiamen special economic zone.

The submarine geomorphology is broad and flat in the north sea area of Gulang Island and to the east of riffle region, with a water depth of generally more than 10 m, so it is the weak silting district in Xiamen harbour tidal current riffle, where the sediment is mainly silt clay. Because its matter sources are mainly the suspended matter diffusing to east with ebb tide which is a part of the sediment flowing from the Jiulong River into sea, and the suspended sediment carried from the open ocean during flood tide, its mineral combination (Ⅳ) is different from that in the riffle region in the estuary, and the content of hornblende and biotite with small specific gravity *etc.* is higher than that of other 3 mineral zones (Tab. 3).

5 Summary

1) There are 49 kinds of heavy minerals with granularity 0.063～0.125 mm in the sediment of surface layer from Jiulong River, which are mainly terrigenous detrital minerals, and only a few authigenic minerals. The dominant and characteristic minerals are magnetite, hematite, epidote, ilmenite, limonite, hornblende, zircon, andalusite, biotite *etc.* The average content of heavy minerals is 9.38 %.

2) Four mineral assemblage zones can be divided based on the heavy mineral contents and the distribution characteristics, which not only relate to the matter sources but also are controlled by the hydrodynamic conditions and the sedimentary environment in Jiulong River estuary.

3) The distribution characteristics of heavy minerals show that the transport of sediment detrital mineral is consistent with the diffusion of sediment. In view of the fact that the riffle region in Jiulong River estuary is now still slowly silting, it is imperative to desilt and dredge the south and north channel of Jiyu Island. Moreover, it should be noted that, only by protecting our environment and reducing soil erosion, can we avoid siltation of the navigation channel and port.

References

[1] Liu Weikun *et al.* The Change of Submarine Geomorphy and Silting in Xiamen harbour. Taiwan strait, 1984, 3(2): 179-188.

[2] Liao Shuimu *et al.* The Distribution Feature of Submarine Sediment Type in Xiamen harbour. Taiwan strait, 1987, 6(2): 158-166.

[3] Cai Aizhis *et al.* The Diffusing of Sediment Enter Sea and the Modern Sediment of the Gulf in Jiulong River estuary in Fujian. marine geology and the Quaternary geology, 1991, 11(1): 57-67.

[4] Chen Jinquan. The Effect to the Transport for Sediment and Contaminant Tidal Current and Residual Current of Xiamen gulf. Taiwan strait, 1985, 4(1): 17-19.

[5] Hong Huiliang. Xiamen Hong Kong's Heavy Mineral Research. Marine journal, 1993, 15(3): 49-62.

[6] Xu Maoquan. The Research of Detrital Mineral in the Sediment of Surface layer from Jiulong River estuary. J. Xiamen university (natural science edition), 1994, 33(5): 675-680.

[7] Liu Weikuns *et al.* The Form and Develop of the Riffle in Xiamen Haicang harbour. Taiwan strait, 1994, 13

(4): 317-322.

[8] Chen Lilong *et al.* The Research of the Heavy Minerals Assemblage and the Distribution Characteristics in Bohai sediment. Oceanologia et Limnologia Sinica, 1980, 11(1): 46-64.

[9] Huang Quanzhen *et al.* edit. Fujian Province Geologic Map (1: 500000) Specification. Fuzhou: Fujian province map press, 1998, 58-69.

[10] National Marine Department 3th Marine Research Institute. The Comprehensive Survey Report of Marine Environment in Xiamen harbour (II). Taiwan strait, 1988, 7(1): 36-96.

[11] Xu Maoquan, Chen Youfei edit. Marine Geology. Xiamen: Xiamen university press,1999, 137-142.

[12] Liu Baojun *et al.* edit. Petrographic Ancient Geography Foundation and Working Method.Peking: Geology impress. 1985.

Study on the Release of Grouper *Epinephelus* for Stock Enhancement

Bo Zhili (薄治礼), Zhou Wanxia (周婉霞)
Marine and Fishery Research Institute of Zhejiang Ocean University and Marine Fisheries Research Institute of Zhejiang Province, Zhoushan 316100

Abstract Two methods, tagging and ink injection, are used in the grouper releasing experiment. The studied fishes are the juvenile of *Epinephelus akaara* and *Epinephelus awoara* both artificially cultivated and caught from natural waters, and their wild adults. Experimental results show that the inhabiting behaviours for both juvenile and adult fishes show distinct regionality, which move within an area of 2 n mile diameter 651 days and 48 days after being released, respectively. With the tagging method, the tagged fishes could only be recaptured in the year of release while, with the injection method, they could be caught in the 1st, 2nd and 3rd years. It is confirmed that in the cement tank, the tagged fishes lose their 1/3 tags. That means that the tagging method is not fit for the release research while the injection method is. Generally, the recaptured rates of injected fishes are 1.4 ~ 4.5 %, 3.1 ~ 13.4 % and 2.7 % for the 1st, 2nd and 3rd years, respectively.

Keywords grouper, enhancement, release

The grouper *Epinephelus* belongs to the fishes of *Serranidae*, widely distributing in the warm waters of the Pacific and Indian Oceans. Rich in variety, it has had 31 species recorded in the offshore sea of China, among which 30 species are in the South China Sea, 8 ~ 9 in the East China Sea and one in the Yellow Sea[1]. Distributed in the coastal waters of Zhejiang are mainly *E. akaara* and *E. awoara.* The grouper *Epinephelus* is a rare edible marine fish. Inhabiting the rock and reef waters, it always hides in the rock caves or gaps in daylight and does not move for long distances, thus depicting distinct regionality. It is an androgynous, female-premature transsexual fish with a long life cycle. Its population age structure is complex and its stock cannot be easily recovered once it has degenerated; Also, owing to the localization of inhabitation, its reserves in a particular fishing ground are not large and once it is overfished, its stock would easily degenerate[2]. As the grouper *Epinephelus* has higher economic value and the fishermen may benefit a lot from it, the fishing intensity is constantly increasing, so that its stock is now fluctuating or being reduced. Therefore, it is essential to enhance its natural stock by means of artificial release. The earliest experiment on the release and enhancement of the grouper *Epinephelus* was reported to be in 1980 when the Marine Fisheries Research Institute of Zhejiang Province released 100 wild adults in the waters around Huangxing Island of Zhoushan, with a recaptured rate of 10% that year[3]. The earliest marking release of the juvenile grouper *Epinephelus* was also carried out by the Marine Fisheries Research Institute of Zhejiang Province in September, 1987, when it released 1 051 marked juveniles, self-cultivated, in the Zhujiajian waters of Zhoushan, and, subsequently, a certain number of juvenile grouper *Epinephelus* has been released every year. Between 1987 and 1995, it had released a total of 164 384 fishes[4]. It was reported that the Naruto Branch of the Fisheries Testing Ground of Tokushimaken, Japan had released 3 000 juvenile grouper

Received on March 6, 2003; accepted on April 22, 2003

Epinephelus in Kameura Harbour near the Naruto-kaikyō in may, 1989[5]. No other reports than this have been available. This paper describes the experiment and results of the marked release of grouper *Epinephelus* by the Zhejiang Marine Fisheries Research Institute and preliminarily discusses the methods of marking and the feasibility of artificially enhancing the stock of grouper *Epinephelus*.

1 Materials and methods

1.1 Origin, size and quantity of the released fish

Most fishes to be released are artificially cultivated fries, which come from the parent male and female fishes of *E. awoara* and *E. akaara* through intensified raising in the Xishan Testing Ground by the grouper *Epinephelus* Project Group of the Institute. The parent male and female fishes are made to spawn naturally and fertilize, and the fertilized eggs are hatched and cultivated artificially to become the juvenile grouper *Epinephelus* with a body length of 3 cm and more. A total of 164 486 grouper fishes were released in 1980 and 1987 ~ 1995, among which 100 in 1986 are the wild adults captured by angling, a small portion in 1991 and 1992 was the wild juveniles caught by angling and the rest are the self-cultivated juveniles.

1.2 Marking methods for released fishes

1.2.1 Tagging method

The marking method adopted in 1980 and 1987 is the tagging method. The tag is a small rectangular, and hexagonal red plastic one, with the two sides engraved with the characters "Zhejiang Provincial Marine Fisheries Research Institute" and the numbering. To one end of the tag are tied two stainless steel wires with a diameter of about 0.21 mm and a length of 50 mm. The tag is 12 mm long and 5.5 mm wide, and the total weight of the tag and the wires is about 0.1 ~ 0.4 g. The marked portion is the fin membrane between the first and second fin spines of the back fin on the fish body. In actual operation, the tag is tied to the fish body by getting the stainless wire on the tag through the fin membrane.

1.2.2 Ink injection method

The LATEX ink injection method was employed in 1991, in which the LATEX colouring liquid made in Japan was used and subcutaneously injection into the back of the fish to be released. The length of the colouring liquid injected was about 1 ~ 2 cm and the colour of the liquid is red or green.

In 1987, the fin-clipping method was tried. But this method would impair the image of the fish, so it is not discussed in this paper.

1.3 Selection of releasing sites

In this experiment, two types of releasing sites are chosen. One is the operation sea area for grouper *Epinephelus* production, such as the Bogumen Waters of Zhujiajian Xiaoao Waters; The other is not the traditional operation sea area for grouper *Epinephelus* production, but has the environmental conditions suitable for the living of the fish, such as the waters around Xishan Island. The time of release is chosen at the ebb and flood slack during the neap tide. Before the release, such environmental factors in the releasing ground as seawater salinity, SST, dissolved oxygen, pH value and transparency, *etc.* are measured.

1.4 Check on the results of release

The results of release are checked mainly according to the tagged fish recovered. Firstly, the foreign-trade purchasing station is entrusted to recover the tagged fish. Most grouper *Epinephelus* fishes caught by fishermen are purchased by the foreign trade corporation, so the purchasing station is the most important distributing centre; Secondly, notices for recovering the tagged grouper are put up in the focal fishing villages where the grouper *Epinephelus* is caught and, at the same time, notices are delivered to the local fisheries administrative department, striving for its propaganda for and assistance in recovering the tagged fish; Thirdly, broad masses of fishermen are to be interviewed so as to expand propaganda and collect as far as possible the data on recapture. In addition, appropriate incentive standards are established in order to recover more tagged fishes. For those who have with them recaptured tagged fish samples and the data on the time place of recapture, a certain amount of money award would be given to them apart from purchasing their fish products at a price higher than the market price. Those who provide the data on recapture but without samples would also be given some bonus as appropriate. The data from the latter would be checked against the original record of release before they are adopted.

2 Results

2.1 Survey of releasing operations

In 1980, 1987 ~ 1995, a total of 164 486 grouper fish were released, among which 2 087 was the tagged fish. Except in 1980 when the wild adult groupers was released, most fishes released in other years were the self-cultivated grouper fries. The released artificial fish fries range from 3 to 22 cm in body length and 1.3 ~ 220 g in body weight. The sites of release are mainly in the Zhoushan sea area. See Table 1 for the releasing operations in different years.

2.1.1 Zhujiajian waters

Release has been carried out twice in the Zhujiajian waters. The first release was on Sept. 14, 1987, when 1 051 tagged and fin- clipped grouper were released in the Bogumen waters with the tagged ranging from 4.5 ~ 22.1 cm in body length and from 4.2 to 220 g in body weight. The second release was conducted on Sept. 5, 1991, when 451 grouper fries marked with the injection method were released in the Xiaoao waters of Zhujiajian, among which the artificially cultivated fries range from 3.5 cm to 520 cm in body length, with a mean of 4.0 cm; from 3.3 g to 5.2 g in body weight with a mean of 4.2 g; The wild fries range from 11.0 cm to 17.3 cm in body length with a mean of 15.6 cm; from 50 g～155 g in body weight, with a mean of 109.6 g.

2.1.2 Xishan Island waters

The place of release is in the waters near Houlongkou to the north of Xishan Island. One kind of grouper fries are tagged and the other not tagged. On Sept. 5, 1991, 67 grouper fries marked with the injection method were released, among which the artificially cultivated fries range from 3.0 cm to 6.0 cm in body length, with a mean of 3.4 cm, 3.1 g to 6.2 g in body weight with a mean of 3.3 g; the wild fries range from 13.0 cm to 17.7 cm in body length, with a mean of 16.0 cm; 73 g to 145 g in body weight, with a mean of 121.7 g. Every year between 1988 and 1995, in the waters to the north of Xishan Island were released a certain amount of artificially cultivated non-tagged fries, over 3 cm in total body length and over 3 g in body weight.

2.1.3 Other water areas

In May～July, 1980, 100 tagged wild groupers were released in the waters around Huangxing Is. of the Zhongjieshan Archipelago, including Miaoao, Yutouzui, Waiyupan, Niaoshijiao, Xiaohuangshan, Anjiao, Tiedingzui, *etc.* their body lengths ranging from 11.0 cm to 34.0 cm and body weights from 40 g to 1 010 g.

Tab. 1 Schedule of artificial marking grouper in 1980, 1897 ~ 1995

Year	Number	Location of release	Body length (cm)	Body weight (g)	Marking methods	Remarks
1980	100	Sea area surrounding Huangxing Is., Zhongjieshan	11 ~ 34	40 ~ 1 010	Tagging	Wild adult
1987	1 051	Bogumen waters of Zhujiajian, Putuo	4.5 ~ 22.1	4.2 ~ 220	Tagging	Fin-clipped artificial fries of the same year and of the previous year
1988	3 890	Sea area to the north of Xishan Is., Putuo	3.0 ~ 5.9	1.3 ~ 4.7	No mark	Artificial fries of the same year
1989	1 657	Sea area to the north of Xishan Is., Putuo	3.0 ~ 4.1	1.3 ~ 2.5	No mark	Artificial fries of the same year
1990	14 222	Sea area to the north of Xishan Is., Putuo	3.4 ~ 6.4	1.8 ~ 6.8	No mark	Artificial fries of the same year
	11 300	Sea area of Haizhamen, TAimen, Liuheng, putuo				
1991	451	Xiaoao waters, Zhujiajian, Putuo	3.5 ~ 17.3	3.3 ~ 155	Injection method	Most are artificial fries of the same year, a small amount of wild fries
	24 269	Sea area north of Xishan Is., Putuo	3.0 ~ 17.7	3.1 ~ 145	67 fish with injection method	
1992	418	Southwest of the Xihu Harbour Mouth, Xiangshan Habour	10.0 ~ 21.20	40 ~ 280	Injection method	Artificial fries of the same year, and wild fries
	31 182	Sea area north of Xishan Is.	2.9 ~ 6.7	3.2 ~ 10.0	No mark	Artificial fries of the same year
1993	15 000	Sea area north of Xishan Is.	3.0 and more	3.0 and more	No mark	Artificial fries of the same year
1994	10 000	Sea area north of Xishan Is.	Over 4.0	About 5	No mark	Artificial fries of the same year
	48 000	Sanheng Is. waters L hua, Shengsi				
1995	3 000	Sea are north of Xishan Is.	Over 3.5	Over 3	No mark	Artificial fries of the same year
Total	164 486					

On Aug. 10, 1990, 11 300 artificially cultivated grouper fries without tags were released in the waters of Haizhamen, Taimen, Liuheng, Putuo, with their body lengths ranging from 3.4 cm to 6.4 g and body weights from 1.8 g to 6.8 g.

On Sept. 20, 1992, 418 artificially cultivated grouper fries of the same year and wild fries tagged

with the ink injection method were released in the southwest of the Xihu Harbour mouth of Xiangshan Harbour, with their body lengths ranging from 10.0 cm to 21.2 cm and body weights from 40 g to 280 g.

In 1994, 48 000 artificially cultivated grouper fries without tags were released in the Shanhengdao waters of Luhua, Shengsi, with their body lengths ranging from 4 cm to 5 cm and body weights over 5 g.

2.2 Temporary cultivation test of tagged fish

Between 1987 when a large number of tagged groupers were released, and 1990, only those released in 1987 have been recovered. Therefore, in 1991, the experiment on the short-term temporary cultivation of tagged fish was made to find out about the activity and survival rate of tagged fish. In 1991, stones were placed in the $20m^3$ cement pond of the Institute's Xishan Testing Ground to simulate the bottom environment for natural inhabitation by grouper. On July 26, 31 tagged grouper fries were put into the pond, their body lengths ranging from 12.8 cm to 17.7 cm, and body weights from 70 g to 180 g. It was found from observation that after 16 days' temporary cultivation, the tags of 6 grouper fish fell off on August 8, amounting to 19.4 % of the fish temporarily cultivated; on September 1, the tag of one fish fell off amounting to 3.2 % and on September 2, the tags of three fish fell off, amounting to 9.7 %. After more than one month's temporary cultivation from July 26 to September 2, nearly one third of the tags fell off. During the temporary cultivation, no tagged fish were found dead with a survival rate of 100 %.

2.3 Refishing of tagged groupers and rate of refishing (Fig. 1, 2) (Tab. 2)

Fig. 1 Sketch map of release and refishing of tagged groupers

2.3.1 Zhujiajian Waters

For the tagged grouper released in 1987, only two were refished in the waters near the place of release in Bogu on Sept. 15 of the same year (*i.e.*, the second day after release), but since then no tagged fish have been recovered.

For the tagged grouper marked with the injection method and released in 1991, 40 grouper fish with red and green colouring marks were recaptured in the waters near the place of release in Xiaoao on September 5 (*i.e.*, the day of release). The recaptured tagged fish range from 14.0 cm to 16.1 cm in body length and from 100 g to 150 g in body weight. As they are captured on the day of release, they are counted in the rate of refishing.

On June 13 ~ August 28 of 1992, the second year of release, 14 grouper fish with red and green marks were recaptured in the waters around Mount Zhaifeng and Mount Wuzei of Zhujiajian, with their body lengths ranging from 17 cm to 21 cm and body weights from 125 g to 255 g. The refishing rate in the second year is 3.1 %.

Tab. 2 Schedule of refishing of tagged grouper

Location	Date	Tagging No.	Body length (cm)	Body weight (g)	Number of fish	Rate of refishing (%)	Days of release	Moving distance	Remarks
Surrounding waters of Huangxing Is.	May ~ July, 1980	C	No	230 ~ 715	10	10	12 ~ 48	B	8 (handline), 2 (Cuttlefish trawl)
Bbogumen waters of Zhujiajian	Sept.15, 1987	89317 121522	6.0 ~ 8.8	6.2 ~ 9.1	2	/	2	A	Shrimp trawl
	Sept.15, 1987	Red Green	14.0 ~ 16.1	100 ~ 150	40	/	1	A	Handline
Surrounding waters of Zhujiajian	Jun. 13 ~ Aug. 28, 1992	Red Green	17.0 ~ 21.0	125 ~ 255	14	3.1	282 ~ 385	B	Handline
	Jun.17, 1993	Red	26.0 ~ 27.0	520 ~ 560	3	0.67	651	A	Handline
Water area north of Xishan Is.	Sept. 20, 1991	Green	5.6 ~ 16.5	6.0 ~ 135	3	4.5	15	A	1 (handline), 2 (pull net)
	Jul. 25 ~ Aug. 11, 1992	Green	18.0 ~ 19.8	185 ~ 220	9	13.4	309 ~ 326	A	Handline
Water area of Xihu Harbour Mouth of Xiangshan Harbour	Oct. ~ Nov., 1992	Green	No	No	6	1.4	41	A	Filter net, seine net

Note: 1. The fish captured on the day of release or the next day are not counted.

2. For the moving distance, A represents less than 1 n mile; B represents less than 2 n mile.

3. For the tagging number C, the numbers are 88241, 88249, 88273, 88275, 88293, 88297, 88299, 88285.

On Jun. 17, 1993, the third year of release, 3 grouper fish with green marks were recaptured in the waters around Mt. Zhaifeng and Mt. Wuzei, with body lengths ranging from 26 cm to 27 cm and body weights from 520 g to 560 g. the refishing rate in the third year is 0.7 %.

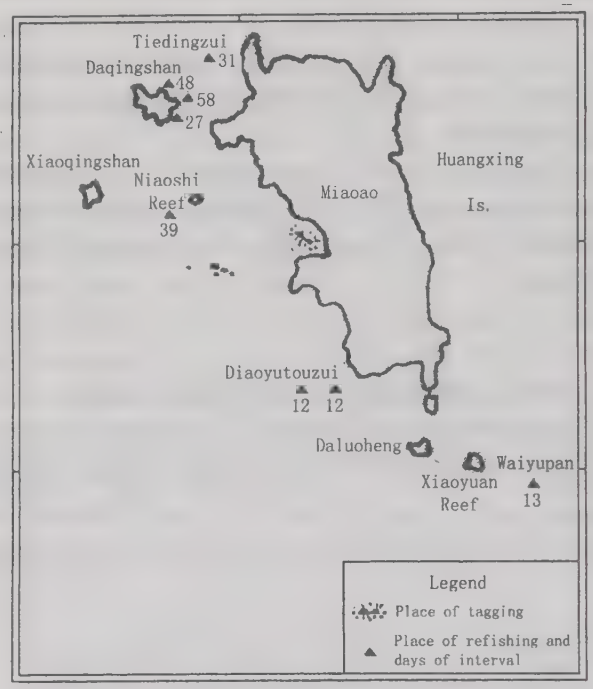

Fig. 2 Sketch map of release and refishing of tagged groupers, 1980

2.3.2 Xishan Island Waters

Three grouper fish with green colouring liquid mark which were released on Sept. 5, 1991 were captured by amateur angling lovers in the waters around the North Wharf of this island on Sept. 20, 1991, *i.e.* 15 days after the release. They range from 5.6 cm to 16.5 cm in body length and from 6.0 g to 135 g in body weight, and the refishing rate is 4.5 %.

On Jul. 25 ~ Aug. 11, 1992, the second year of release, 9 grouper fish with green colouring marks were recaptured in the waters north of Xishan Island and west of Dongshan Island, with body lengths ranging from 18.0 cm to 19.8 cm and body weights from 185 g to 220 g. The refishing rate in the second year was 13.4 %.

In addition, in the waters surrounding Xishan Island where no grouper fish had been fished before, the amateur angling lovers have fished the grouper many times, and in the prawn ponds of this island juvenile grouper fish over 10 cm in body length have been found a number of times.

2.3.3 Other water areas

On Sept. 20, 1992, grouper fish marked with the ink injection method were released in Xiangshan Harbour. In the late October and early November of the same year, *i.e.*, one month after the release, 6

tagged fish were recaptured near the location of release. The refishing rate was 1.4 %.

One hundred wild adult grouper fish were released in the surrounding waters of Huangxing Island. Ten of them were recaptured and the refishing rate was 10 %.The shortest interval between release and recapture was 12 days and the longest 58 days (See Tab. 2 and Fig. 2).

2.4 Refishing rates in several operations

In 1980 and 1987 — 1993, a total of 87 tagged grouper fish were recaptured, among which 75 were captured by handline, accounting for 86.2; 2 by shrimp trawl, amounting to 2.3 %; 2 by cuttlefish trawl, amounting to 2.3 %; 2 by pull net, amounting to 2.3 % and 6 in other operations (including filter and seine nets), amounting to 6.9 %.

2.5 Movement of tagged fish

2.5.1 Movement of tagged juvenile fish

It can be seen from Tab.2 and Fig.1 that the longest time between release and recapture was 651 days and the location of recapture was in the Wuzeishan Waters of Zhujiajian at the farthest, which was less than 2 n mile away from the place of release, the Xiaoao Waters of Zhujiajian; while the tagged fish recaptured in the same year were basically found near the place of release.

2.5.2 Movement of tagged adult fish

It can be seen from Tab. 2 and Fig. 2 that the grouper fish released in the Miaoao Waters of Huangxing were recaptured after 31 days and 43 days respectively in the waters of Tiedingzui and Waiyupan which are relatively farther from Miaoao. These waters are both about 1 n mile away from Miaoao. And 30 % of the tags of the recaptured fish were overgrown with attaching organisms such as polypite or algae.

It may be confirmed from the above-mentioned results that the grouper fish, whether juvenile or adult, do not move a long distance and their inhabitation is characterized by distinct localization.

3 Discussion

The tagged fish used in this experiment are mostly the artificially-cultivated juvenile grouper fish and a small portion is the wild grouper adult. The tagged fish from the two sources both have recapture records.The fact that they could be recaptured 2 n mile within the location of release after 651 days of release suggests that their moving range is small. It is believed that both the artificially cultivated and wild juvenile fish may be released for stock enhancement and regarded as the object of stock enhancement in the artificial fish reef zone. In the meanwhile, as their inhabiting behaviours are similar to the adult fish and have distinct localization, and whoever release them may be benefit, their artificial release for stock enhancement is easily accepted locally. Furthermore, if rational management measures are taken, the artificial release of the natural stock of grouper for stock enhancement is feasible.

Tow marking methods, tagging and ink injection, are introduced in this paper. But it can be seen from the results of recapture that only the records of recapture in the same year are available for the tagged grouper juvenile, but the records of recapture for the same year, second year and third year may be obtained for the grouper juvenile marked with the ink injection method. Judging from the recapture in the same year of release, in the Zhujiajian waters, the number of tagged fish released in 1987 was 2.3 times that of the tagged fish marked with the injection method and released in 1991, but the

recaptured number of the former was only 5 % of the latter. The authors think that the main reason is that the grouper fish are living in the rock and reef waters and moving about among the rocks so that their tags may easily fall off due to the infriction with rocks. This may be evidenced by the condition of the tagged grouper fish temporarily cultivated in the cement pond. It is believed, therefore, that, for the marking release of rock and reef fish such as grouper, it is suitable just to tag the fish. The ink injection marking leaves permanent marks in the fish body, which are easily recognized, so it can check the results of release more rationally and hence it is suitable for studying the population growth. But in terms of the research on the individual growth, it is best to adopt the method combining the marking in vitro and in vivo. New exploration should be made into the rational marking method in vitro.

References

[1] Cheng Qingtai and Yang Wenhua. Preliminary Study on the Geographic Distribution of China's Fishes of Serranidae. Beijing: Science Press. Collected Papers on Ichthyology, Vol.1[C], 1981, 1-8.

[2] Bo Zhili and Zhou Wanxia. Monitoring of Zhejiang's Offshore Grouper Resource Dynamics and the Countermeasures. Marine Fishery, 1992, (4): 151-152.

[3] Bo Zhili and Zhou Wanxia. First Tagging in China of the Artificially Cultivated Grouper Fries. Marine Fishery, 1988, (2): 80-83.

[4] Bo Zhili and Zhou Wanxia. Tagging and Refishing Experiment on Juvenile Grouper in the Littoral Waters of Shenjiamen, Zhejiang Province. Journal of Aquatic Products, 1999, (3): 304-307.

[5] Lu Zhongkang. Research Status of and Problems in the Grouper Cultivation. Modern Fishery Information, 1996, 11(1): 8-12.

Marine Science Bulletin

Marine Science Bulletin publishes papers on marine science and technology including physical oceanography, chemical oceanography, marine biology, marine geology, environmental oceanography, estuarine & coastal sciences, marine technology, digital ocean, coastal zone management, ocean engineering, marine economics, etc., and aims to promote international academic exchange.

Editor-in-Chief: Wang Hong（王　宏）
Deputy Editor-in-Chief: Lin Baofa（林宝法） He Guangshun（何广顺）
Yang Ying （杨　鹰）
Executive Editor: Xu Jie（徐 杰） He Xuewu （何学武） Zhang Deshan（张德山）
Zhang Xiaoxian（张潇娴） Wang Zhankun（王占坤）
Computer typist: Cheng Xiuchun （程秀春）

Marine Science Bulletin **(Vol . 5 No. 1 May 2003)**

Responsible Institution:
State Oceanic Administration of China
Edited and Published Semi-annually by:
National Marine Data and Information Service
Address: 93 Liuwei Road, Hedong District, Tianjin 300171, China
E-mail: msb@mail.nmdis.gov.cn

ISSN1000-9620
CN12-1271/N